Elaboration of magnetic micro/nano-tweezers for biotechnological applications

Cécile Iss

UNIVERSITÉ DE GRENOBLE

THÈSE

Pour obtenir le grade de

DOCTEUR DE L'UNIVERSITÉ DE GRENOBLE

Spécialité: **Nanophysique**

Arrêté ministériel: 7 août 2006

Présentée par

Cécile ISS

Thèse dirigée par **Bernard DIENY**
codirigée par **Yanxia HOU-BROUTIN**

préparée au sein du **Laboratoire SPINTEC**
dans **l'École Doctorale de Physique**

Elaboration de micro/nanopinces magnétiques pour applications biotechnologiques

Elaboration of magnetic micro/nano-tweezers for biotechnological applications

Thèse soutenue publiquement le **18 Juin 2015**
devant le jury composé de :

Mme Nora DEMPSEY
Directrice de recherche, Présidente du jury
M. Bernard DOUDIN
Professeur, Rapporteur
Mme Véronique DUPUIS
Directrice de recherche, Examinatrice
M. François MONTAIGNE
Professeur, Rapporteur
Mme Yanxia HOU-BROUTIN
Chargée de recherche, Co-Encadrante
M. Bernard DIENY
Directeur de recherche, Directeur de thèse

Université Joseph Fourier / Université Pierre Mendès France /
Université Stendhal / Université de Savoie / Grenoble INP

Remerciements

Ces 3,666667 années de thèse ont constitué pour moi une tranche de vie inoubliable, un parcours initiatique riche en découvertes et apprentissages de toutes sortes... Maintenant que cette page se tourne, je souhaite marquer un temps pour remercier toutes celles et ceux qui m'ont accompagnée dans cette aventure...

Je tiens en premier lieu à exprimer mes plus profonds remerciements à mon directeur de thèse, Bernard Dieny, pour son précieux soutien tout au long de la thèse et en particulier au cours des derniers mois d'analyse et de rédaction. Ce fut un grand plaisir de travailler et d'apprendre à ses côtés ! Toute ma gratitude va aussi à Yanxia Hou-Broutin, ma co-encadrante de thèse au SPrAM, souriante et attentive et dont les conseils toujours pertinents et motivants ont su orienter mes travaux ! Merci également à Hélène Joisten pour son aide et son soutien au quotidien !

J'adresse toute ma gratitude à Frank Hekking, directeur de l'école doctorale de physique en 2011, sans les efforts de qui je n'aurais pas pu effectuer ma thèse à Spintec.

Je remercie tout autant les membres de mon jury de thèse d'avoir accepté d'évaluer mon travail et d'avoir participé à ma soutenance : mes rapporteurs Bernard Doudin (professeur à l'Université de Strasbourg) et François Montaigne (professeur à l'Université de Lorraine), ainsi que Nora Dempsey (directrice de recherche à l'Institut Néel) et Véronique Dupuis (directrice de recherche à l'Institut Lumière Matière).

Ce travail de thèse n'aurait pas abouti sans mes chers collègues que je remercie vivement pour leur collaboration ! Merci en particulier à Éric Gautier, avec qui j'ai partagé de longues heures de suspense insoutenable devant le FIB de la PFNC, ainsi que les plus grandes joies de la thèse en avant-première ! Je remercie aussi, bien sûr, la fameuse « Bioteam » : Guillermo Tulio Ortiz pour ses conseils avisés, ses critiques constructives et son soutien, Selma Leulmi, Thomas Dietsch et Mélissa Morcrette pour nos échanges et le plaisir de se retrouver à nos réunions hebdomadaires ! Un énorme merci à toute l'équipe de la PTA et du Service technologie et caractérisation, en particulier Frédéric Gustavo, Christophe Lemonias, Jean-Luc Thomassin, Thierry Chevolleau, Marlène Terrier, Corinne

Perret et Stéphane Litaudon qui m'ont prodigué des conseils vitaux et donné de nombreux coups de pouces... bref, une aide précieuse ! Je salue au passage tous les collègues de salle blanche, notamment l'enthousiaste Laurent Vila ! Merci également à toute l'équipe CREAB du SPrAM qui m'a accueillie et formée dans son laboratoire de chimie ; en particulier Nora Reinhardt avec qui j'ai eu la joie de collaborer dans le cadre du projet ANR Nanoshark.

Je souhaite aussi remercier tous les membres du laboratoire Spintec que j'ai eu la chance de côtoyer pendant ces 3 années. J'ajoute une mention spéciale au secrétariat de Spintec pour son incroyable patience, ainsi qu'à Mairbek Chshiev qui a aussi soutenu ma candidature pour l'école d'été d'IEEE Magnetics Society 2013, Guillaume Prenat, Gilles Gaudin, Mihai Miron, Liliana Prejbeanu... et tous ceux avec qui j'ai eu le plaisir d'échanger ! Je tiens aussi à ajouter Emmanuel Hadji à cette liste non-exhaustive, même s'il n'est pas « Spintecois » mais d'un service voisin !

Je tiens par ailleurs à remercier Frédéric Né et Philippe Brincard de m'avoir embarquée dans l'aventure du Rhône-Alpes Challenge pour l'épreuve VTT « Les Chemins du Soleil ». Bien que cela ne paraisse pas directement lié à mon travail de thèse, cette aventure a profondément marqué cette période de ma vie et fut l'occasion pour moi d'approfondir des disciplines propres à une thèse : ténacité, persévérance et dépassement de soi ! Les éditions 2013 et 2014 ont en plus été l'occasion de faire l'heureuse rencontre de collègues d'autres services du CEA que je salue au passage !

Autres événements marquants : tous les bons moments passés avec les jeunes du laboratoire, sans qui cette thèse aurait été une expérience tristement différente ! Le bureau des supers nanas (Magali, Léa, Claire, re-Mélissa et Alex !) et le bureau des mecs (Marc, Pierre-Yves, Alex et Christophe), les personnages endémiques du deuxième étage: Kamil, Miguel, Pablo, Karla, Marina... Et l'inclassable Dr. Karol Marty ! Merci à tous pour ces excellents souvenirs intra et extra-muros ! Pourvu que ça dure !

Et pour finir, j'embrasse mes proches pour les remercier de m'avoir accompagnée et supportée durant ces difficiles mais tellement belles années ! Merci à ma famille, merci à Benjamin, Adrien, Michouquette et Ufukum... et à Éric qui m'a donné la force de finir cette thèse en beauté...

Abstract

The objective of this thesis was to elaborate magnetic micro/nano-tweezers remotely actuable by the application of a magnetic field. This innovative idea consists in binding two parallelepiped magnetic microparticles by one of their sides with a flexible gold nano-hinge. Intended for biotechnological and medical applications, these tweezers aim at capturing biochemically targeted micro/nano-objects, in order to exert forces on them and perform force measurements.

In this project starting from a simple idea, the challenge was to carry out theoretical and technological studies leading to a first proof of concept. To this end, an analytical model was first elaborated to predict the magneto-elastic behavior of the tweezers, depending on various physical parameters. Then, a fabrication process inspired from microelectronic techniques was developed to complete a functional prototype of tweezers. Finally, the remote actuation of such tweezers, kept attached to a substrate, by the application of a magnetic field, was demonstrated using an original experiment set up inside a scanning electron microscope. These experiments yielded results in good agreement with our theoretical predictions and allowed the quantification of the gold nano-hinge elastic behavior.

Attached to a substrate, these tweezers constitute an array of reflective micro-surfaces, which can find applications in microfluidics (biochips) or in nano-physics. Released in solution, the tweezers could be used in an original way for biological objects micro-manipulation or cell diagnostic and therapy.

Résumé

Cette thèse propose de réaliser des micro/nano-pinces magnétiques articulées dont l'actionnement à distance est obtenu par l'application d'un champ magnétique. Cette idée innovante consiste à relier par l'un de leurs côtés deux microparticules magnétiques parallélépipédiques à l'aide d'une nano-charnière en or flexible. Destinées à des applications biotechnologiques et médicales, ces pinces ont pour finalité de capturer des micro/nano-objets ciblés biochimiquement pour y appliquer et mesurer des forces.

Le défi de ce projet était de mener, à partir d'une idée simple, un ensemble d'études à la fois théoriques et technologiques, pour aboutir à une première preuve de concept. Dans ce but, un modèle analytique a d'abord été construit pour prédire le comportement magnéto-mécanique des pinces en fonction de divers paramètres physiques. Ensuite, un procédé de fabrication inspiré des techniques de la microélectronique a été développé pour parvenir à la réalisation d'un prototype de pince fonctionnel. Enfin, l'ouverture par l'action d'un champ magnétique de pinces fixées à un substrat, a pu être démontrée à l'aide d'une expérience originale installée dans un microscope électronique à balayage. Les résultats de ces expériences, en bon accord avec nos prédictions théoriques, ont permis de quantifier le comportement mécanique de la nano-charnière en or.

Fixées à un substrat, ces pinces forment un réseau de micro-surfaces réfléchissantes qui trouveront des applications en microfluidique (bio-puces) ou en nano-physique. Libérées en solution, les pinces pourraient être employées de manière originale en micro-manipulation d'objets biologiques ou diagnostic et thérapie cellulaire.

Table of contents

1 Introduction

1.1 Position of the subject in the global context of biotechnologies

Magnetic micro/nanoparticles have constituted the basis of numerous multidisciplinary studies for several decades. In particular, magnetic particles offer broad perspectives of applications in the wide area of research in biotechnology and biomedicine [1, 2]. Research focuses especially on their use in diagnosis with, for instance, magnetic contrast agents for magnetic resonance imaging (MRI), magnetic particles imaging (MPI) [3] and cell sorting, as well as in therapy with drug delivery, tissue engineering, hyperthermia and more recently targeted cancer cells destruction by micro-particles vibrations [4].

The use of magnetic particles for these applications is mainly motivated by their ability to be remotely actuated, manipulated and detected using external magnetic fields. The fact that magnetic fields penetrate biological solutions or tissues enables magnetic particles to be steered remotely in biological media, including in living organisms [1].

The displacement of magnetic particles is usually obtained with magnetic field gradients. However, gradients decrease quickly with the distance. Yet the magnetic tractive force should be maximized to efficiently steer magnetic particles in viscous media and in the case of *in vivo* applications, overcome the drag of blood flow. The magnetic gradient can be replaced by a uniform (alternating or constant) magnetic field that can exert a magnetic torque on anisotropic particles [5]. Otherwise, the particles magnetic volume can be increased. However, enlarged particles loose the advantage of high surface to volume ratio reached at nanoscale, which can be of great interest in biotechnologies [6, 7, 8].

Another critical feature for magnetic particles is their ability to spontaneously redisperse in zero field when they are suspended in solution, since a spontaneous agglomeration would prevent their use in a biological media.

To address this issue, two different types of magnetic micro/nano-particles are nowadays used in biological and biomedical applications. On one hand, conventional and widely used magnetic particles, such as iron oxide superparamagnetic particles (SPION) [9, 10], rely on the superparamagnetic behavior of nanoparticles and are produced by bottom-up approaches based on chemical routes [11]. On the other hand, an innovative type of micro and nanoparticles were developed by top-down approaches, using micro/nano-electronics fabrication techniques [12]. The recent emergence of this approach opened up many possibilities by allowing the elaboration of three-dimensional functional micro/nano-objects built from several materials and releasable in solution, similarly to magnetic particles. In particular, it led to the emergence of magnetic micro/nano-tweezers [13] aimed at biotechnological and medical applications, object of this thesis work. These magnetic micro/nano-tweezers are intended to be used either remaining fixed to their substrate or dispersed in solution.

The reason why superparamagnetic magnetic particles are preferred over ferromagnetic particles is that the latter exhibit remanence, whereas the former do not. As a result, the superamagnetic particles do not aggregate once the magnetic field is removed. Indeed, even though ferromagnetic particles are attractive due to their effective coupling to an external field, their remanent magnetization is responsible for their aggregation once dispersed in suspension in a solution.

The superparamagnetic behavior is obtained in ferromagnetic materials when reduced to nanometric dimensions (around 5-10nm for typical ferromagnets [2]). At that point, thermal fluctuations can overcome the magnetocrystalline anisotropy energy barrier (proportional to the volume) which maintains the magnetization in a given direction [14]. The magnetization is then randomized and appears null in zero field over a characteristic measurement time (typically over 100 s in most practical situations [15]).

Moreover, at these dimensions, particles are generally small enough to be in single domain state (around 3 nm (CoPt) to 30 nm (Fe_3O_4) [16]), which enhances their magnetic response. As a matter of fact, the segmentation in magnetic grains oriented in random directions lowers a particle overall magnetization, as the grains partially compensate each other. For comparable volumes, a single domain particle can more easily reach full

saturation magnetization under the application of a magnetic field, thus relatively increasing the magnetic forces and torques which can be created on it. However, the volumes considered are so small that these forces are quite weak; too weak, for instance, to overcome the drag force of blood flow.

Thus, it appears necessary to develop alternative synthesis methods yielding larger magnetic volumes to increase the driving force, while preserving the superparamagnetic-like behavior. That's why, for instance, the synthesis of larger magnetic microparticles, based on sets of superparamagnetic nanoparticles incorporated into various matrices is the object of investigations [17, 18, 19].

Towards this goal, an innovative fabrication method of novel biologically relevant magnetic particles arose, inspired from the advances in the seemingly distant field of microelectronics [20, 21, 22]. It consists in the top-down approach mentioned above, based on micro/nano-electronics fabrication techniques, which allows fabricating magnetic particles with a complete control of the magnetic particles constituting materials, shapes and dimensions. This allows providing the particles with advantageous magnetic properties, such as a superparamagnetic-like behavior and higher magnetic susceptibilities resulting in enhanced responses to lower applied magnetic fields [23] than SPIONs obtained by chemical route (bottom-up approach) [24, 25, 26, 27].

In particular, a first magnetic composition has been proposed for such particles: SAFs (Synthetic AntiFerromagnetic particles) [28, 29, 30, 5] consisting in stacks of ferromagnetic layers (such as Permalloy), antiferromagnetically coupled through non-magnetic spacers (such as ruthenium) (***Figure 1***). In the absence of external magnetic field, the antiparallel coupling between the magnetic layers is such that the average magnetization over the total volume is null, resulting in zero remanence. Provided that the magnetic susceptibility remains lower than a susceptibility threshold established and modeled in a previous study [27], no aggregation occurs in zero field, despite their micrometric volumes (typically 1 µm side and a few hundreds of nanometers thick), larger than superparamagnetic nanoparticles.

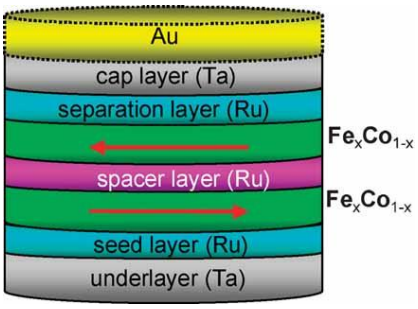

***Figure 1**: "Layer structure of disk-shaped SAF nanoparticles containing ferromagnetic layers separated by a nonmagnetic spacer. Additional layers that inhibit corrosion and impart other functional properties, such as Au for selective surface chemistry, are indicated."*
Figure and legend extracted from [29].

Another very attractive example of magnetic particles fabricated by a top-down approach is the vortex particles named after their magnetic configuration: the vortex magnetic state. It consists in an in-plane magnetic flux closure distribution resulting in a zero net magnetization in zero field. More than SAFs, vortex particles always redisperse in solution once the applied field is removed, their magnetic susceptibility being always lower than the agglomeration susceptibility threshold [31].

Both types of particles find very promising applications in biology and medicine. Of particular interest, current studies at Argonne [4] and Spintec [32] labs focus on using these magnetic particles for cancer cell destruction following an innovative approach. Like for hyperthermia [33], magnetic particles are functionalized to bind to cancer cells in the purpose of killing them without harming healthy cells, by applying alternating magnetic fields. The difference between these two approaches lies in the mechanism which triggers cell death. In the case of hyperthermia, cells are heated above 42°C thanks to fields of hundreds of kHz, while the other approach uses mechanical vibrations on the cells membrane, requiring fields of much lower frequencies (tens of Hertz). Proper mechanical stimuli to the membrane trigger a biochemical cascade within the cells, resulting in their apoptosis (***Figure 2***), *i.e.* their "suicide". Unlike heat, mechanical stimuli apply only to targeted cells, causing less (if any) harm to the neighboring cells. Furthermore, apoptosis does not lead to inflammation like the necrosis induced by heating. This new approach

offers exciting perspectives for cancer treatment and already yields promising results [4, 32].

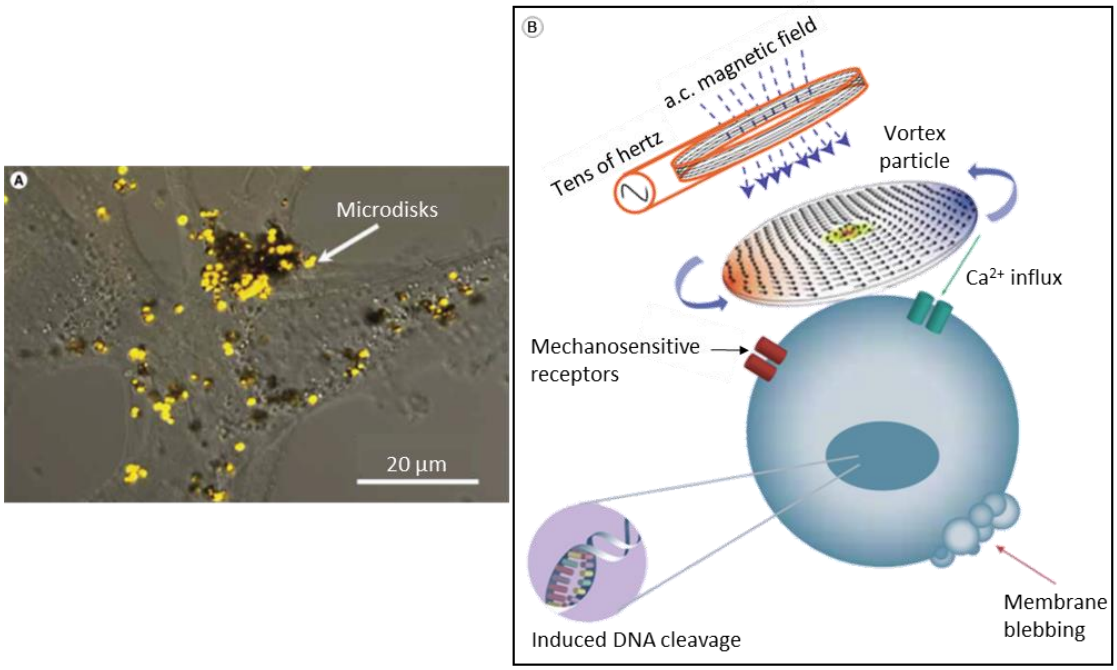

***Figure 2**: "Ferromagnetic microdisks targeted to a cancer cell for magnetomechanical cell stimulation. (A) Confocal optical image of microdisks on the A172 glioblastoma cell surface. (B) The principle of magnetomechanical actuation of cell membrane triggering apoptosis." Original figures and legend extracted from [21].*

As mentioned above, in the context of biotechnologies, the top-down approach used for fabricating this new type of magnetic particles (SAF and vortex particles) has likewise allowed the invention of a more complex micro/nano-object for biotechnology, the subject of this thesis.

The micro/nano-tweezers elaborated in this study constitute innovative collection of nano-robots designed to be used either attached to their substrate or dispersed in solution. Thus, the tweezers are a cross between colloidal magnetic particles and NEMS (Nano-Electromechanical Systems with a least one feature's dimension below 100 nm) or MEMS (Micro-Electromechanical Systems with at least one feature's dimension between 100 nm and 200 µm).

The state of the art provides micro/nano-manipulation tools intended for biological and medical purposes covering a wide range of dimensions (from 1 mm [34] to 50 nm [35]). However, most of these devices operate at the scale of a single cell [36, 37, 38, 39, 40, 41] or more [42]. In addition, the fabrication process and implementation of such devices is not always compatible with collective fabrication and utilization. In most cases, the energy and signals required to operate them are transmitted through wires or tethers connecting them to controls outside of the biological medium, excluding the perspective of *in situ* applications. This also applies to optical tweezers [35, 41], which, although they can address nanoscale objects, do not allow exerting mechanical stress on the trapped objects.

Magnetically actuated devices offer the opportunity to get rid of wires and tethers. As a matter of facts, magnetic tweezers using magnetic microbeads to exert torsional and tensional stress are popular to study DNA interactions with other molecules [43]. Such setup has even been adapted to collective measurements [44], the acquisition of statistical data being of particular interest in biology. However, magnetic tweezers require the analytes to be bound to a fixed surface, which is not compatible with *in situ* applications. Besides, they do not allow mechanical grabbing like the micro/nano-tweezers presented in this study.

Regarding *in situ* applications, untethered devices are highly preferable when it comes to access difficult–to-reach objects in a sample or in an organism. In this framework, the development of magnetic microgrippers already yielded promising results [45, 46] but besides being quite large (~500 µm), they exploit magnetism only for their motion, while their actuation is triggered by other mechanisms such as pH variation [45] currently too high to match with biological applications, optical [44] or thermal [41] stimulation which allows only one actuation (closure).

Our micro/nano-tweezers are currently the only magnetically actuated devices which can be released in solution in the manner of magnetic microparticles and remotely actuated on demand to capture objects of the order of 1µm large. Indeed, their actuation is based on the well-known principle of attraction and repulsion between two magnetic bodies [47, 48].

The fabrication process of such tweezers being compatible with chemical functionalization, these devices can also benefit from chemical functionalization features such as passivation to enhance their biocompatibility and chemical selectivity toward a targeted analyte. Tailoring the tweezers chemical properties can give rise to interesting applications presented in section **1.2.2**. Therefore, these magnetic micro/nano-tweezers constitute an original and promising prototype of gripping BioNEMS (NEMS for biomedical applications).

1.2 Presentation of the study

Within this context, this project aims at providing new perspectives for selective grabbing of targeted biological samples at micro or nano-scale in liquid environment. It combines on one hand an innovative technological approach inspired from micro/nano-electronics to fabricate complex magnetic micro/nano-particles with a precise control of materials in composition, shape and size, with on the other hand, a state of the art chemical functionalization method. The original idea implemented in these tweezers consists in binding two magnetic particles by a flexible nano-hinge to create an articulated magnetic nano-tweezer capable of a jaw-like opening (***Figure 3***). Taking advantage of the magnetostatic interactions between a pair of magnetic micro-particles, the tweezers actuation can be triggered remotely by the application of an external magnetic field.

1.2.1 General concept

More precisely, these micro/nano-tweezers consist in two magnetic particles placed one on top of the other and linked by one of their ends by a flexible hinge. Their magnetic actuation, triggered by the application of a magnetic field, is enhanced by the magnetostatic

interaction between the two particles. The repulsive or attractive nature of this interaction depends on their respective magnetization direction as sketched in ***Figure 3***.

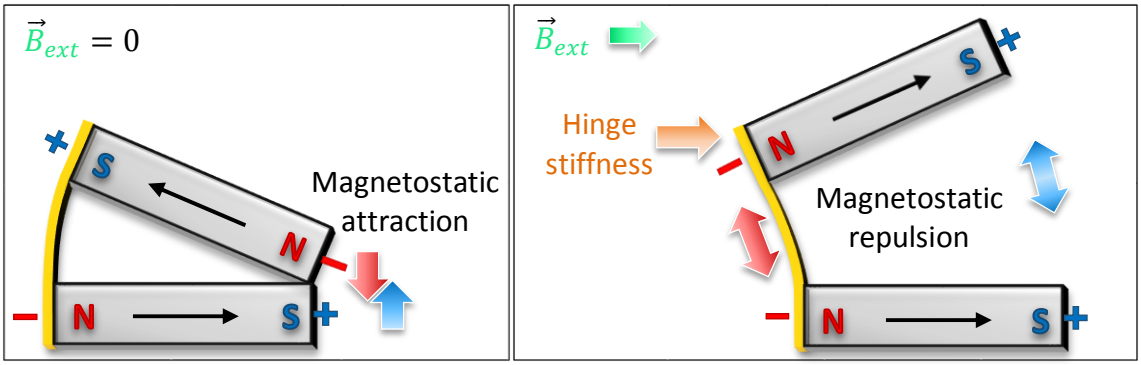

Figure 3*: Magnetic micro/nano-tweezers working principle. The top jaw is here assumed to be made of a soft magnetic material (switchable magnetization) whereas the bottom jaw can be made either of a soft or a hard magnetic material (fixed magnetization as a permanent magnet). In zero applied field, the particles spontaneously attract each other by setting their magnetization anti-parallel to each other (left). The application of a magnetic field tends to align both magnetizations in the same direction, causing the particles mutual repulsion. The resulting magnetic torque is balanced by the elastic torque from the hinge which tends to maintain the jaws in a close configuration (right).*

Thus, a tweezer is closed when the two particles standing for its jaws have their respective magnetizations in an anti-parallel configuration. For a tweezer made of two magnetic jaws of proper composition and shape, this can occur spontaneously in zero field, in the same way as two macroscopic magnets. However, under the application of a sufficient magnetic field, both magnetizations are forced to align along the field, reaching parallel configuration. In this state, their mutual repulsion contributes to the tweezer opening while the hinge holds the jaws together. The opening amplitude is then determined by the balance between the magnetic torque and the elastic torque. So, the hinge should be flexible enough to allow a wide opening, but strong enough so that the tweezer is not excessively fragile. In addition, the elasticity of the hinge can assist the closing back of the tweezers.

Therefore, by remotely applying a magnetic field and turning it off, the magnetic micro/nano-tweezers can be opened and closed so that they can grab small objects at the micro/nano-scale and release them at specific locations. In particular, thanks to proper

surface functionalization, the tweezers can interact specifically with targeted biological entities. Therefore, the nano-tweezers constitute an original and promising tool for interacting with biological objects such as small cells, bacteria, DNA and RNA strands, viruses or coated particles (***Figure 4***), as previously addressed by magnetic micro/ nanoparticles. They can find applications in biotechnologies, and the biomedical field by enabling the exploration of additional applications compared to monolithic nanoparticles, thanks to their nano-mechanical and nano-optical properties.

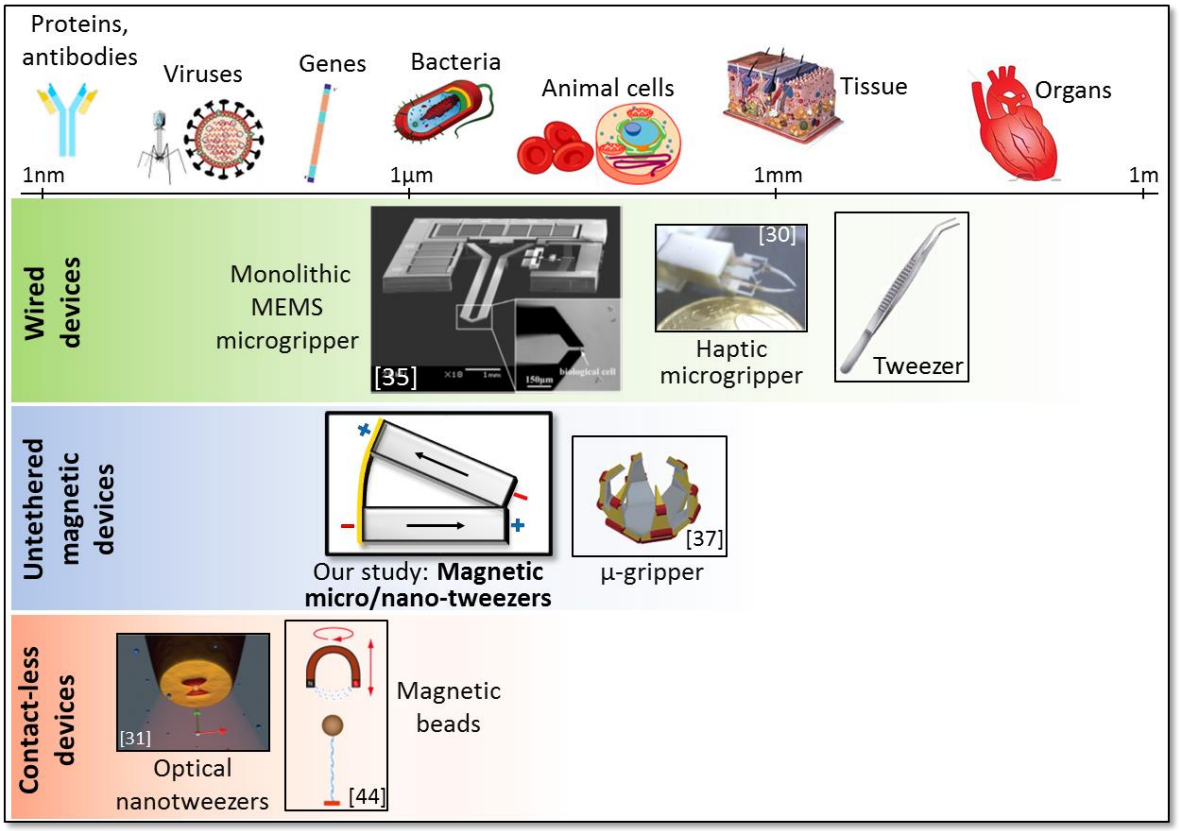

Figure 4*: Comparison of the length scale of various biological assemblies [49] with a few examples of tweezers [34, 35, 41, 43, 44], including the tweezers presented in this study, sorted according to the typical size of objects they interact with.*

Depending on the application, the tweezers can be utilized either attached to the substrate or released in solution. Accordingly, the jaws magnetic properties can differ along with their constituting material. When the tweezers are released in solution, their opening and closing can be remotely controlled only if both jaws are magnetic. The two jaws can either be both made of a soft magnetic material or one made of a soft material and the

other of a hard one. In contrast, when the tweezers remain attached to a substrate, only the mobile jaw needs to be magnetic. The fixed jaw can be magnetic as well as non-magnetic.

These two scenarios, a semi-magnetic tweezer attached to a substrate and a fully magnetic tweezer released in solution, involve different actuation mechanisms and balance of forces, as sketched in ***Figure 5***.

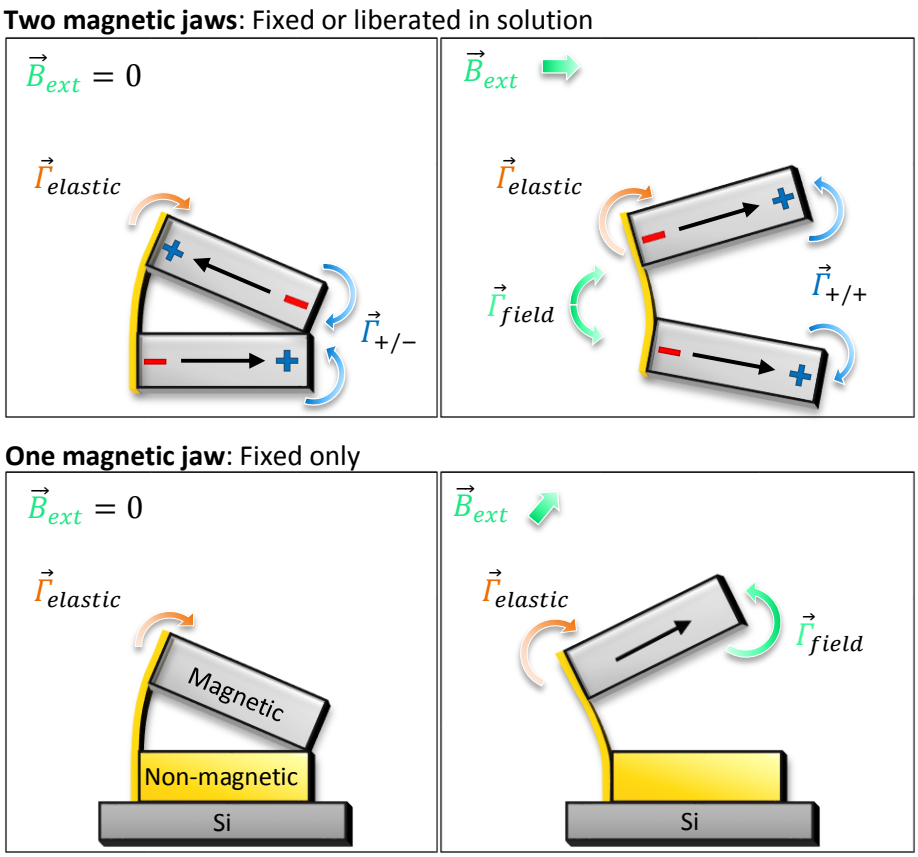

Figure 5*: Comparison of the torques involved in the two main scenarios considered in this study. Arrows indicate qualitatively the direction of the motion induced by each torque.*
Up: when both jaws are magnetic, the equilibrium opening angle is reached when the jaws magnetostatic repulsion is balanced by the hinge restoring torque. If the tweezer is liberated in solution, it will adjust its orientation with respect to the applied field direction.
Down: when only the upper jaw is magnetic, the balance occurs between the magnetic torque due to the external field and the hinge restoring torque. Although this configuration is slightly simpler than the previous one, it requires the lower jaw to be fixed on a substrate to open the tweezer.

A qualitative description of these two scenarios is given below and further details will be discussed extensively in chapter 3, sections **3.1.2** and **3.3**.

1.2.1.1 Tweezers comprising one mobile magnetic jaw, the other being fixed and non-magnetic

When a tweezer comprises only one magnetic jaw, the other one being in a non-magnetic material, the actuation mechanism is due to the torque exerted by the applied magnetic field on the upper jaw magnetization (***Figure 5***). Therefore, the tweezer needs to be attached to a substrate in order to be actuated. If the lower jaw wasn't fixed, this would result in the whole tweezer rotation rather than its opening. As a matter of facts, the field should be preferably applied out-of-plane to yield significant opening. The equilibrium opening angle is reached when the magnetic torque exerted by the field is balanced by the elastic torque due to the hinge restoring force.

To make the actuation efficient, the upper jaw has to be made of a magnetic material with in-plane magnetization. This way, the plane of the jaw tends to align with the applied field direction. If the magnetization was allowed to go out-of-plane, it would rotate within the jaw without inducing any mechanical motion. For a given material, this feature relies on the shape of the magnetic volume, using here the shape anisotropy of thin films which tends to maintain their magnetization in-plane. Thus, the magnetic layer constituting the upper jaw should be rather thin (more details in section **2.1.2** and chapter 2).

To optimize this actuation mechanism, a material with high saturation magnetization is preferable for the upper jaw. A higher saturation magnetization increases the magnetic torque responsible for the tweezer opening. Indeed, the force applied by an external magnetic field on a magnetic volume is proportional to its magnetization, which reaches its maximum at saturation. Iron (2.15 T), Cobalt (1.79 T), Cobalt-Iron (1.8-2.4 T depending on the composition), Cobalt-Iron-Boron (1-1.6 T), Iron-Silicon (2 T) and Neodymium-Iron-Boron (~1.3 T) are examples of magnetic materials with high saturation magnetization.

This scenario can be used for instance for molecular bonding strength measurements or incorporated in biochips for detection and measurements assays. These applications are presented in section **1.2.2**.

1.2.1.2 Tweezers consisting in two magnetic jaws

If both jaws are magnetic, their magnetostatic interaction adds up to the magnetic field influence and the hinge stiffness. As mentioned in section **1.2.1**, the tweezer dimensions and material can be adjusted so that the magnetostatic coupling between two magnetic jaws leads to the tweezer locking by favoring antiparallel alignment of their respective magnetizations. Under the application of a magnetic field, the tweezer will resist to its opening until the field is large enough to bring the magnetization of the two jaws in parallel alignment. From that point, the mutual repulsion between the two micro-magnets will contribute to the jaws separation (***Figure 5***).

Therefore, tweezers combining two magnetic jaws could be actuated without being fixed to a substrate and can then be released in solution, and thus find interesting applications in microfluidics and biotechnologies (see section **1.2.2**). The tweezers displacement in liquid environment could be achieved collectively using magnetic field gradients. However, the simultaneous control of displacement and the opening/closing of a set of tweezers is not easily achievable by the only use of magnetic fields and their gradients in microfluidics channels. Indeed, due to gradient distribution, only a few tweezers can be submitted to a given field, while the neighbors necessarily undergo another field. Nevertheless, moving and actuating the tweezers can be achieved by combining dielectrophoresis for motion and magnetic fields for actuation in specific microfluidic channels.

Compared to the previous case with only one magnetic jaw, here magnetization reversal is a key feature for actuation. Therefore, the choice of materials with proper coercivity for the jaws is of particular importance.

The coercivity is the intensity of the magnetic field required to reverse the magnetization of a material once it has been saturated and is intrinsic to each material. Magnetic materials can be classified in two categories: “soft” materials with low coercivity such as Permalloy (nickel 80% - iron 20%), mu-metal (composed of approximately 77% nickel, 16% iron, 5% copper and 2% chromium or molybdenum), Sendust (84% iron, 17%

silicon and 6% aluminum), and CoFe (90%-10%) on one hand, and “hard” materials on the other hand, with a coercive field large enough to be considered as permanent magnets, such as some ferric oxides $CoFe_2O_3$, or samarium-cobalt and neodymium-iron-boron or exchange biased ferromagnets like Co/IrMn for example [50].

As mentioned before, the tweezers actuation, when released in solution, would imply the switching of at least one jaw’s magnetization to go from the antiparallel (closed) state to the parallel (open) state. For this purpose, at least one jaw should be magnetically “soft”, whereas the other can be “soft” or “hard”, giving rise to two different actuation mechanisms when liberated in solution.

If both jaws are made of a magnetically soft material, the tweezer is expected to open and rotate to align with the applied field at the same time. Indeed, as the jaws get polarized by the applied field, the tweezer will open due to magnetostatic repulsion between the two jaws. In addition, the tweezer will tend to rotate in the fluid to align its easy axis of magnetization with the field direction. In most practical cases, if the jaws have an elongated shape with the longest dimension perpendicular to the hinge, then this long dimension will constitute the easy axis of magnetization due to shape anisotropy. The rotation of the tweezer will occur with a maximum angle of +/- 90°, since both jaws magnetizations directly point towards the same direction as the applied field. Following the example of two antiferromagnetic moments observing a Spin-flop transition [51], two identical jaws will have an opening symmetric with respect to the field direction (***Figure 6***).

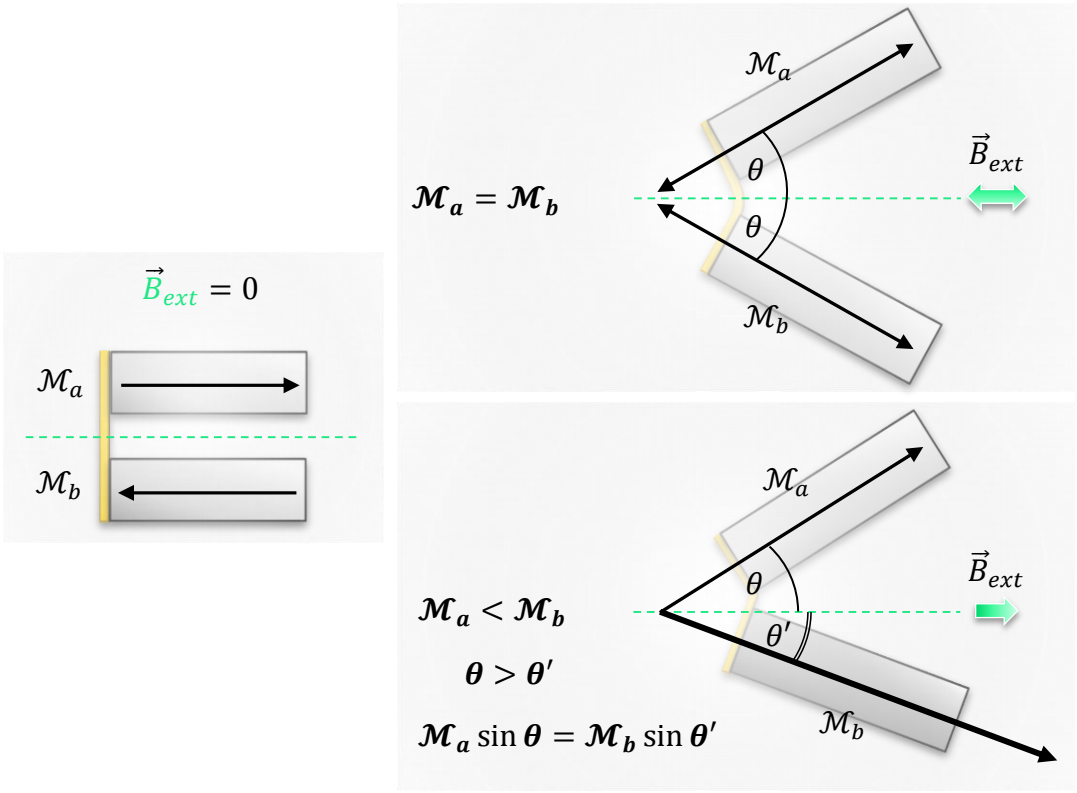

***Figure 6**: The opening of a tweezer released in solution can be compared to the Spin-flop transition in antiferromagnets if the jaws are assimilated to antiparallel coupled magnetic moments. When submitted to a field parallel to their initial magnetization direction, the two moments split on both sides of the field direction. Whereas two identical moments split symmetrically, two unequal moments adjust their position to balance the torques exerted by the field on their respective transverse components. If both jaws are soft, the tweezer aligns with the field axis, independently of its direction. On the other hand, if one jaw has a magnetization hard to reverse, the tweezer rotates until this magnetization is in the same direction as the applied field.*

Conversely, when one jaw is made of a hard material while the other is made of a soft material, the harder jaw will tend to induce the tweezer rotation so that its permanent magnetization will align to the field. In this case, the rotation of the tweezer will occur with a maximum angle of +/- 180°. The soft jaw will then get magnetized parallel to the hard one, triggering the tweezer opening. Here again, if the two jaws have the same moment, they will align symmetrically with respect to the field direction. If their moment are different, they will align so that their respective component transverse to the applied field are opposite and balance each other. This way, the overall torque exerted by the field on the tweezer is zero (***Figure 6)***.

1.2.2 Potential applications

Whether they are kept attached to a substrate or liberated in solution, the magnetic micro/nano-tweezers offer promising perspectives of applications for biological sample grabbing in dry or liquid environment at micro/nano-scale.

Most of these applications implies that the inner side of the tweezers jaws undergo surface chemical functionalization to provide them with specific interaction with targeted biological entities. Likewise, the outside of the tweezers can be passivated to prevent them from oxidizing and have non-specific interaction with the environment. This topic is addressed in chapter 6, section **6.3**.

Interestingly, the chemical bounding between the jaws inner surface and the analyte can modify the tweezers actuation mechanism. The strength of the ligand-analyte interaction can actually compete with the magnetostatic torques which open the tweezers. Thus, the capture of a sample can either definitely lock a tweezer or require the application of an increased magnetic field to open back the tweezer, depending on the torques involved. This interplay can be exploited to measure the strength of molecular bonds within captured biological complexes (***Figure 7***). For this application, the tweezers should be fixed on the substrate, so only their upper jaw requires to be magnetic.

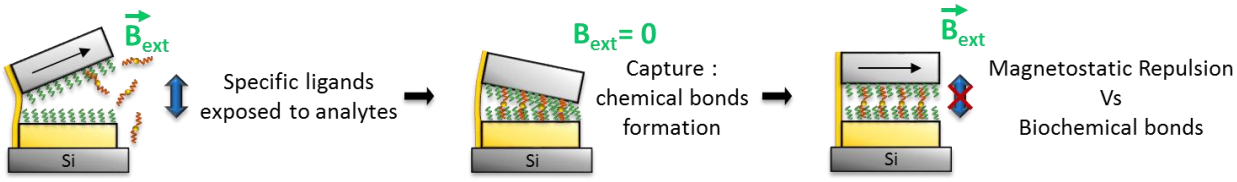

Figure 7*: Molecular bonds force measurements principle with functionalized tweezers attached to a substrate and comprising only one magnetic jaw.*

This principle could be implemented in biochips by incorporating the tweezers in microfluidic channels. Taking advantage of the tweezers magneto-optic property, the sample capture of a collection of tweezers fixed on their substrate can be monitored by optical microscope, which is a rather simple technique compared to other labs-on-chip.

Indeed, a tweezers assembly constitutes a micro-array of reflective micro surfaces whose reflectivity can be modified by the application of a magnetic field. When a tweezer

gets “locked” by creating chemical bonds with its target, it modifies its reaction to the magnetic field application. It will stay closed when empty tweezers open and conversely if the sample is large with respect to the jaws. This difference of behavior can be revealed by monitoring the reflectivity of the tweezers top surface with an optical microscope, while applying and removing an external magnetic field. The concept of such magneto-optical biochip is illustrated in ***Figure 8***.

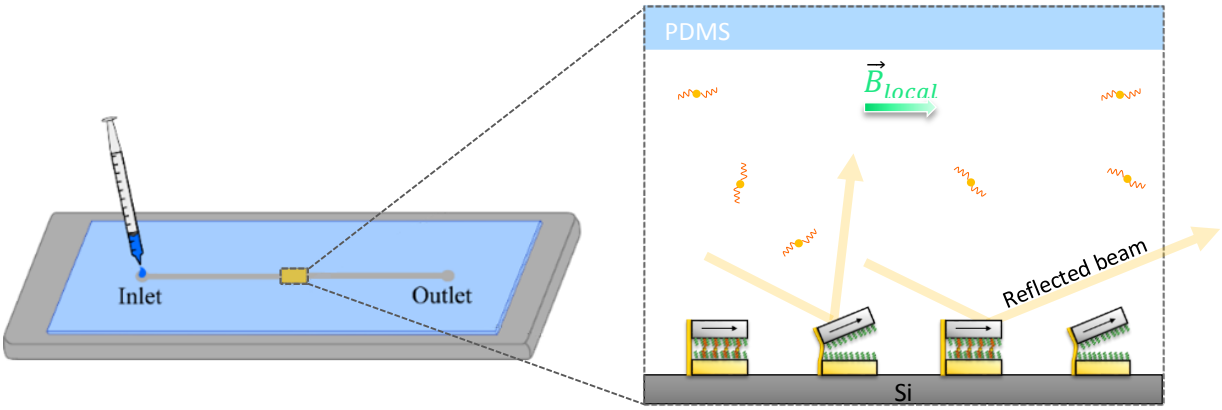

Figure 8*: Principle of a biochip using an assembly of tweezers fixed onto the bottom of a microfluidic channel as an array of magneto-optical detectors. The capture of a targeted sample in suspension (or flowing) in the microchannel via chemical binding locks the tweezer closed and modifies its reflectivity compared to empty tweezers when a magnetic field is applied.*

Tweezers with two magnetic jaws can as well find many applications in biotechnologies. For instance, they could be used for extremely local hyperthermia. Once a target is captured, a magnetic field (typically tens of mT) can be applied at the usual frequencies used for hyperthermia (hundreds of kHz [52]). Too high to induce mechanical motion, this frequency will rather result in the magnetic jaws heating. Compared to single particles, the temperature can get more elevated between the two sources of heat, inside the tweezers, than outside. This way, the tweezers can be used as magnetic “micro-oven”, heating the captured sample.

On the other hand, if lower frequencies are applied (for instance 1 to 20Hz), the tweezers could adopt a very original behavior: they could literally “chew” the caught object. Cells mechanical properties and their response to mechanical stimuli have been an active field of research the past few years [53, 54, 55]. In particular, recent studies demonstrated

the possibility to trigger apoptosis in cells by submitting them to proper mechanical stimuli [4, 32]. Depending on their size, our tweezers could be well adapted, compared to particles or AFM probes, to exert forces on cell membranes. Moreover, this approach would enable highly parallel studies and statistical analysis of mechano-transduction within biological entities.

Finally, if tweezers with two magnetic jaws are released in solution, their motion can be controlled by dielectrophoresis inside adapted microfluidic channels. Their ability to grab and transport the micro/nano-objects to a desired location seems to be a promising approach. This offers the perspective of using the nano-tweezers for cell sorting, magnetic field-mediated transfection into living cells, drug delivery.

One can even think of using magnetic nano-tweezers for non-invasive nano-biopsy in a similar way as another recent study which reports performing non-invasive biopsy with tweezers comprising a ferromagnetic material and thermally activated, and retrieved using a magnetic catheter [56]. In that study, the fabricated tweezers have sizes ranging from 10µm to 1mm to target cells which are in the range of 10–100µm. For the magnetic micro/nano-tweezers presented in this work, biting in the cells, or catching bacteria or cell organelles could be targeted instead. Of course, this kind of application requires further investigation and cannot be envisaged in living organisms in short or medium term.

1.3 Environment and objectives of the thesis

This thesis is directly coupled to the Nanoshark project funded by the ANR (French Research National Agency) P2N program (support reference: ANR-11-NANO-001). The project involved a collaboration between three laboratories: Spintec and SPrAM, part of the INAC (Institut Nanosciences et Cryogénie), and the LTM (Laboratory of Microelectronic Technologies). The collaboration between these three laboratories aims at gathering the diverse skills and means required to carry out this multidisciplinary work, which combines materials science, physics, engineering, chemistry and biology. Spintec brings its technological and theoretical expertise on thin layers magnetic properties, SPrAM brings its expertise in biochemistry and surface functionalization and LTM in microfluidics. The

Nanoshark project lasts 4 years and this thesis covered the first 3 years of the project. This thesis work was carried out in collaboration between Spintec and SPrAM mostly, the microfluidic application being investigated in the 4th year of the project.

The goals of the thesis were the followings:

First, to build an analytical model to guide the micro/nano-tweezers technological development and support experimental characterizations afterwards.

Second, to achieve the fabrication of remotely actuable tweezers with proper materials, dimensions and magnetic properties. This challenging technological work was enabled by a full access to the Plateforme Technologique Amont (PTA), born in 2007 from a sharing of resources between CEA, CNRS (Centre National de la Recherche Scientifique), Grenoble-INP (Grenoble-Institut National Polytechnique), and UJF (Université Joseph Fourier, Grenoble I) [http://pta-grenoble.com/index.php].

Finally, the demonstration and characterization of the tweezers magnetic actuation was the final goal of this thesis. For that, an innovative experiment was set up and carried out at the Plateforme de Nano-caractérisation (PFNC), involving a FIB (Focused Ion Beam) and a micro-manipulated tip to which a microscopic magnetic sphere of permanent magnet (NdFeB) was attached to actuate the tweezers with a local magnetic field.

1.4 Outline

The first chapter of this manuscript (chapter **2**) deals with the tweezers design in-depth, from the definition of their shape and constitutive materials, to a first analysis of the forces involved in their actuation, compared to other the forces at stake between the jaws at such dimensions.

The magneto-mechanical torques responsible for the tweezers actuation are addressed more extensively in chapter **3**, in which a theoretical model combining analytical and numerical approaches is proposed to describe the tweezers behavior. The study of different types of tweezers using this model concludes this chapter.

The technological development of the tweezers is described step by step from the mere silicon wafer to the completed tweezers in chapter **4**. The exploration of various materials and dimensions (jaws width and hinge thickness) is also addressed in this chapter.

The mechanical and magnetic actuations of individual tweezers were achieved inside a SEM, using a micro-manipulated tip to interact with individual tweezers. These experiments, presented in chapter **5**, were modelled and interpreted using the model built previously.

Finally, the main achievements of this thesis work are summarized in chapter **6**, followed by a discussion on the perspectives of continuation of this work and proposals for long-term applications for these magnetic micro/nano-tweezers.

1.5 References

[1] Q. Pankhurst, J. Connolly, S. Jones et J. Dobson, «Applications of magnetic nanoparticles in biomedicine», *Journal of Physics D: Applied Physics,* vol. 36, 2003.

[2] K. M. Krishnan, «Biomedical Nanomagnetics: A Spin through Possibilities in Imaging, Diagnostics, and Therapy», *IEEE Transactions on Magnetics,* vol. 46, n°17, pp. 2523-2558, 2010.

[3] B. Gleich et J. Weizenecker, «Tomographic imaging using the nonlinear response of magnetic particles», *Nature,* vol. 435, pp. 1214-1217, 2005.

[4] D.-H. Kim, E. A. Rozhkova, I. V. Ulasov, S. D. Bader, T. Rajh, M. S. Lesniak et V.

Novosad, «Biofunctionnalized magnetic-vortex microdiscs for targeted cancer-cell destruction» *Nature Materials,* vol. 9, p. 165–171, 2010.

[5] T. Courcier, H. Joisten, P. Sabon, S. Leulmi, T. Dietsch, J. Faure-Vincent, S. Auffret et B. Dieny, «Tumbling motion yielding fast displacements of synthetic antiferromagnetic nanoparticles for biological applications», *Applied Physics Letters,* vol. 99, n°19, 2011.

[6] A. Verma et F. Stellacci, «Effect of surface Properties on Nanoparticle-Cell Interactions», *Small,* vol. 6, n°11, p. 12–21, 2010.

[7] A. E. Nel, . L. Mädler, D. Velegol, T. Xia, E. M. V. Hoek, P. Somasundaran, F. Klaessig, V. Castranova et M. Thompson, «Understanding biophysicochemical interactions at the nano–bio interface», *Nature Materials,* vol. 8, pp. 543-557, 2009.

[8] W. Jiang, B. Y. S. Kim, J. T. Rutka et W. C. W. Chan, «Nanoparticle-mediated cellular response is size-dependent», *Nature Nanotechnology,* vol. 3, pp. 154-150, 2008.

[9] M. Mahmoudi, S. Sant, B. Wang, S. Laurent et T. Sen, «Superparamagnetic iron oxide nanoparticles (SPIONs): Development, surface modification and applications in chemotherapy», *Advanced Drug Delivery Reviews,* vol. 63, n°11-2, pp. 24-46, 2011.

[10] S. Yoffe, T. Leshuk, P. Everett et F. Gu, «Superparamagnetic iron oxide nanoparticles (SPIONs): synthesis and surface modification techniques for use with MRI and other biomedical applications», *Current Pharmaceutical Design,* vol. 19, n°13, pp. 493-509, 2013.

[11] S. Hasany, N. Abdurahman, A. Sunarti et R. Jose, «Magnetic iron oxide nanoparticles: chemical synthesis and applications review», *Current Nanoscience,* vol. 9, pp. 561-575, 2013.

[12] W. Hu, R. J. Wilson, A. Koh, A. Fu, A. Z. Faranesh, C. M. Earhart, S. J. Osterfeld, S.-J. Han, L. Xu, S. Guccione, R. Sinclair et S. X. Wang, «High-Moment Antiferromagnetic Nanoparticles with tunable Magnetic Properties», *Advanced Materials,* pp. 1479-1483, 2008.

[13] B. Dieny, P. Sabon et H. Joisten, «Microscale or nanoscale magnetic tweezers and process for fabricating such tweezers»,. FR, US Brevet WO2012017024 A1, 04 08 2010.

[14] F. Himpsel, J. Ortega, G. Mankey et R. Willis, «Magnetic nanostructures», *Advances in Physics,* vol. 47, n°14, pp. 511-597, 1998.

[15] K. M. Krishnan, A. B. Pakhomov, Y. Bao, P. Blomqvist, Y. Chun, M. Gonzales, K. Griffin, X. Ji et B. K. Roberts, «Nanomagnetism and spin electronics- materials, microstructure and novel properties», *Journal of Materials Science,* vol. 41, n°13, p. 793–815, 2006.

[16] J.-J. Lee, K. J. Jeong, M. Hashimoto, A. H. Kwon, A. Rwei, S. A. Shankarappa, J. H. Tsui et D. S. Kohane, «Synthetic Ligand-Coated Magnetic Nanoparticles for Microfluidic Bacterial Separation from Blood», *Nano Letters,* vol. 14, pp. 1-5, 2014.

[17] S. K. Suh, K. Yuet, D. K. Hwang, K. W. Bong, P. S. Doyle et T. A. Hatton, «Synthesis of Nonspherical Superparamagnetic Particles: In Situ Coprecipitation of Magnetic Nanoparticles in Microgels Prepared by Stop-Flow Lithography», *Journal of the American Chemical Society,* vol. 134, p. 7337−73, 2012.

[18] H. Nguyen Hoang, L. Nguyen Hoang, C. Nguyen et T. Ngo Quy, «Preparation of magnetic nanoparticles embedded in polystyrene microspheres», *Journal of Physics: Conference Series,* vol. 187, n°1012009, 2009.

[19] F. C. Fonseca, G. F. Goya, R. F. Jardim, R. Muccillo, N. L. V. Carreno, E. Longo et E. R. Leite, «Superparamagnetism and magnetic properties of Ni nanoparticles embedded in SiO_2», *Physical Review B,* vol. 66, n°1104406, 2002.

[20] B. D. Gates , Q. Xu, M. Stewart, D. Ryan, C. G. Willson et G. M. Whitesides, «New Approaches to Nanofabrication: Molding, Printing, and Other Techniques», *Chemical Reviews,* vol. 105, n°14, p. 1171–1196, 2005.

[21] E. A. Vitol, V. Novosad et E. A. Rozhkova, «Microfabricated magnetic structures for future medicine: from sensors to cell actuators», *Nanomedicine (Lond),* vol. 7, n°110, pp. 1611-24, 2012.

[22] D. Canelas, K. Herlihy et J. DeSimone, «Top-Down Particle Fabrication Control of Size and Shape for Diagnostic Imaging and Drug Delivery», *Interdisciplinary Reviews Nanomedecine and Nanobiotechnology,* vol. 4, pp. 391-404, 2009.

[23] H. Joisten, T. Courcier, P. Balint, P. Sabon, J. Faure-Vincent, S. Auffret et B. Dieny, «Self-polarization phenomenon and control of dispersion of synthetic antiferromagnetic nanoparticules for biological applications», *Applied Physics Letters,* vol. 97, n°1253112, 2010.

[24] K. Wilson, L. Harris, J. Goff, J. Riffle et J. Dailey, «A generalized method for magnetite nanoparticle steric stabilization utilizing block copolymers containing carboxylic acids», *European cells and Materials,* vol. 3, n°1Suppl.2, pp. 206-20, 2002.

[25] F. Elaissari Abdelhamid (Lyons, F. Pichot Christian (Corbas, F. Mandrand Bernard (Villeurbanne et F. Sauzedde Florence (Lyons, «Superparamagnetic monodisperse particles»,. US Brevet 6,133,047, 15 01 1998.

[26] A. Hütten, D. Sudfeld, I. Ennen, G. Reiss, K. Wojczykowski et P. Jutzi, «Ferromagnetic FeCo nanoparticles for biotechnology», *2005,* vol. 293, p. 93–101, Journal of Magnetism

and Magnetic Materials.

[27] R. Asmatulua, M. A. Zalich, R. O. Claus et J. S. Riffle, «Synthesis, characterization and targeting of biodegradable magnetic nanocomposite particles by external magnetic fields», *Journal of Magnetism and Magnetic Materials,* vol. 292, p. 108–119, 2005.

[28] S. X. Wang, R. J. Wilson et W. Hu, «Synthetic antiferromagnetic nanoparticles»,. US Brevet 20080206891, 16 08 2007.

[29] W. Hu, R. J. Wilson, A. Koh, A. Fu, A. Z. Faranesh, C. M. Earhart, S. J. Osterfeld, S.-J. Han, L. Xu, S. Guccione, s, R. Sinclair et S. X. Wang, «High-Moment Antiferromagnetic Nanoparticles with tunable Magnetic Properties», *Advanced Materials,* vol. 20, n°18, pp. 1479-1483, 2008.

[30] A. Fu, W. Hu, L. Xu, R. J. Wilson, H. Yu, S. J. Osterfeld, S. S. Gambhir et S. X. Wang, «Protein-Functionalized Synthetic Antiferromagnetic Nanoparticles for Biomolecule Detection and Magnetic Manipulation», *Angew Chem Int Ed Engl.,* vol. 48, n°19, pp. 1620-4, 2009.

[31] S. Leulmi, H. Joisten, T. Dietsch, C. Iss, M. Morcrette, S. Auffret, P. Sabon et B. Dieny, «Comparison of dispersion and actuation properties of vortex and synthetic antiferromagnetic particles for biotechnological applications», *Applied Physics Letters,* vol. 103, n°1132412, 2013.

[32] S. Leulmi-Pichot, *Destruction de cellules cancéreuses par vibrations magnéto-mécaniques de micro/nano particules magnétiques: Elaboration des particules par approche top-down, biofonctionnalisation et tests in vitro,* Grenoble: Thesis manuscript, 2014.

[33] K. Okawa, M. Sekine, M. Maeda, M. Tada, M. Abe, N. Matsushita, K. Nishio et H. Handa, «Heating ability of magnetite nanobeads with various sizes for magnetic hyperthermia at 120 kHz, a non-invasive frequency», *2006,* vol. 99, n°18, p. 08H102, Journal of Applied Physics.

[34] K. Houston, A. Sieber, C. Eder, O. Tonet, A. Menciassi et P. Dario, «Novel Haptic Tool and Input Device for Real Time Bilateral Biomanipulation addressing Endoscopic Surgery», chez *Proceedings of the 29th Annual International Conference of the IEEE EMBS*, Lyon, 2007.

[35] J. Berthelot, S. S. Aćimović, M. L. Juan, M. P. Kreuzer, J. Renger et R. Quidant, «Three-dimensional manipulation with scanning near-field optical nanotweezers», *Nature Nanotechnology,* vol. 9, pp. 295-9, 2014.

[36] F. Beyeler, A. Neild, S. Oberti, D. J. Bell, Y. Sun, J. Dual et B. J. Nelson, «Monolithically

fabricated microgripper with integrated force sensor for manipulating microobjects and biological cells aligned in an ultrasonic field», *Journal of Microelectromechanical Systems,* vol. 16, n°11, pp. 7-15, 2007.

[37] N. Chronis et L. P. Lee, «Electrothermally Activated SU-8 Microgripper for Single Cell Manipulation in Solution», *Journal of Microelectromechanical Systems,* vol. 14, n°14, pp. 857-63, 2005.

[38] C. Yamahata, D. Collard, B. Legrand, T. Takekawa, M. Kumemura, G. Hashiguchi et H. Fujita, «Silicon Nanotweezers With Subnanometer Resolution for the Micromanipulation of Biomolecules», *Journal of Microelectromechanical Systems,* vol. 17, n°13, pp. 623-31, 2008.

[39] K. Kim, X. Liu, Y. Zhang et Y. Sun, «Nanonewton force-controlled manipulation of biological cells using a monolithic MEMS microgripper with two-axis force feedback», *Journal of Micromechanics and Microengineering,* vol. 18, n°1055013 (8pp), 2008.

[40] B. K. Chen, Y. Zhang, D. D. Perovic et Y. Sun, «MEMS microgrippers with thin gripping tips», *Journal of Micromechanics and Microengineering,* vol. 21, n°1105004 (5pp), 2011.

[41] H. Zhang et K.-K. Liu, «Optical tweezers for single cells», *Journal of the Royal Society Interface,* vol. 5, n°124, p. 671–690, 2008.

[42] S. Yamanaka, F. M. Selaru, E. Gultepe, J. S. Randhawa, S. Kadam, E. Shin, A. Kalloo et D. H. Gracias, «Biopsy with Thermally-Responsive Untethered Microtools», *Advanced Materials,* vol. 25, p. 514–519, 2013.

[43] A. Celedon, I. M. Nodelman, B. Wildt, R. Dewan, P. Searson, D. Wirtz, G. D. Bowman et S. X. Sun, «Magnetic Tweezers Measurement of Single Molecule Torque», *Nano Letters,* vol. 9, n°14, pp. 1720-25, 2009.

[44] I. D. Vlaminck, T. Henighan, M. T. van Loenhout, I. Pfeiffer, J. Huijts, J. W. J. Kerssemakers, A. J. Katan, A. van Langen-Suurling, E. van der Drift, C. Wyman et C. Dekker, «Highly Parallel Magnetic Tweezers by Targeted DNA Tethering», *Nano Letters,* vol. 11, p. 5489–5493, 2011.

[45] J. S. Randhawa, T. G. Leong, N. Bassik, B. R. Benson, M. T. Jochmans et D. H. Gracias, «Pick-and-Place Using Chemically Actuated Microgrippers», *Journal of the American Chemical Society,* vol. 130, n°151, p. 17238–17239, 2008.

[46] C. J. Morris, K. E. Laflin, W. A. Churaman, C. R. Becker, L. J. Currano et D. H. Gracias, «Initiation of nanoporous energetic silicon by optically-triggered, residual stress powered microactuators», chez *IEEE 25th International Conference on Micro Electro Mechanical Systems (MEMS)*, 2012.

[47] D. Ciudad, C. Aroca, M. Sánchez, E. Lopez et P. Sánchez, «Modeling and fabrication of a MEMS magnetostatic magnetic sensor», *Sensors & Actuator A,* vol. 115, pp. 408-416, 2004.

[48] H.-T. Su, T.-L. Tang et W. Fang, «A novel underwater actuator driven by magnetization repulsion/attraction», chez *IEEE 22nd International Conference on Micro Electro Mechanical Systems*, 2009.

[49] G. Paumier, P. Ronan, NIH, A. Jan Fijałkowski, J. Walker, M. D. Jones, . T. Heal, M. Ruiz, S. P. (National Center for Biotechnology Information), Liquid_2003 et Arne Nordmann & The Tango! Desktop Project, «Comparison of various biological assemblies and technological devices», Wikimedia, 5 July 2008. [Online]. Available: http://commons.wikimedia.org/wiki/File:Biological_and_technological_scales_compared-en.svg.

[50] M. M. Ali, C. H. Marrows, M. Al-Jawad, B. J. Hickey, A. Misra, U. Nowak et K. D. Usadel, «Antiferromagnetic layer thickness dependence of the IrMn/Co exchange bias system», *Phys. Rev. B,* vol. 68, n°121, 2003.

[51] S. G. E. te Velthuis, J. S. Jiang, S. D. Bader et G. P. Felcher, «Spin Flop Transition in a Finite Antiferromagnetic Superlattice: Evolution of the Magnetic Structure», *Physical Review Letters,* vol. 89, 2002.

[52] B. Kozissnik, A. C. Bohorquez, J. Dobson et C. Rinaldi, «Magnetic fluid hyperthermia Advances, challenges, and opportunity», *International Journal of Hyperthermia,* vol. 29, n°18, pp. 706-14, 2013.

[53] P. Tseng, J. W. Judy et D. Di Carlo, «Magnetic nanoparticle-mediated massively parallel mechanical modulation of single-cell behavior», *Nature Methods,* vol. 9, n°111, p. 1113–1119, 2012.

[54] T. G. Kuznetsova, M. N. Starodubtseva, N. I. Yegorenkov, S. A. Chizhik et R. I. Zhdanov, «Atomic force microscopy probing of cell elasticity», *Micron,* vol. 38, pp. 842-833, 2007.

[55] B. Geiger, J. P. Spatz et A. D. Bershadsky, «Environmental sensing through focal adhesions», *Nature Reviews Molecular Cell Biology,* vol. 10, pp. 21-33, 2009.

[56] E. Gultepe, J. S. Randhawa, S. Kadam, S. Yamanaka, F. M. Selaru, E. J. Shin, A. N. Kalloo et D. H. Gracias, «Biopsy with Thermally-Responsive Untethered Microtools», *Advanced Materials,* vol. 25, p. 514–519, 2013.

2 Micro/nano-tweezers general description

The micro/nano-tweezers presented in this study are the first of their kind, so their design and development started from scratch. The purpose of this work is to set the cornerstones of the tweezers elaboration and actuation with a simple model. After a first proof of concept, it will be possible to refine their design. Thus, the project started with a simple and robust structure, protected by a patent, which could be built by the means of microelectronic fabrication technics.

As pictured in ***Figure 9***, the tweezers are made of two evaporated jaws, one being magnetically soft, whereas the other can be soft, hard or non-magnetic. They are held apart by a metallic hinge evaporated on one of their side. The hinge flexibility is one of the key features of the tweezers actuation. Therefore, its material and dimensions need to be chosen carefully to meet technological requirements with expectations on their mechanical properties. Idem for the jaws, whose size and shape are as determinant for their magnetic state as their constitutive material.

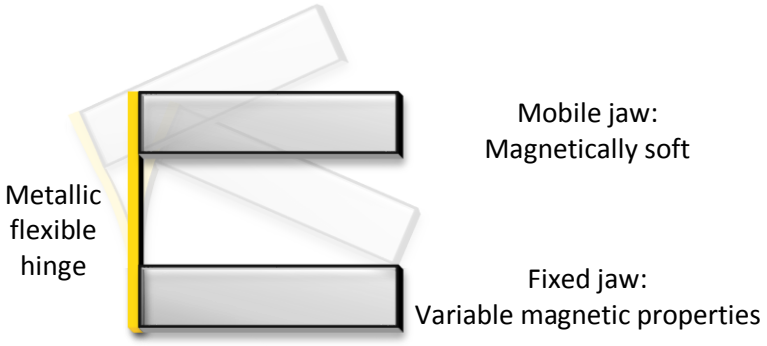

Figure 9*: Design of a technologically feasible tweezer. The upper jaw is mobile and magnetically soft, while the lower one is fixed to the substrate (in a later stage, one could consider releasing the tweezer from the substrate but this has not been done in the framework of this thesis). The latter can be made of a non-magnetic material, a soft magnetic material or a hard magnetic material. The flexible hinge binding the jaws together will be an evaporated metallic layer.*

The conception of the jaws will be addressed first in section **2.1**. The choice of geometry, dimensions and materials for the three types of jaws (non-magnetic, soft and

hard) will be explained in detail. The attractive or repulsive nature and the force of the interaction between the two magnetic jaws depend on their respective magnetic state. Therefore, the micromagnetic structure and dynamic of soft jaws will be described to formulate the main hypotheses on which subsequent calculations will be based. Finally, the description and a preliminary estimation of the magnetic forces behind the tweezers actuation will be provided.

The hinge design is then given in part **2.2**. The choice of its constitutive material was made in the perspective of optimizing its mechanical response to the jaws motion under magnetic forces. Its stiffness will be evaluated to predict the amplitude of the tweezers opening.

However, at such submicronic dimensions the jaws could also be exposed to physical microforces (van der Waals, Casimir, etc...), which could have a non-negligible impact on the tweezers behavior. Therefore, the order of magnitude of the forces potentially involved will be estimated in section **2.3** and compared to verify if the magneto-elastic forces are indeed dominant.

2.1 Jaws design

2.1.1 Materials selection

Since the fabrication process of the tweezers represents a challenging part of the overall work, materials and fabrication technics were selected as simple as possible to limit the complexity of this fabrication.

The fabrication of three types of tweezers is intended (“soft/soft”, “soft/hard” and “soft/non-magnetic” tweezers), so three different materials need to be selected.

Regarding the non-magnetic jaws, Chromium was selected among the available materials for its availability in our evaporation units and relatively straightforward growth properties.

To make a hard magnetic jaw, a permanent magnet material must be used. Compared to the soft jaws, the hard magnet magnetization must remain stable while the magnetization of the soft jaw reverses under the application of an external magnetic field.

Among the materials presented in the introduction, Neodymium-Iron-Boron (NdFeB) has the strongest coercivity (670 to 750 $kA.m^{-1}$) so it was selected for the theoretical calculations. As the NdFeB deposition requires a specific process, the first technological realizations of soft/hard tweezers were made using exchange biased multilayers i.e. multilayers in which antiferromagnetic layers (in Iridium-Manganese) alternated with ferromagnetic layers (in Cobalt) (see chapter **4**, section **4.2.1**).

Concerning the soft jaws, more parameters should be considered. Actually, the main criterions to make a choice are, ranked by importance: a) a low coercivity for an easy magnetization reversal under an applied field, b) a high permeability or susceptibility to reach saturation faster and c) a high magnetization value at saturation to enhance magnetostatic interactions between the jaws.

Among the very soft materials listed in the introduction, only NiFe was available in the evaporators at the beginning of this study. And for good reason, Permalloy (80 % Nickel, 20 % Iron) is the most commonly used soft ferromagnetic material in microelectronics. Indeed, it is easy to deposit in the form of thin film form by sputtering or evaporation and it is quite resistant to corrosion. This means that its quality is almost independent from the provider and ensures constant properties over long period of time. Furthermore, NiFe has the great advantage to exhibit no magnetostriction, *i.e.* its magnetic properties are not sensitive to uncontrolled strain in the samples, besides being stable with temperature. As a comparison, FeCoB, a soft material with higher saturation magnetization than Permalloy, is very sensitive to annealing, even in zero applied field. A good control of the jaws magnetic properties is highly preferable for the beginning of the study to facilitate preliminary characterization. Therefore, even if Permalloy has a rather low magnetization at saturation (8.10^5 $A.m^{-1}$ [1]) compared to other materials like Fe and Co, it was selected as constituent of the soft jaws.

It is not bad as a starter, since the NiFe coercive field is extremely low: 80-160 $A.m^{-1}$ (1-2 Oe in CGS units). In addition, Permalloy saturation field, for which magnetic saturation is reached, is only 800 $A.m^{-1}$ (10 Oe) for the bulk material.

Regarding biocompatibility, Permalloy is not a perfect candidate, not to mention NdFeB, Co or IrMn. However, the risk of cytotoxicity is rather low as long as the tweezers are kept attached to their substrate while put in contact with living biological samples. For reinforced precautions, the tweezers surface can be chemically passivated.

For *in vitro* or *in vivo* applications of tweezers released in solution, the fabrication process can be adapted to replace Permalloy by magnetite, a ferromagnetic material considered as biocompatible. This will not be carried out in the frame of this work.

The magnetic properties of ferromagnetic particles also depend strongly on their sizes and geometry for magnetostatic reasons. In this study, we focused on square shaped jaws, which represent a good trade-off between technological difficulties and expected magnetic properties. Indeed, an interesting magnetic configuration for soft jaws would be the vortex structure (more details given in section **2.1.2**) but round dots are more difficult to bind by a hinge than rectangular dots and vortex state can also be generated in square dots. In this thesis, the tweezers were patterned by photolithography to size of the order of 2 µm. If further miniaturization appears to be required, photolithography can be replaced by nano-imprint or electron beam lithography.

The magnetic jaws thickness was set at 200 nm to begin with, as a compromise between the maximization of the magnetic volume to ensure stronger magnetostatic interactions under applied magnetic fields and the proper adhesion of the magnetic metallic layer during its deposition process.

2.1.2 Micromagnetism of magnetic soft jaws

Since the “hard” jaws are considered as permanent magnets and thus endowed with a fixed, monodomain magnetization, this section only focuses on “soft” jaws in Permalloy, whose magnetic response versus field is more complex due to their micromagnetic behavior. Indeed, the magnetic state of a magnetic micro- or nano-structure is determined by the balance between various energy terms (mostly magnetostatic, exchange, and Zeeman as will be detailed further). Among the various possible magnetic configurations, the one which minimizes the total energy is favored.

Magnetic force microscopy (MFM) measurements were performed on tweezers composed of two jaws in Permalloy and revealed a vortex-like magnetic structure (***Figure 10***). Magnetic vortices occur in ferromagnetic disks and are characterized by an in-plane magnetization rotating around a small core with out-of-plane magnetization located in the center of the disk (or sometime pinned on a defect). When the sample is not a disk but square-like, it adopts a configuration hybrid between the vortex in disks and the Landau structure in rectangles [2]. The development of 90° domain walls, regions where the magnetization rotates, dividing the volume in four domains is highlighted by the contrasts in the MFM image below.

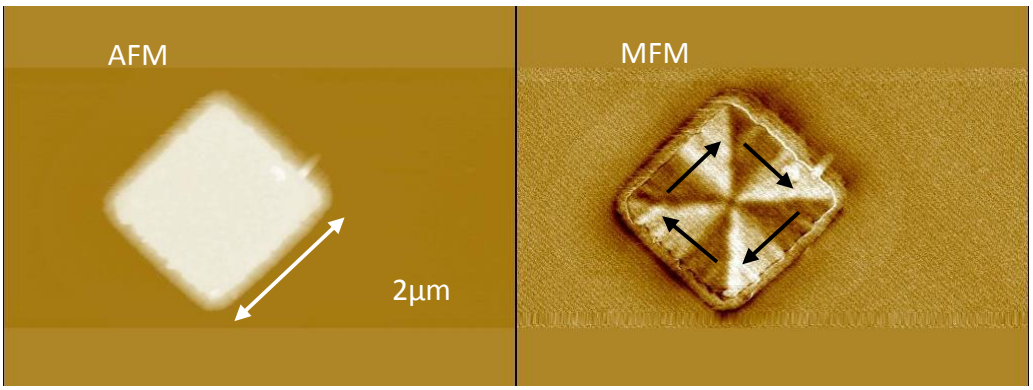

Figure 10*: Atomic force microscopy images of a soft/soft tweezer of 2x2 µm² with Permalloy jaws of 100 nm thick: topography on the left and magnetic field on the right. The upper jaw exhibits a perfect vortex-like structure (black arrows indicate the magnetization direction).*

Like the shape, the size of a sample has also a strong influence on its magnetic structure, for a given material. Particles smaller than a domain wall width (around 100 to 300 nm in Permalloy [3]) are usually composed of a single domain, so-called a monodomain. The apparition of domains in larger samples, when no external field is applied, is due to the magnetostatic energy minimization. It aims at closing the demagnetizing flux and preventing it as much as possible from leaking out of the sample. However, the creation of domain walls has a cost as it increases the exchange energy. Indeed, this energy due to interactions between closest neighbor atomic moments favors

parallel magnetic alignment in ferromagnetic materials. The energy locally increases within domain walls due to the presence of magnetization gradients.

This balance between magnetostatic and exchange energies restricts the apparition of vortex structure to disk with intermediate size and weak magnetocrystalline anisotropy [4]. As shown in ***Figure 11***, the aspect ratio is also determinant for the vortex stability.

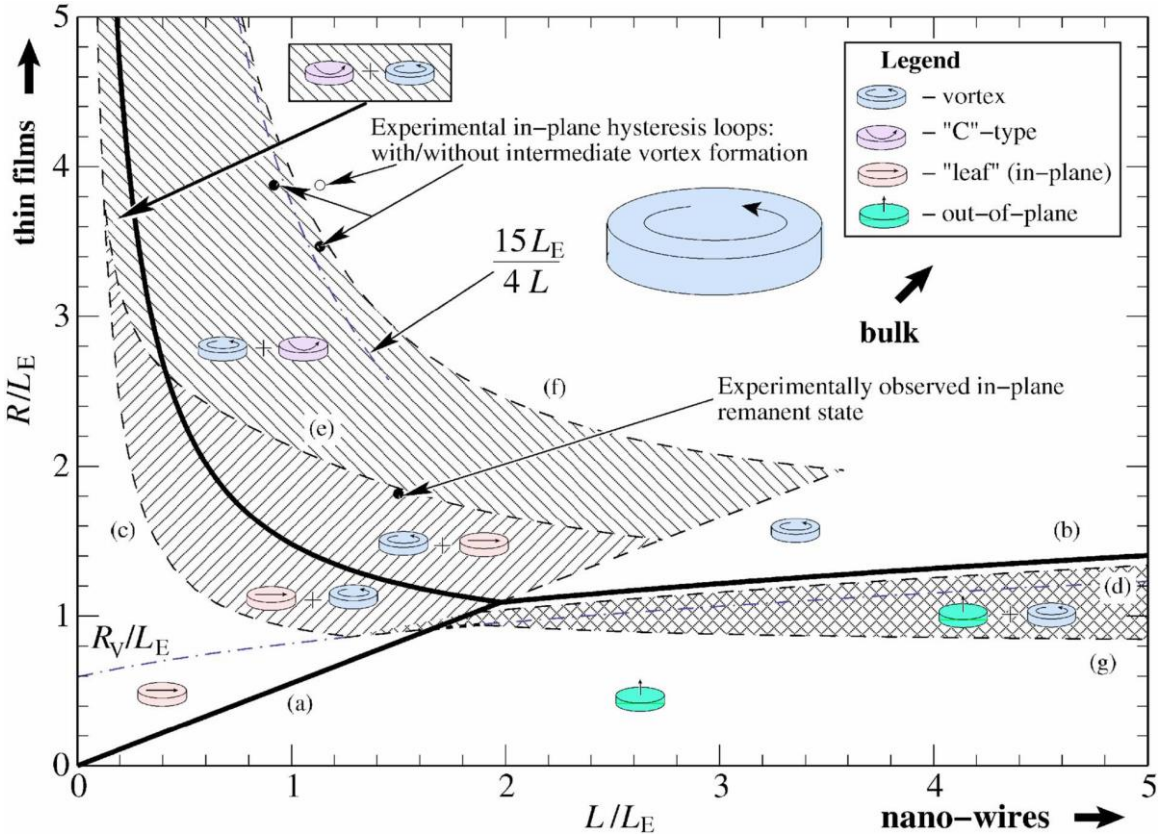

Figure 11*: Map of metastable circular nanocylinders. Solid lines represent the equality of the equilibrium energies of the bordering ground states. Dashed lines correspond to the stability loss. More than one state _represented by symbols with arrows_ can be stable in the shaded regions. The leftmost in each group of symbols indicates the ground state. The formula gives the asymptotic to the C-vortex transition line, and the other dash-dotted line is the equilibrium radius of the vortex core. Image and legend extracted from the reference [4]. L is the particle thickness, R its radius and L_E the exchange length.*

The map above gives the regions of stability of the magnetic states available for ferromagnetic nanocylinders depending on their aspect ratio. As expected, out-of-plane magnetization occurs in rather thick samples wherein the thickness is larger than the diameter, whereas in-plane configuration occurs in thinner samples due to their easy-plane shape anisotropy.

Regarding the tweezers, in-plane magnetization is preferable for their actuation. For the magnetic torque applied on the jaws magnetization to produce a mechanical torque, the magnetization must have some anisotropy. It cannot be allowed to rotate in any direction without energy cost. Otherwise, the magnetization may rotate out-of-plane without inducing any mechanical torque and thus no opening.

There is a critical aspect ratio (thickness/radius) below which in-plane magnetization is more stable than out-of-plane magnetization. For ferromagnetic disks, the ratio between the disk thickness L and its radius R should be below this critical value to ensure in-plane magnetization: $L/R \ll 1.81$ [4, 5]. In our experiments, the tweezers jaws aspect ratio is about 0.18, so their magnetic actuation *via* the application of an external field or magnetostatic mutual repulsion should be possible.

When submitted to an external field, the Zeeman energy tends to align every magnetic moment along the applied field. As a consequence, the vortex core is progressively shifted in a direction transverse to the applied field. Such vortex displacement depends linearly with the applied field (***Figure 12***). When the magnetic field reaches the annihilation field, the vortex vanishes completely and the sample stabilizes in the saturated monodomain state.

At saturation, the Zeeman energy is minimized but the magnetostatic energy is maximized, leading to strong emission of demagnetizing field. Regarding the tweezers, this means greater magnetostatic interactions between the two magnetic jaws.

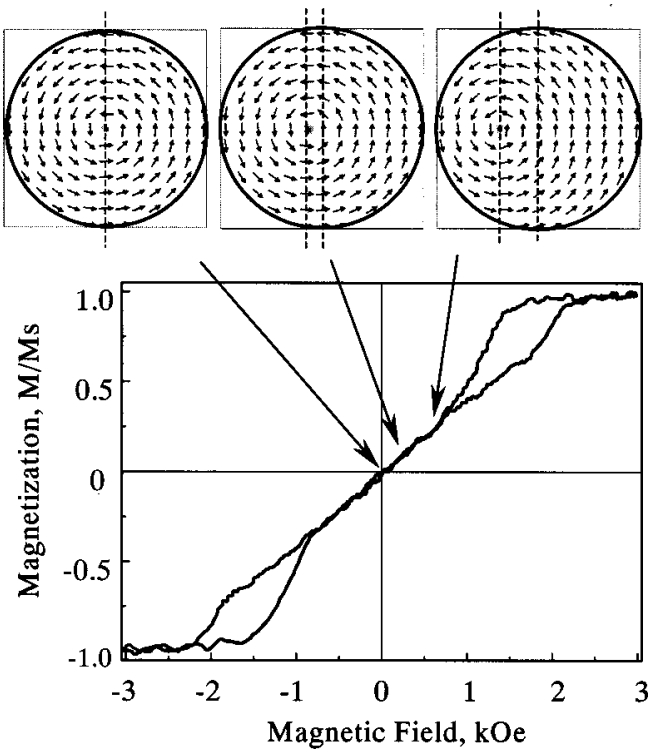

***Figure 12**: Measured hysteresis loop and calculated field evolution of magnetic vortex for Permalloy disk with diameter 0.2 µm and thickness 60 nm. Image and legend extracted from reference [5].*

Guslienko *et al.* [5] showed that the slope of the linear part of hysteresis loop is size-dependent. This slope represents the magnetic susceptibility χ of the ferromagnetic disks in polycrystalline NiFe. The team determined its dependence on the aspect ratio $\beta = L/R$, with (L is the disk thickness and R its radius):

$$\chi^{-1} = 2\beta[\ln 8/\beta - 1/2] \quad (1)$$

As a comparison, VSM (Vibrating Sample Magnetometer) measurements were performed on square NiFe particles with comparable dimensions, developed by Spintec and dedicated for biological applications [6]. These particles exhibit vortex-like cycles with a quasi-linear response to the applied field until magnetic saturation (***Figure 13***).

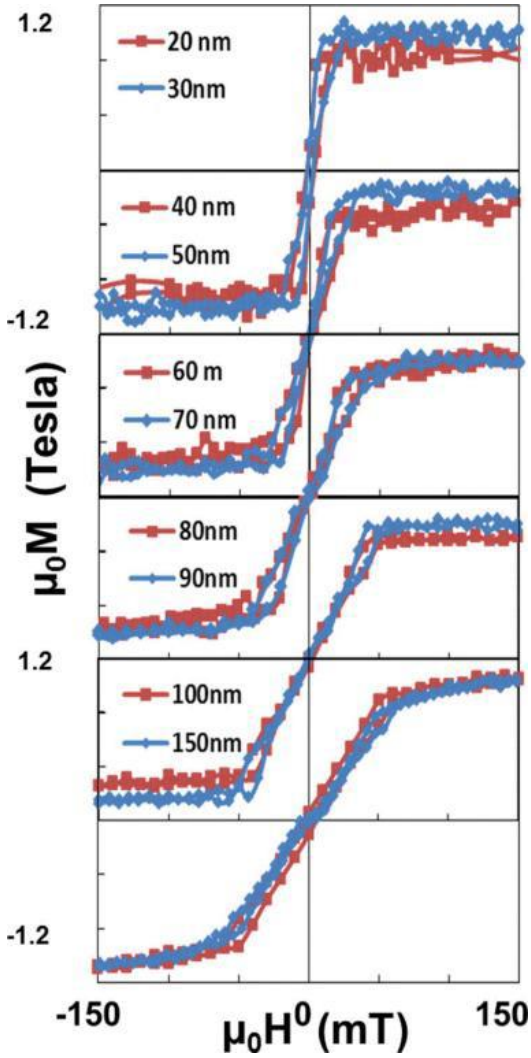

***Figure 13**: Hysteresis cycles of an array of micro-vortex particles in Permalloy fixed to a silicon substrate. These VSM measurements were performed on particles of 1.3 µm in size for varying thicknesses (from 20 nm to 150 nm). The magnetization shows a linear response to the applied field when |H|<60 mT and a plateau elsewhere.*

In addition, these curves reveal a very low coercivity, like in ***Figure 12***. This is characteristic of low magnetocrystalline anisotropy and ensures an easy magnetization reversal, which is essential to benefit from the magnetostatic interactions between the two magnetic jaws to control the jaws opening/closing. In particular, when a soft jaw and a hard one are put together, both parallel (open) and antiparallel (close) magnetization configurations are available due to the soft jaw magnetization reversal while the hard magnetization remains unchanged.

To conclude, these results indicate that the magnetic configuration observed in the square magnetic structures that we used as jaws can be assimilated to vortex configuration. Therefore, in the theoretical calculations aiming at predicting the tweezers behavior under magnetic field (chapter **3**), the jaws are considered to behave like vortices. Thus, the following main hypotheses are made:

a linear and reversible response to an applied field. The saturation field of soft jaws is set at about 0.1 T, like particles with an aspect ratio close to our jaws (***Figure 13***).

the magnetization remains confined in the plane of the jaw (the influence of the out-of-plane magnetized vortex core can be neglected considering on one hand the dimension of our jaws (around 2 µm) and on the other hand the size of this vortex core which is the exchange length of the order of 5 nm in Permalloy).

2.1.3 Upper jaw motion due to magnetic torques

This section aims at calculating the magnetic torque exerted on the micro/nano-tweezers upper jaw and determining its order of magnitude. Three torque terms determine the motion of the upper jaw with respect to the fixed lower jaw. i) The first one is the Zeeman coupling between the magnetic moment of the magnetically soft upper jaw and the applied field; ii) the second one is the magnetostatic interaction between the two magnetic jaws. Of course, this second torque term does not exist when the bottom fixed jaw is non-magnetic. These tweezers made of only one magnetic jaw (soft/non-magnetic tweezers) can be used to highlight the role actually played by the magnetostatic interactions in tweezers made of two magnetic jaws (soft/soft and soft/hard). iii) These two magnetic torque terms are balanced by the mechanical torque exerted by the hinge on the top jaw. The equilibrium position is reached when the three torque terms balance each other.

The magnetostatic interaction between the two magnetic jaws is due to the mutual influence of the stray magnetic field created by each jaw on the magnetization of the other one. At remanence (zero field), these soft jaws adopt a vortex configuration and as a result do not emit any field. However, under the application of a magnetic field, the Zeeman energy gradually overcomes the other energy terms (exchange, magnetostatic), leading to

an increase of the net magnetization, and eventually annihilation of the vortex configuration and saturation, resulting in a monodomain configuration. Correlatively, the stray field emitted by the jaw increases. When two magnetized soft jaws are put in close proximity, their magnetization mutually influence each other *via* their magnetostatic stray field.

Concerning soft/hard tweezers, the magnetostatic interactions depend less on the applied field since the hard jaws are assumed to be made of permanent magnets *i.e.* having a fixed magnetization. Therefore, hard jaws create a stray field even at remanence. The torque they exert on the upper jaw can be attractive or repulsive depending on the applied field. Indeed, when one jaw is made of a hard magnetic material, the magnetization of the soft jaw can align antiparallel to the hard one at low magnetic field, generating an attractive torque between the two jaws. In contrast, when the applied field exceeds the stray field created by the hard jaw on the soft one, the magnetization of the soft jaw reverses and the torque becomes repulsive. This contrasts well with the behavior of soft/soft tweezers, at least in the case where the two jaws have similar thicknesses. In this case, the two soft jaws get polarized by the applied field in a similar way so that they exert a repulsive torque on each other. When the field is large enough so that the two soft jaws reach magnetic saturation, their mutual repulsion is usually stronger than the one between a hard and a soft jaw due to the saturation magnetization value which differs in the two kinds of jaws. For soft jaws (Permalloy), the saturation magnetization is 8×10^5 A.m^{-1}, while it is of the order of 5.8×10^5 A.m^{-1} in hard jaws (NdFeB).

In ***Figure 14***, numerical simulations (using finite elements method in Flux3D) illustrate the stray fields emitted by the two soft jaws in space. In this example, the stray field lines are represented for a tweezer opening at 45° and assuming the jaws are magnetically saturated. Both jaws are soft and have square geometry, measuring 2 µm of the side and 200 nm of the thickness.

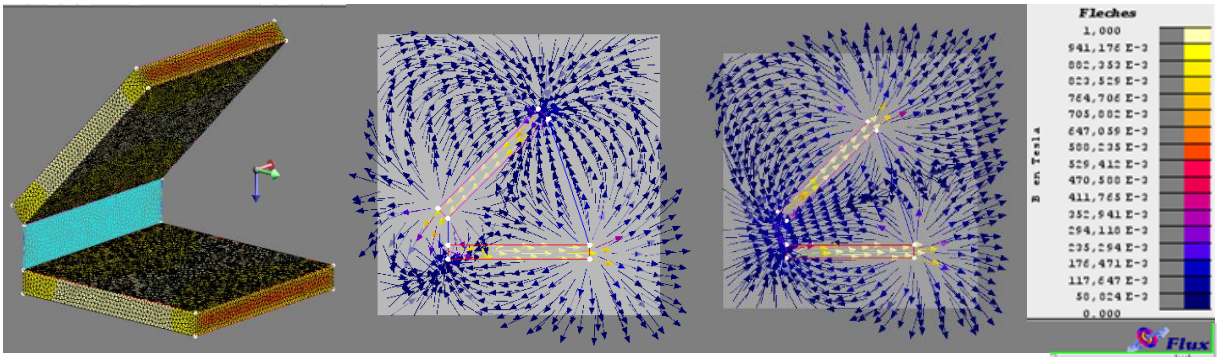

***Figure 14**: Flux3D simulation of a soft/soft tweezer artificially brought at saturation in absence of an applied field. Left: three dimensional sketch of the tweezer. Right: stray field lines spatial distribution for two magnetic orientation of the upper jaw magnetization (middle graph: the magnetization points towards the bottom left corner; right graph: the magnetization of the upper jaw points towards the upper right corner).*

In presence of an applied field of 0.01 T and at 45° with respect to the lower jaw, ***Figure 15*** shows how the same tweezer deflects the field lines depending on its opening angle.

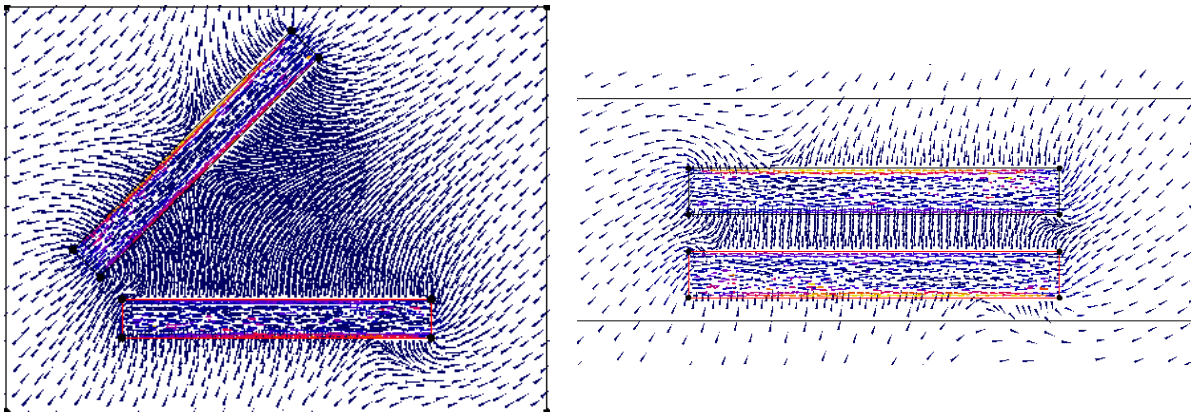

***Figure 15**: Magnetic field lines inside and outside the jaws of a soft/soft tweezer (2x2x0.2 µm^3) when submitted to a uniform magnetic field of 0.014 T, applied at 45°. On the left: tweezer open at 45° (color scale: from dark blue=0 T to yellow=0.84 T), on the right tweezer with parallel jaws (color scale: from dark blue=0 T to yellow=0.5 T).*

The torque exerted on the soft mobile jaw in this situation was also calculated for several angular positions of the upper jaw (from 0° to 90°) in presence of the 0.01 T field applied at 45° above the plane of the bottom jaw. ***Figure 16*** gives the evolution of the torque related to the applied field and stray field from bottom jaw on top jaw versus this

opening angle. Two cases are considered: i) the two jaws are magnetically soft, ii) only the top jaw is magnetic whereas the bottom one is non-magnetic.

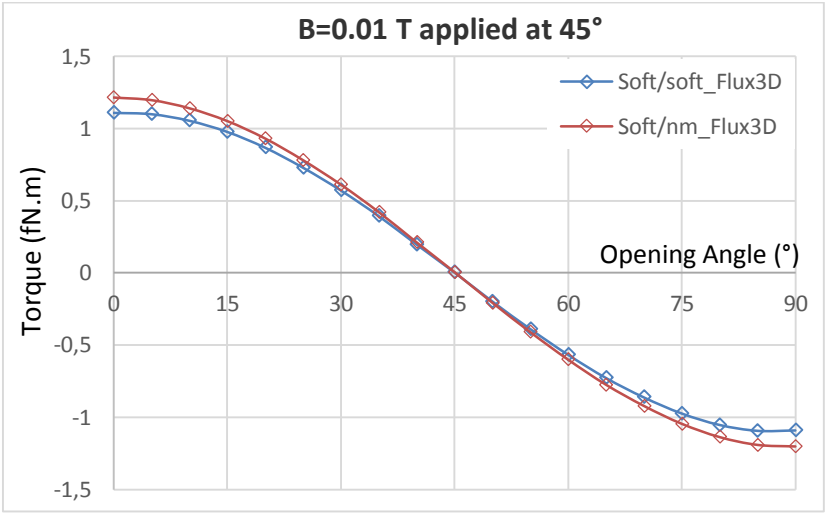

***Figure 16**: Magnetic torque exerted on the upper jaw (magnetically soft) of soft/soft and soft/non-magnetic tweezers according to its angular position, corresponding to the tweezer opening angle. A magnetic field of 0.01 T was applied at 45° with respect to the substrate. In both case, the torque tends to open the tweezer until the latter opens at 45°. At this point, the torque becomes zero since the jaw magnetic moment is aligned with the applied field. If the tweezer opens more, the torque tends to close it back to 45°. Note that the torque is slightly smaller for the soft/soft tweezer than for the soft/non-magnetic tweezer because the stray field from the bottom soft jaw on the top jaw tends to oppose the applied field, resulting in weaker net field acting on the top jaw.*

On this graph, the torque calculated for a soft/non-magnetic tweezer has also been plotted and appears very close to the result of the soft/soft case. The difference between the two cases gives the contribution of the magnetostatic interactions between two magnetic jaws to the total magnetic torque. Here, it appears to be very small (0.1 fN.m) because the applied field is rather weak so that the soft jaws magnetizations are themselves small. As a comparison, the torque exerted by a hard jaw on a soft jaw reaches 28 fN.m at remanence.

The curves plotted in ***Figure 16*** demonstrate clearly that the tweezers actuation is mainly due to the torque exerted by the external magnetic field on the mobile jaw magnetization. Like any magnetic dipole, the upper jaw experiences a magnetic torque

when submitted to a magnetic field $\vec{B}$, which tends to align its dipolar magnetic moment $\vec{m}$ to the field due to Zeeman energy:

$$\vec{\Gamma} = \vec{m} \times \vec{B} \quad (2)$$

The magnetic moment is a function of the jaw magnetization $\vec{M}$ and volume V:

$$\vec{m} = \iiint \vec{M} dV \quad (3)$$

As explained previously, the jaws are supposed to exhibit a linear response to the applied field (vortex-like response), so that their magnetization can be expressed versus the applied field $\vec{H} = \vec{B}/\mu_0$:

$$\vec{M} = \chi^{-1}\vec{H} \quad (4)$$

where χ is the magnetic susceptibility defined in equation (1) for a vortex.

The torque should be maximal when the field is applied at 45° with respect to the mobile jaw orientation. Indeed for an applied field H oriented at an angle φ with respect to the plane of the upper jaw, the magnetization acquired by the upper jaw will vary as the in-plane component of the field, *i.e.* as $H.cos\,\phi$. Correlatively, the torque varies as $H.M.sin\,\phi$, so that the torque is a $cos\,\phi.sin\,\phi$ function of ϕ, which is maximum at 45°. According to equation (1), the saturation field is 0.86 T. Hence, the maximal torque would be of 280 fN.m and the corresponding force exerted on the 2 µm lever arm about 140 nN. These values are quite encouraging and show that the tweezers, even comprising only one magnetic jaw, have good chance to overcome the hinge stiffness. To make sure of this, the hinge will be studied in the next section.

An analytical model was established to better understand the mechanisms occurring during the tweezers opening and to predict their behavior under various conditions. It is explained in chapter 3, section **3.1**.

2.2 Hinge design

2.2.1 Material selection

The hinge mechanical properties are decisive for the tweezer behavior. It should be flexible to let the tweezer open widely, elastic to come back to its initial position after deformation and thus apply a slight restoring force to help the tweezer close back, and also ductile to avoid breaking under plastic deformation.

To this purpose, both polymers and metals were considered. Polymers are flexible and elastic, so a bond between the jaws or even their embedding in a polymer matrix constituted an interesting idea (see more in section **6.2.2** in chapter 6). However, the fabrication process of polymer hinges would be more difficult than that of metal hinges. Indeed, the deposition of a thin metal layer by PVD (Physical Vapor Deposition) is a mastered technic at the PTA (CEA cleanroom) and can be easily implemented in a very reproduce manner. Therefore, the idea of a polymer hinge was kept as a spare option.

Among the metals available in the PTA's evaporators, Aluminum (Al) and Gold (Au) distinguish from the others by their high ductility and elasticity. Gold was chosen over Aluminum because it is noble, biocompatible and usually adheres well to other materials, ensuring a good contact with the jaws. In addition, it can be easily chemically functionalized if necessary. Besides, Aluminum is also the most convenient material for the sacrificial layer used to create the gap between the jaws, which discards the possibility of using it for the hinge.

Gold tensile strength was measured between 260 to 300 MPa [7], while it is 150 MPa for Aluminum [7]. This value defines the limit of the elastic regime of gold (discussed in chapter 3, section **3.2**). The Young modulus of bulk gold was reported to be from 57 to 120 GPa (80 GPa for Al) [7]. In addition, a study showed that the Young modulus of e-beam evaporated gold is 55-62 GPa [8], reported lower than sputtered gold. The mean value of 59 GPa was used for theoretical calculations of the hinge behavior. E-beam evaporation was preferred over sputtering also for its better directionality to ensure the hinge deposition on only one side of the tweezers.

2.2.2 Elastic forces

The jaws motion due to the magnetic torque discussed previously in section **2.1.3** is transferred as a mechanical torque on the hinge (***Figure 17***). Under this load, the hinge bends and undergoes stress and deformations. Its restoring force balances the magnetic torque to reach an equilibrium position. The amplitude of the tweezer opening at equilibrium depends on the hinge stiffness.

To evaluate the order of magnitude of the hinge stiffness, we will assume that it remains in the linearly elastic regime. Such materials are supposed to deform proportionally to the applied load (Hooke's law) and undergo only reversible deformations. Otherwise, beyond a given threshold of stress (yield stress), materials behave plastically and experience non-linear irreversible deformations. Since the hinge is expected to undergo repeated opening and closing of the jaws, it is highly preferable that it stays within its elastic regime. Therefore, the hinge will be assimilated to an elastic beam and the validity of this hypothesis will be discussed in chapter 3, **3.2**.

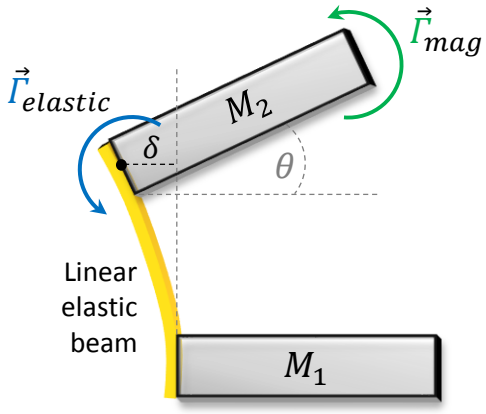

Figure 17*: Sketch of a tweezer illustrating the hinge deflection under the application of an elastic torque due to the jaw motion induced by the magnetic torque.*

According to Euler-Bernoulli elastic beam theory, the relation between the applied torque Γ and the hinge elastic deflection δ is given by [9]:

$$\Gamma = \frac{E\ w\ t^3}{6\ L^2}\ \delta \tag{5}$$

with E the Young modulus of e-beam evaporated Gold (59 GPa), w the width of the hinge (equals the width of the tweezer), t its thickness and L its height. The proportionality

factor between the torque and the deflection is the stiffness constant of the beam according to Hooke's law.

The equivalent relation can be obtained for the angle of deflection and thus the tweezer opening angle θ provided that: $\sin\theta = \delta/2L$ and that for small angles: $\sin\theta \approx \theta$, which is one of the definitions of the elastic linear regime. Thus, the expected opening angle resulting from a given torque application can be deduced for a given set of physical parameters. For example, submitted to the previously estimated maximum magnetic torque of 280 fN.m, a hinge of 2 µm in width, 350 nm in height and thickness of 15 nm, would yield a tweezer opening of 71°. The graph below (***Figure 18***) gives the results of the same calculation for several hinge thicknesses.

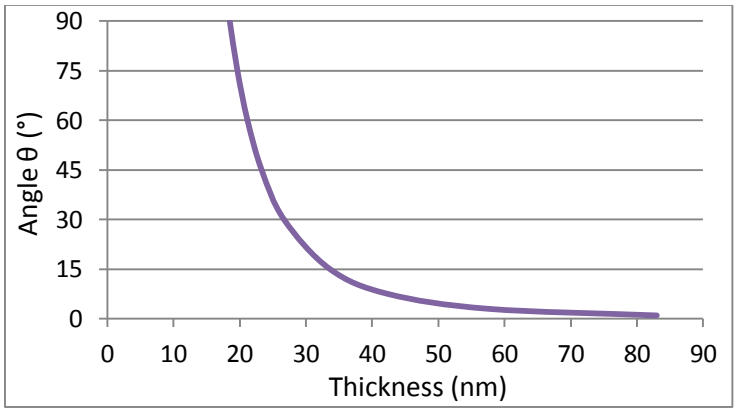

Figure 18*: Opening angle of a tweezer whose upper jaw is submitted to an ideal torque of 280fN.m depending on the hinge thickness.*

Although such a result is very encouraging, this calculation does not take the magnetic torque dependence on distance into account. If it did, the opening angle would be significantly smaller. Moreover, the limit of the elastic regime may be overpassed for thin hinges. To achieve more accurate estimations of the parameters optimizing the tweezer opening, further calculations and numerical modeling were done and presented in chapter 3, section **3.2**.

However, the tendency for the angle to decrease quickly while the thickness of the hinge increases should be realistic and encourages, from a technological point of view, to make hinges as thin as possible.

2.3 Other microscopic forces acting on the jaws

Although the magneto-elastic forces are the main operators of the tweezers actuation, the dimensions of these objects at the boundary between nanoscale and microscale, invite to ponder on the significance of molecular interactions and quantum effects on their behavior. In particular, long-range molecular forces and quantum effects could contribute to the jaws mutual attraction or keep the tweezers closed once contact between the jaws has been established. It appears then crucial to check if these forces can overcome the magnetic force responsible for the tweezers opening. Therefore, this discussion aims at comparing the order of magnitude of the magnetic force responsible for the tweezer opening with all the forces likely to close the tweezers or keep them closed.

For that purpose, the order of magnitude of the Casimir effect and the Van der Waals interactions between the jaws will be estimated and compared to the magneto-elastic forces presented earlier. Gravity can be neglected at these dimensions and electrostatic effect ruled out since the considered system consists of two metallic plates linked by a metallic hinge.

2.3.1 Casimir effect

The Casimir effect, named after the Dutch physicist Hendrik Casimir who predicted it in 1948, is a quantum attractive force between two parallel uncharged conducting plates in vacuum. This effect is remarkable as it is an observable consequence of vacuum quantum fluctuations. Experimental validation of the Casimir effect constituted a real challenge as the first accurate measurement of this force between two plates was achieved after several trials in 2001 only, at the University of Padua (Italy).

The quantum phenomenon at the root of the Casimir effect is vacuum fluctuations. Indeed, in virtue of the wave-particle duality, vacuum possesses a zero-point energy different from zero, around which its energy fluctuates due to Heisenberg's uncertainty principle. These fluctuations, in the manner of gas molecules colliding with a wall, can exert a pressure on a surface.

In the case of two perfectly parallel mirrors, the confinement of the vacuum between the plates leads to the discretization of vacuum energy levels, in the same way as electromagnetic waves are selected by their wavelengths inside a Fabry-Perot cavity. As a consequence, the amount of energy inside the cavity is decreased compared to energy continuum on the outside. This difference of energy results in a motive force that pushes the plates toward each other: the Casimir effect. This force is proportional to the plates surface A and increases drastically when the distance L between the plates decreases:

$$F_{Cas} = \frac{\pi^2 \hbar c}{240\, L^4} A \tag{6}$$

With $\hbar$ the reduced Planck constant, c the speed of light and $A \gg L^2$ [10].

This formula is ideal and was established for perfectly reflecting mirrors. For real mirrors, the Casimir effect depends on frequency, wavevector and polarization of the waves trapped inside the cavity. This situation can be described by a model based on the interaction between surface plasmons from each plate, coupled through vacuum energy [10]. However, to evaluate the order of magnitude of the Casimir effect between the jaws of the micro/nano-tweezers presented in this study, the ideal formula is ample. One could just keep in mind that the force between non-perfectly reflecting mirrors is smaller as it results from a balance between resonant and non-resonant modes (erased in the ideal case) in the cavity. Besides, thermal fluctuations and surface roughness have marginal influence (<1 %) according to reference [10].

In the case of our tweezers, the two parallel metallic particles constituting the jaws are separated by a few hundreds of nanometers and could be affected by this effect. The estimation of the Casimir force for two parallel plates of 2 µm side and separated by 350 nm gives approximately 2 pN, which is at least 2 orders of magnitude smaller than the magnetic repulsion between two magnetic jaws, typically ranging from tenths to tens of nanoNewtons.

However, when the tweezer closes, the distance between the jaws decreases until the jaws extremities enter in contact. Hence, infinitesimal surfaces parallel to each other are brought very close to each other, experiencing a greater Casimir effect (***Figure 19***).

Considering a contact area of 1 % of the jaws total length - so 20 nm-, the length on which the force should be integrated is λ=1.98 µm.

***Figure 19**: The Casimir force between a tweezer jaws is of the order of picoNewtons when they are parallel (left) or closed (right). In comparison, the magnetic force exerted on the upper jaw by an external magnetic field can reach 140 nN.*

The force between two infinitesimal surfaces $dA = wd\lambda$ can be written:

$$dF_{Cas} = \frac{\pi^2 \hbar c}{240} \frac{wd\lambda}{L(\lambda)^4} \tag{7}$$

The distance L is a function of λ multiplied by the slope of the upper jaw with respect to the lower jaw. Integrated on the surfaces measuring 2 µm large and 1.98 µm long, the force is 6 pN, only slightly higher than previously.

Concerning the contact area, its surface A is supposed to be 20 nm by 2 µm. The separation distance can be set at 10 nm, assuming a minimal roughness of the jaws surface. In such an ideal situation, the force could reach tens of nanoNewtons. However, the jaws roughness should be significantly higher due to the polycrystalline growth of Permalloy films, which leads to columnar structures. Given that the jaws are 200 nm thick, the grains curvature can reach about 40 nm, drastically increasing the mean separation distance on which the force depends to the power 4. Moreover, this granularity decreases considerably the occurrence of parallelism between the surfaces, so that the Casimir effect should be most likely negligible in these tweezers.

2.3.2 Van der Waals interactions

The van der Waals forces arise from interactions between uncharged atoms or molecules and play a crucial role in matter cohesion. This universal attractive force (repulsive only in special cases) is relatively weak compared to covalent bonds but has observable effects on macroscopic bodies and is namely responsible for surface tension [11] and adhesion within nanostructures [12].

One can distinguish three different source of van der Waals according to electrostatic nature of the interacting atoms or molecules:

The Keesom force arises from electrostatic interactions between permanent dipoles (molecular ions, polar molecules...). This interaction is rather rare as atoms hardly carry permanent dipole.

The Debye force, or induction, is the interaction between a permanent dipole and an induced dipole. The polar molecule distorts the charge cloud of a neighboring non-polar molecule, which will be temporarily polarized. The induced and permanent dipoles are then mutually attracted.

The weakest interaction is the London force, or dispersion, which occurs between two temporarily induced dipoles. It arises from the electron cloud random fluctuations of all atoms and molecules, which produces oscillating electric field acting upon the polarizability of neighboring atoms or molecules. The resulting shifting of their charges gives them instantaneous dipolar moments and causes mutual attraction.

Except for highly polar materials such as water, the London dispersion gives the largest contribution (70–100 %) to the van der Waals attraction [7]. Indeed, all materials are polarizable, whereas Keesom and Debye forces require permanent dipoles. That's why only London forces will be estimated here and compared to the magneto-elastic torques involved in the tweezers behavior.

When the distance between two dipoles exceeds 10nm, the time for the electric field to make a full loop between them can become comparable to their fluctuation period. In this situation, named retarded regime, the dispersion energy decays faster [13]. Thus, the

London force has more chance to be significant between the parts of the jaws in contact, when the tweezer is closed. That is why, it is evaluated in this particular situation.

The Van der Waals force between to macroscopic bodies was first expressed by Hamaker [14]. Here, between two flat surfaces of surface S separated by a distance d in the non-retarded regime the expression is [7, 11]:

$$F_{vdW}(d) = -\frac{\mathrm{A_H}\, S}{6\pi d^3} \tag{8}$$

where $\mathrm{A_H}$ is the Hamaker constant specific to the two interacting bodies and their medium. In particular, it is typically $4\text{x}10^{-19}$ J for metals in vacuum and water [11]. Thus, for two surfaces of 2 µm by 20 nm separated by 10 nm, the force would be about 1 nN, which could compete with the magnetic force exerted by an external magnetic field on the upper jaw. But as discussed for the Casimir effect, the high roughness of the surfaces in contact should considerably decrease their Van der Waals interactions.

To conclude on this evaluation of the micro-forces potentially involved between the jaws, quick estimations have shown that magnetic and elastic forces are indeed dominant and the tweezers actuation should not be hindered by other physical phenomena. However, particular attention should be paid to the tweezers closure during experimental characterization. Indeed, Van der Waals forces and the Casimir effect might become significant when the two jaws are in contact.

To better describe this interplay and predict the behavior of a tweezer depending on the given parameters, a model combining analytical and numerical calculations was further built and presented in the next chapter (**3**).

2.4 References

[1] E. du Trémolet de Lacheisserie, «Magnétisme. 1- Fondements», Presses Universitaires de Grenoble, 1999.

[2] R. Hertel, «Thickness dependence of magnetization structures in thin Permalloy rectangles», *International Journal of Materials Research,* pp. 957-962, 2002.

[3] «Investigations into domain wall widths of thick Permalloy films by high-voltage Lorentz microscopy», *J. Phys. Colloques 32 ,* 1971.

[4] K. L. M. a. Y. Lee, «Map of metastable states for thin circular magnetic nanocylinders», *Appl. Phys. Lett.,* vol. 92, n° 1112506, p. 112506, 2008.

[5] K. Y. Guslienko, V. Novosad, Y. Otani et H. Shima, «Field evolution of magnetic vortex state in ferromagnetic disks», *Applied Physics Letters 78,* p. 3848, 2001.

[6] S. Leulmi, H. Joisten, T. Dietsch, C. Iss, M. Morcrette, S. Auffret, P. Sabon et B. Dieny, «Comparison of dispersion and actuation properties of vortex and synthetic antiferromagnetic particles for biotechnological applications», *Appl. Phys. Lett.,* vol. 103, n° 1132412, 2013.

[7] B. B. (ed.), «Nanotribology and Nanomechanics II, Nanotribology, Biomimetics, and Industrial Applications», chap13, p107-202, Springer-Verlag Berlin Heidelberg, 2011.

[8] L. Wang et B. C. Prorok, «The Influence of Deposition Technique on the Mechanical Properties of Freestanding Gold Films» chez *SEM Annual Conference & Exposition on Experimental and Applied Mechanics*, 2007.

[9] «Engineering Vibrations», 2013. [Available Online]: http://ruina.tam.cornell.edu/Courses/ME4730%20Fall%202013/Rand4770Vibrations/BeamFormulas.pdf.

[10] Genet et al., «Electromagnetic vacuum fluctuations, Casimir and Van der Waals forces», *Ann. Fond. L. de Broglie ,* vol. 29, pp. 311-328, 2004.

[11] F. L. Leite, C. C. Bueno, A. L. Da Róz, E. C. Ziemath et O. N. Oliveira Jr., «Theoretical Models for Surface Forces and Adhesion and Their Measurement Using Atomic Force Microscopy», *Int. J. Mol. Sci.,* vol. 13, n° 112777, 2012.

[12] J.-H. Choi, Z. Li, P. Cui, X. Fan, H. Zhang, C. Zeng et Z. Zhang, «Drastic reduction in the growth temperature of graphene on copper via enhanced London dispersion force», *Scientific Reports,* vol. 3, n° 11925, 2013.

[13] D. Tabor, «Surface Forces and Surface Interactions», *Journal of Colloid and Interface Science,* vol. 58, n° 11, 1977.

[14] H. C. Hamaker, «The London-Van der Waals attraction between spherical particles», *Physica,* vol. IV, 1937.

3 Tweezers actuation modeling

A theoretical model was built to evaluate the magnetostatic and elastic torques exerted on the mobile jaw to predict the behavior of the three types of tweezers as a function of various parameters and be able to calculate their opening angle in particular. This study provided a better understanding of the magneto-elastic mechanisms involved and confirmed the hypotheses made in chapter 2, section **2.1.2**.

First, the magnetic torque exerted on the upper jaw, which arises from magnetostatic interaction and external field application, was expressed analytically and calculated numerically (**3.1**). Then, the elastic torque from the hinge was calculated by the finite elements method (**3.2**). Finally, equilibrium position was determined by balancing the elastic and magnetic torque on the upper jaw. Thus, calculating both torques allows determining the corresponding opening angle of the tweezer (**3.3**).

These calculations were carried out assuming the lower jaw fixed in space while the upper jaw was mobile. This assumption was intended to facilitate both the calculations and the comparison with experimental results, since the tweezers mechanical and magnetic characterizations were planned to be performed on tweezers fixed to the substrate.

3.1 Magnetic actuation

3.1.1 Analytical modeling and numerical solution

The tweezers jaws are conceptualized as two parallelepiped ferromagnetic bodies submitted to an in-plane external magnetic field. Their magnetization $\vec{M}$ is considered uniform and in-plane (chapter 2, section **2.1.2**). Therefore, following the Coulomb approach, the jaws present magnetic charges only at their surfaces, where a rupture in the magnetization component normal to the surface occurs. As is well-known from standard magnetostatics, the surface magnetic charge on each surface is:

$$\sigma_m = \vec{M}.\hat{n} \tag{9}$$

Given the jaws geometry, this scalar product results in only two opposite magnetic surface charges on the two surfaces perpendicular to the magnetization (see ***Figure 20***).

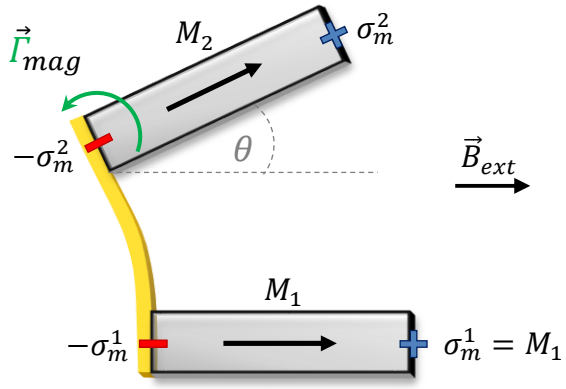

Figure 20*: Tweezer model (side view) made of two parallelepiped jaws with uniform and in-plane magnetization presenting opposite magnetic surface charges one both surfaces perpendicular to their magnetization when submitted to a uniform external magnetic field.*

Finally, one tweezer forms a system of four interacting magnetic surface charges $\sigma_m^i = \pm M^i$, $i = 1,2$. Each surface pole creates a magnetic field which writes by analogy to the electrostatic field as:

$$\mathrm{H} = \frac{1}{4\pi}\frac{\sigma'_m}{r^2} \tag{10}$$

where r is the distance between the source and the point of measurement.

The magnetic fields created by the two charged surfaces of the lower jaw sum up with the externally applied field to yield the total magnetic torque acting on the upper one which drives its opening. This torque can be determined knowing the mobile jaw's magnetostatic energy:

$$E_2 = -\vec{M}_2 V.\vec{H}_{total} \tag{11}$$

with $\vec{M}_2$ the upper jaw magnetization, V its volume and $\vec{H}_{total}$ the sum of the magnetic fields exerted on the jaw in every point of its volume. The magnetic torque is then derived from this energy:

$$\Gamma_{mag} = \frac{\partial E_2}{\partial \theta} \tag{12}$$

However, the calculation of $\vec{H}_{total}$ acting on the upper jaw is more or less complex, depending on the lower jaw magnetic properties. To compare how the jaws magnetic

properties influence the actuation mechanism of a tweezer and evidence the contribution of magnetostatic interactions between two magnetic jaws to the opening, three types of tweezers were modeled. The first type of tweezers comprises only one magnetic jaw (referred as soft/non-magnetic). In the second type, the tweezers are composed of one soft jaw and one hard jaw (referred as soft/hard). And in the third type, the tweezers are made of two soft jaws (referred as soft/soft). In all cases, the upper jaw is made of a soft material, whereas the lower jaw is the one with varying properties.

The non-magnetic material is defined by its zero magnetization. A jaw made of this material does not interact with external magnetic fields nor creates any field on the upper jaw.

The magnetically hard material is supposed to have homogeneous and in-plane magnetization, parallel to the jaw length, independent of the applied field and set as M_{hard}=581 000 A.m^{-1}, which corresponds to the remanent magnetization of NdFeB, *i.e.* with random grain orientation (half of NdFeB saturation value ~1.035x10^{6} A m^{-1}).

The magnetically soft material is also assumed to have a homogeneous and in-plane magnetization, and to exhibit a linear response to external magnetic fields up to its saturation field H_{sat}. Thus, its magnetization M_{soft} goes from zero magnetization in zero applied field to magnetic saturation M_{sat}=800 000 A.m^{-1} when the field reaches H_{sat}, set at around 0.1 T. This assumption is based on our former observation (chapter 2, section **2.1.2**) that the square jaws in NiFe that we are using have a spontaneous vortex configuration, which gradually gets polarized under magnetic field application up to saturation at around 0.1 T (this value depends on the thickness of the jaw and its lateral dimension). This was also confirmed by micromagnetic simulations. Thus, this linear response is described as follows:

$$M_{soft} = M_{sat} \cdot H_{applied}/H_{sat} \text{ as long as } \left|H_{applied}\right| < H_{sat} \quad (13)$$

$$M_{soft} = M_{sat} \text{ when } \left|H_{applied}\right| \geq H_{sat} \quad (14)$$

The three calculations corresponding to the three types of tweezers are detailed below.

- ***Soft/non-magnetic tweezer***

For a soft/non-magnetic tweezer, the calculation is rather simple as the torque exerted on the upper jaw is due to the external field only. There is no magnetostatic interaction with the lower jaw. So first, the applied field is projected in the plane of the upper jaw. This component of the field is then averaged on the upper jaw volume and compared to the saturation field H_{sat}, characteristic of the soft material. The value of the field determines the magnetization M_2 in the magnetic upper jaw following the linear response mentioned earlier (equation (13)).

When the lower jaw is magnetic, with a magnetization M_1, it generates a magnetic field which affects the magnetization of the upper jaw. Therefore, this field needs to be calculated and summed with the applied field before determining M_2 in the upper jaw.

For that purpose, the fields emitted by the two poles of the lower jaws are calculated and summed to the applied magnetic field.

- ***Soft/hard tweezer***

In the case of a soft/hard tweezer, the lower jaw is made of a hard material so M_1 is fixed and equals M_{hard}. Therefore, the magnetic field created by the lower jaw can be calculated by assuming the presence of two surface magnetic charges distributions of density $\sigma_m = \pm M_{hard}$.

The magnetic fields emitted by these two charges are calculated on each point of the upper jaw following the Coulomb approach. Their sum $\vec{H}_{12}$ is then projected in the upper jaw plane and averaged over its volume. Finally, M_2 is calculated as previously according to the linear law (equation (13)) with $H_{total} = (\vec{H}_{12})_{\parallel} + (\vec{H}_{ext})_{\parallel}$ (where $(\vec{H}_i)_{\parallel}$ is the component of the field $\vec{H}_i$ parallel to the upper jaw plane, *i* standing for "*12*", "*ext*", etc...).

- ***Soft/soft tweezer***

However, when the lower jaw is made of a soft material (soft/soft tweezer), both magnetizations depend on the field created by the other jaw. This phenomenon of auto-induction follows the reciprocity theorem of the magnetostatic energy:

$$\int \vec{M}_1 \vec{H}_{21} dV_1 = \int \vec{M}_2 \vec{H}_{12} dV_2 \quad (15)$$

Therefore, the equilibrium state between the two magnetizations needs to be determined through an auto-consistent calculation for a given opening angle and external applied field.

The strategy consists in defining the mutual magnetic susceptibility $\chi = M_2/(\vec{H}_{21})_{\parallel} = M_1/(\vec{H}_{12})_{\parallel}$ to calculate faster the field created by one jaw on the other knowing the magnetization of the former. Due to the reciprocity theorem: $\chi_{12} = \chi_{21}$, which indeed has been checked numerically. In turns, the magnetization of each jaw is calculated depending on the field emitted by the other, until the results converge.

To do so, a preset value of the lower jaw magnetization ($M_1 = M_{sat}$) is used to calculate the field $\vec{H}_{12}$ emitted on the upper jaw (by surface magnetic charges methods, like previously). Averaged and projected on $\vec{M}_2$, this field allows determining the mutual susceptibility $\chi = M_1/(\vec{H}_{12})_{\parallel}$. Then $(\vec{H}_{12})_{\parallel}$ is summed with the averaged and projected (on M_2) external field to determine M_2 following the linear response to the total applied field, as previously (equation (13)).

From this point, the field created by the upper jaw on the lower one is simply given by $H_{21} = M_2/\chi$. Again, this field is summed with the projection on M_1 of the mean external field to determine M_1. This new value of M_1 is used to carry on the same calculation over again, until both magnetizations converge. The convergence threshold was set at 1A.m^{-1}, 6 orders of magnitude smaller than the typical values.

3.1.2 Qualitative evaluation of the tweezers behavior under the application of a magnetic field

This calculation gives the magnetic torque for a given set of parameters (the tweezer opening angle θ, the external field $\vec{H}_{ext}$ and the jaws dimensions). Therefore, for a given intensity and orientation of the external field, the calculation was performed as a function of θ varying from 1° to 90° by steps of 1. In this modelling study, the jaws are assumed to measure 2 µm x 2 µm x 200 nm (except when their thickness is varied) and to be constituted of Permalloy for soft jaws and NdFeB for hard jaws.

The evolution of the torque with the opening angle was studied for the three types of tweezers and under various external field applications. The comparison between various scenarios provided insight into the most effective way to actuate the tweezers.

The results obtained with this method are in good semi-quantitative agreement with Flux3D simulations (introduced in chapter 2, section **2.1.3**), as shown in ***Figure 21***.

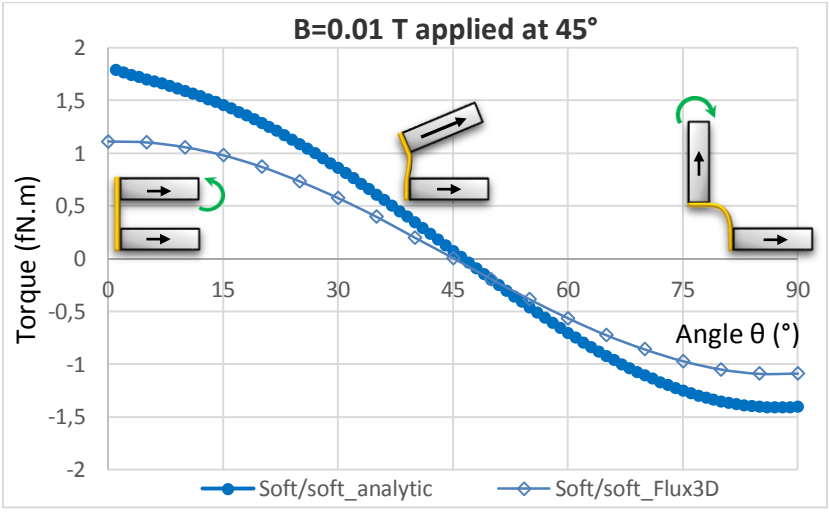

Figure 21*: Magnetic torque versus the tweezer opening angle: comparison between the results obtained by Flux3D (diamond dots) simulations (presented in chapter 1) and the present calculations (rounded dots). Here the calculation was done for a soft/soft tweezer submitted to a uniform magnetic field of 1 mT applied at 45° with respect to the substrate. Sketches accompany the curves to illustrate the tweezer configuration with qualitative evaluation of the magnetization within the jaws (black arrows) and the torque (green arrows).*

Both calculations yield zero torque at ϑ=45°, when the mobile jaw is aligned on the applied field. The difference observed between the present results and Flux3D simulations lies in the magnetic susceptibility definition. In the analytical model, the susceptibility is modelled according to the vortex particles described in chapter 2, section **2.1.2** and the magnetization is artificially fixed in-plane. With Flux3D, the susceptibility is set at 1000 for the bulk material, typical for ferromagnets, and the shape anisotropy is automatically taken into account during the finite element calculation by the software. Therefore, the magnetization is allowed to have out-of-plane components and the in-plane component is lowered. In addition, edges effects, which are disregarded in the analytical model, can also lower the magnetization of the jaw (***Figure 22***). This is why the torque obtained analytically is slightly greater than the torque yielded by Flux3D. The advantage of our own calculation over Flux 3D is the calculation speed which was much faster for comparison with experiments and the possibility to easily vary numerous parameters.

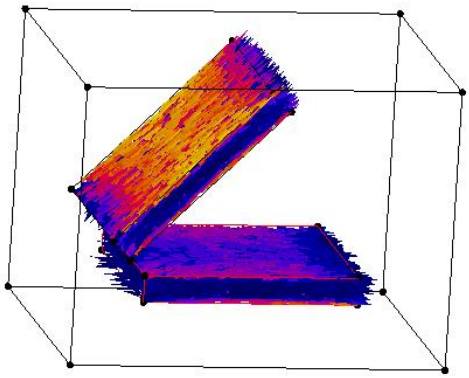

Figure 22*: Map of the magnetic field within the jaws of a soft/soft tweezers submitted to a uniform field of 0.014 T and applied at 45°. The field is drops at the jaws edges, lowering the overall magnetization of the jaws. Color scale: from dark blue=0 T to yellow=1 T. Figure obtained by Flux3D simulations.*

Among all the situations explored, the first case to mention is when no external field is applied, which is plotted for the three types of tweezers in ***Figure 23***. The soft/non-magnetic tweezer is the simplest case as there is no interaction between the jaws, only the external field can exert a torque on the upper jaw. Thus, magnetostatic interactions are highlighted by the comparison between the three types of tweezers. For instance, soft/hard tweezers contrast with soft/soft tweezers by yielding negative values of the torque for small

angles (when the tweezer is almost closed). This is due to the hard jaw remanent magnetization which allows magnetostatic attraction to play a role even at weak applied field.

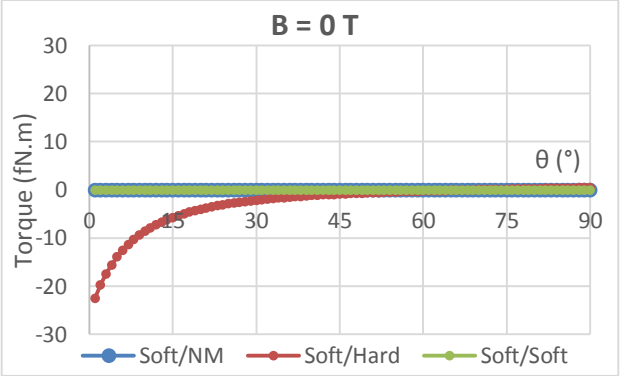

***Figure 23**: Magnetic torque exerted on the upper soft jaw versus tweezers opening angle in 0 applied field. Only the soft/hard tweezers exhibit a non-zero torque due to magnetostatic attraction allowed by the fixed magnetization of hard jaws.*

In the presence of an external field, the torque behaves differently depending on the orientation and intensity of the field (***Figure 24***, **Figure 28** and ***Figure* 30**). However, the general shape of the torque variation versus opening angle is rather similar between the three types of jaws. This indicates that for the materials and dimensions that we used, the dominant source of torque is the direct torque due to the applied field on the upper jaw rather than the torque due to magnetostatic interactions between upper and lower jaws.

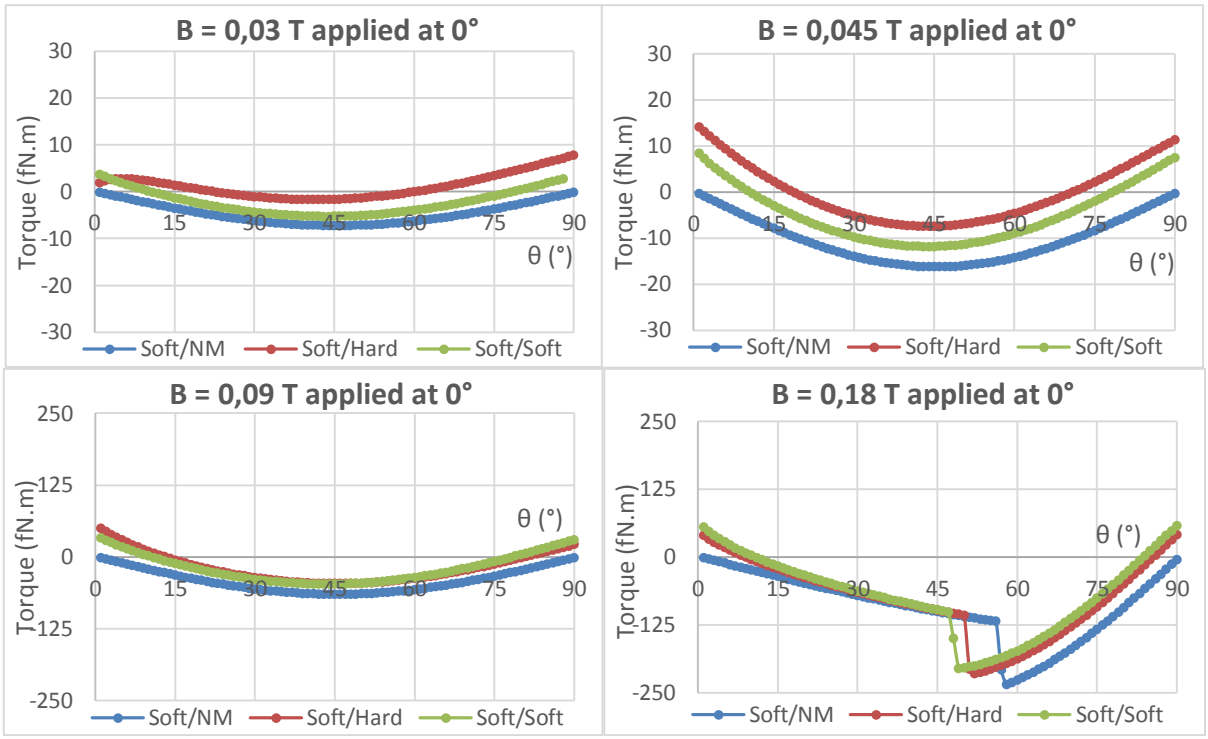

***Figure 24**: Magnetic torque exerted on the upper soft jaw versus tweezers opening angle under the application a magnetic field applied at 0°. Each graph was acquired for an increasing value of the field and for the three types of tweezers.*

When the field is applied at 0°, parallel to the lower jaw, it tends to keep the mobile jaw at 0° due to Zeeman coupling. Therefore, for soft/non-magnetic (soft/NM) tweezers, the torque exerted on the mobile soft jaw is zero when it is parallel to the field and gets more and more negative as the angle increases until 45°, meaning that the applied field tends to maintain the tweezer in closed configuration. For larger angles, the soft jaw is so misaligned with the field that it progressively loses its magnetization, making the torque null again at 90°.

For soft/soft tweezers, the torque at small angles is slightly repulsive (positive values), due to the magnetostatic interaction between the jaws as they get magnetized. The stronger the field, the higher their magnetization and the stronger the repulsive torque. For larger angles, this interaction appears as an off-set in the torque compared to the curve for soft/non-magnetic tweezer. It vanishes when the field becomes stronger, dominated by the contribution of the coupling with the external field.

Regarding soft/hard tweezers, they tend to provide larger torques at moderate fields than soft/NM and soft/soft tweezer due to the larger magnetization of the hard layer in this

range of field. However at large fields, this is no longer true because the soft material exhibit larger magnetization at saturation compared to the hard material.

The drop in the torque observed for high fields (0.18 T in ***Figure 24*** and ***Figure* 30**, 0.085 T in ***Figure 28***) occurs when the mobile jaw reaches saturation. Indeed, at this point, the magnetization derivative has a discontinuity. Since the torque is associated to the angular derivative of the Zeeman energy, this magnetization discontinuity yields a torque discontinuity which shows up as a sudden drop in magnetic torque amplitude. If on the contrary, the magnetization gets no longer saturated because the in-plane projection of the applied field decreases below the saturation value, an upward jump of the torque may appear.

Figure 25 displays the magnetization of a soft/soft tweezer jaws evolution under an increasing magnetic field applied at 0°. When the jaws are parallel (θ=1°), they yield the same reaction to the applied field and both jaws are saturated at 0.15 T. As the tweezer opens, the jaws do not experience the same magnetic field and behave differently. At 45° opening, the lower jaw gets saturated more easily (0.135 T) than the upper one (0.18 T) which is now misaligned with the applied field. The fact that the saturation field of the lower jaw decreases when the tweezer is open shows that magnetostatic interactions between the two soft jaws tend to demagnetize them, at least in the longitudinal direction. In the soft/hard case, it seems that the fixed magnetization of the lower jaw maintains a higher longitudinal magnetization in the soft upper jaw which gets saturated more easily (by comparing the graph in the bottom right of ***Figure 25*** with the right graph of ***Figure 26***).

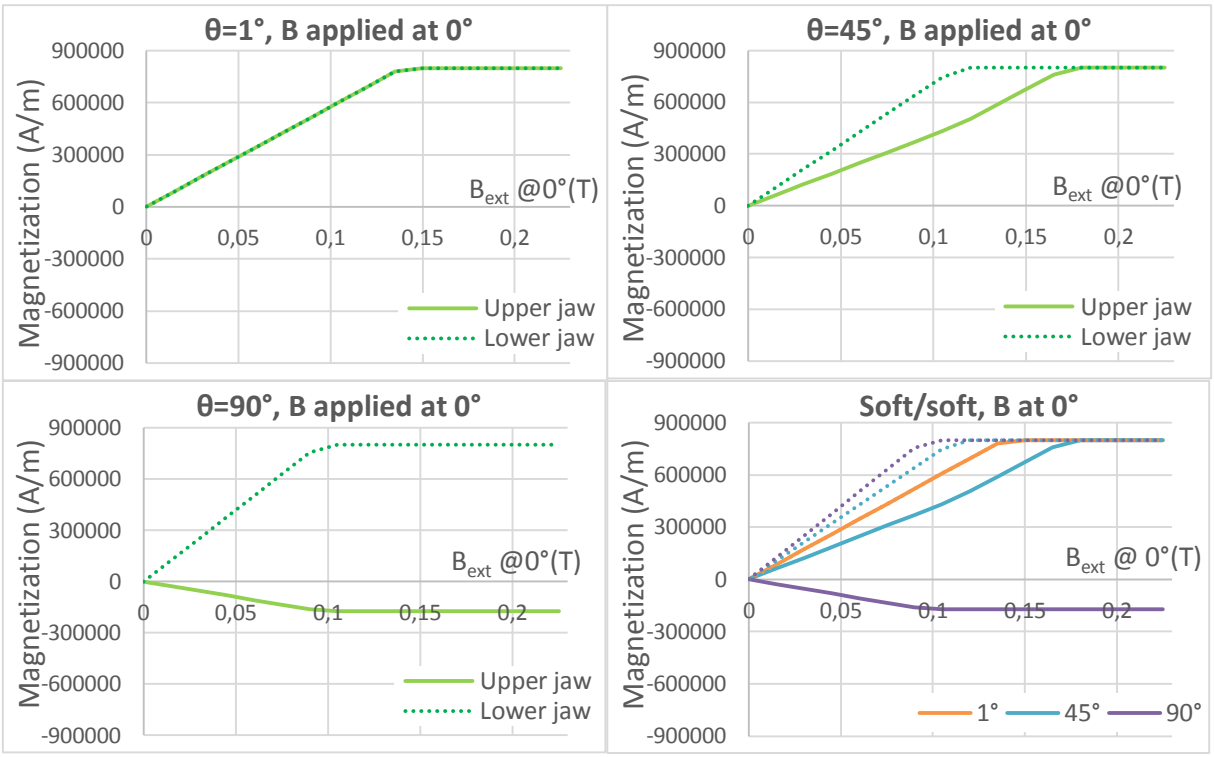

***Figure 25**: Magnetization (longitudinal component) of soft/soft jaws under the application of an increasing in-plane magnetic field. The fourth graph summarizes the three previous ones (upper jaws in full lines and lower jaws in dotted lines).*

Figure 26 shows the magnetization evolution in the same conditions for soft/non-magnetic and soft/hard tweezers. The comparison with the soft/non-magnetic tweezers highlights the influence of magnetostatic interactions and gives a reference value of the saturation field under various conditions.

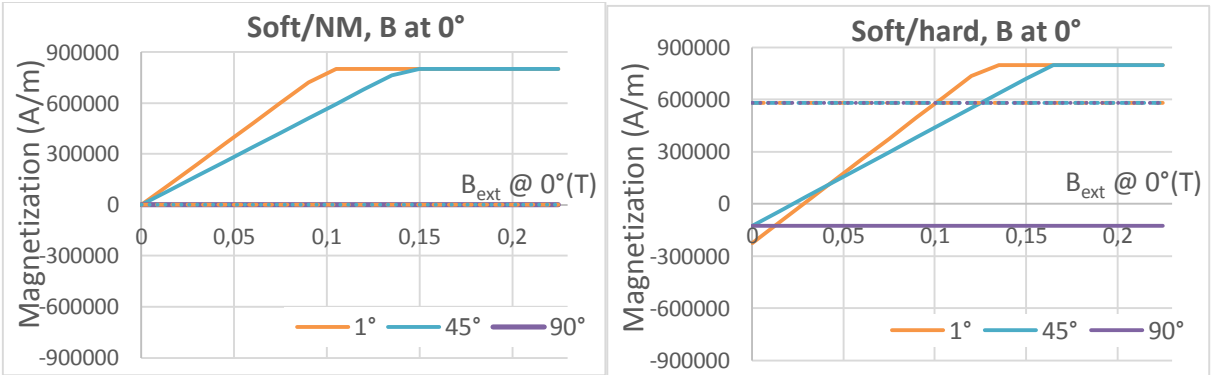

***Figure 26**: Magnetization (longitudinal component) of soft/non-magnetic jaws (left) and soft/hard jaws (right) for three different opening angles under the application of an increasing in-plane magnetic field (upper jaws in full lines and lower jaws in dotted lines).*

In the case of a soft/hard tweezer, the magnetization of both jaws can be anti-parallel at low field, associated with flux closure between the two jaws. This results in an attractive interaction (negative torque) which tends to close the tweezer. When the field is large enough, the magnetization of the upper jaw switches to be parallel to the field, resulting in a positive repulsive torque. The occurrence of a similar behavior in soft/soft tweezers was confirmed by micromagnetic simulations, when the jaws length is extended to 3 times their width. ***Figure 27*** shows for which combination of applied field and upper jaw position the upper jaw magnetization reverses in soft/hard tweezers.

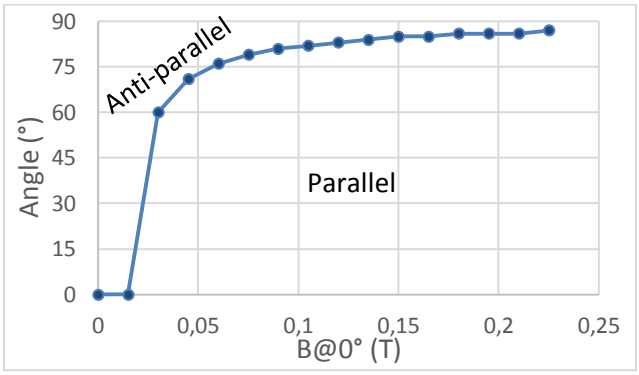

Figure 27*: Map of the opening angle θ and in-plane applied field combination yielding anti-parallel and parallel alignment of both jaws magnetization within soft/hard tweezers.*

When the external field is applied at 45°, the trends are similar, except that the torque becomes null around 45° (a shift can be observed in the graphs in ***Figure 28*** at low applied field due to magnetostatic interactions).

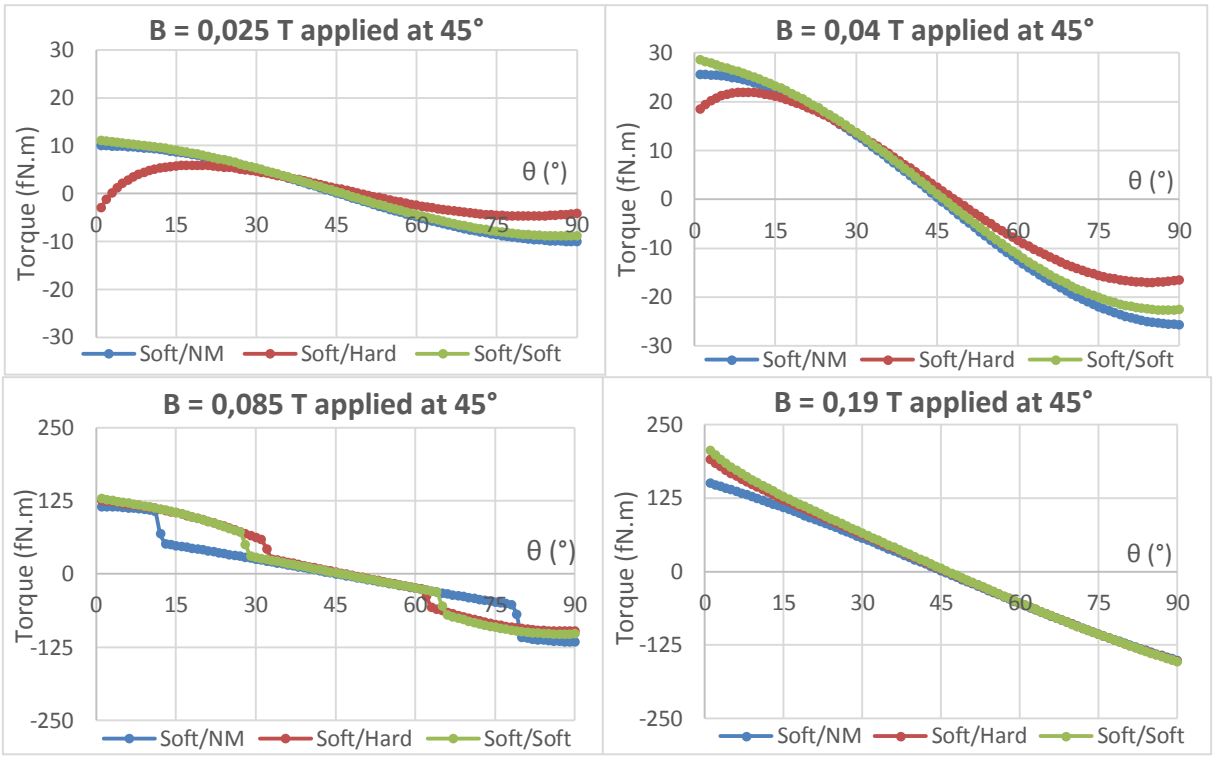

***Figure 28**: Magnetic torque exerted on the upper soft jaw versus θ under the application of increasing field applied at 45° for the three types of tweezers.*

At angles below 45°, the torques are positive, meaning that the upper jaw is pulled upwards due to the fact that the upper jaw magnetization tends to align with the field applied at 45° from the horizontal direction.

Small differences can be seen at small angles between the various types of tweezers due to the repulsion between two soft jaws or the attraction between a soft and a hard jaw. For larger fields (0.19 T), the soft/soft repulsion is greater than the soft/hard one because the saturation magnetization value of the hard jaw (581 $kA.m^{-1}$) is lower than that of the soft one (800 $kA.m^{-1}$).

As the opening angle increases around 45°, the torque on the upper jaw goes to zero and changes sign. This reflects that the dominant effect is again the action of the external field on the upper jaw magnetization, rather than the magnetostatic interactions between the two jaws.

For angles larger than 45°, the behaviors of the three types of tweezer differ again because the net field acting on the upper jaw magnetization is affected by the stray field from the lower jaw, the projection of the latter in the plane of the upper jaw being opposite in sign to that of the applied field (for hard and soft lower jaws). This results in the upper

jaw having a lower magnetization and therefore lower torque, in particular in the case of hard lower jaw compared to soft or NM lower jaws.

The graph plotted for B=0.085 T is particularly interesting as it clearly shows the differences between the three cases to reach (1st jump corresponding to a decrease in absolute value of the torque) and leave (2nd jump corresponding to an increase in absolute value of the torque) magnetic saturation.

Like previously, ***Figure 29*** gives the evolution of the longitudinal component of the magnetization in the jaws of each type of tweezer under the application of an increasing magnetic field at 45°.

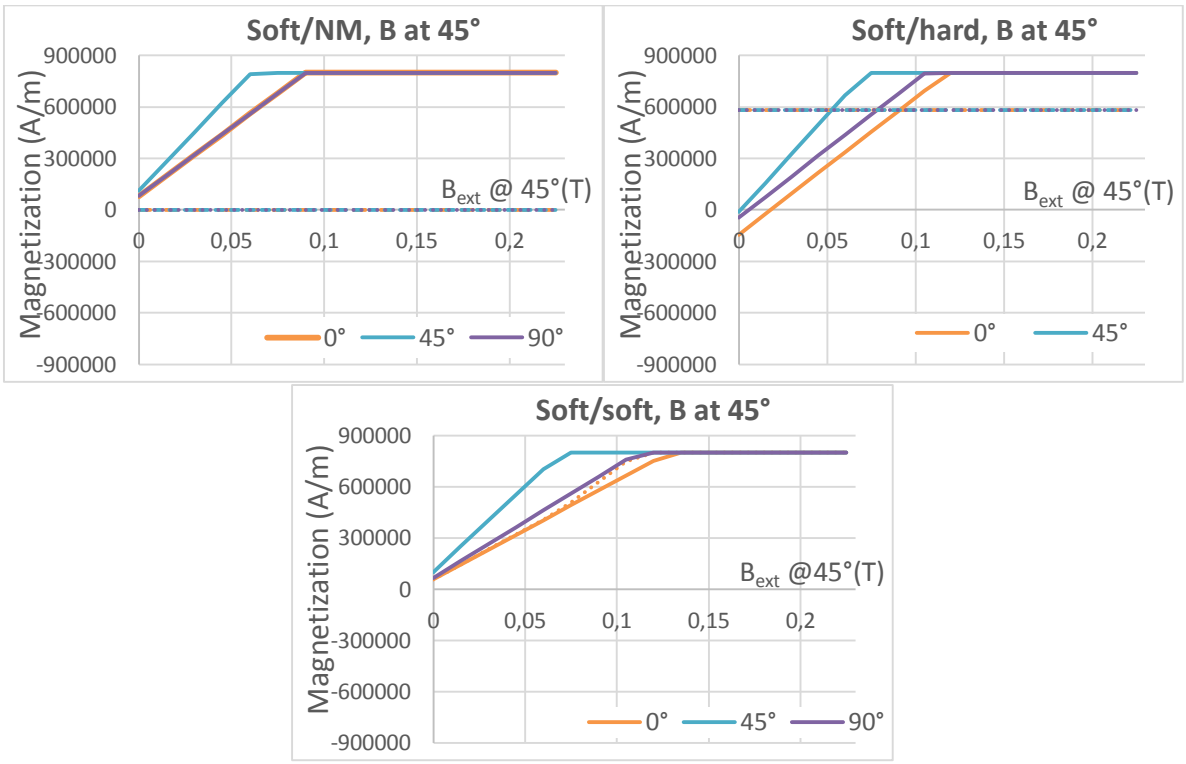

Figure 29*: Magnetization (longitudinal component) of a soft/non-magnetic tweezer jaws (left), soft/hard tweezer (right) and soft/soft tweezer (bottom) for three different opening angles under the application of an increasing magnetic field applied at 45° (upper jaws in full lines and lower jaws in dotted lines).*

Finally, the study of the torque (***Figure 30***) and the magnetization (***Figure 31***) evolution under the application of an out-of-plane field completes the understanding of the

interplay between the external field and the field emitted by the lower jaw on the upper jaw motion.

For the soft/hard tweezer, the torque at low opening angle is negative. Indeed, the external field applied out-of-plane creates almost no polarization in the upper jaw. In contrast, the stray field from the hard lower jaw polarizes the upper jaw magnetization in the negative direction, resulting in an attraction between the two jaws (negative torque) which tends to maintain the tweezer closed. For the soft/soft and soft/NM cases, the torque is zero at low opening angle because the magnetization is very weak, since the field is applied out of plane. Similarly, close to 90°, the upper jaw magnetization is parallel to the external field while the magnetostatic interactions with the lower jaw are weak, therefore the torque is zero. The torque is maximal at about 45°, which can be explained by considering that the magnetization of the upper jaw varies like the cosine of the angle between the applied field and the upper jaw plane, while the torque varies as the sine of the angle between the upper jaw plane and the field (45° is the maximum of the function cosine*sine).

At large field (0.18 T), a clear discontinuity in the torque versus opening angle is observed when the magnetization of the upper jaw reaches saturation. The variation between each type of tweezer highlights the influence of the stray field emitted by the lower jaw on the upper one, depending on the former's nature.

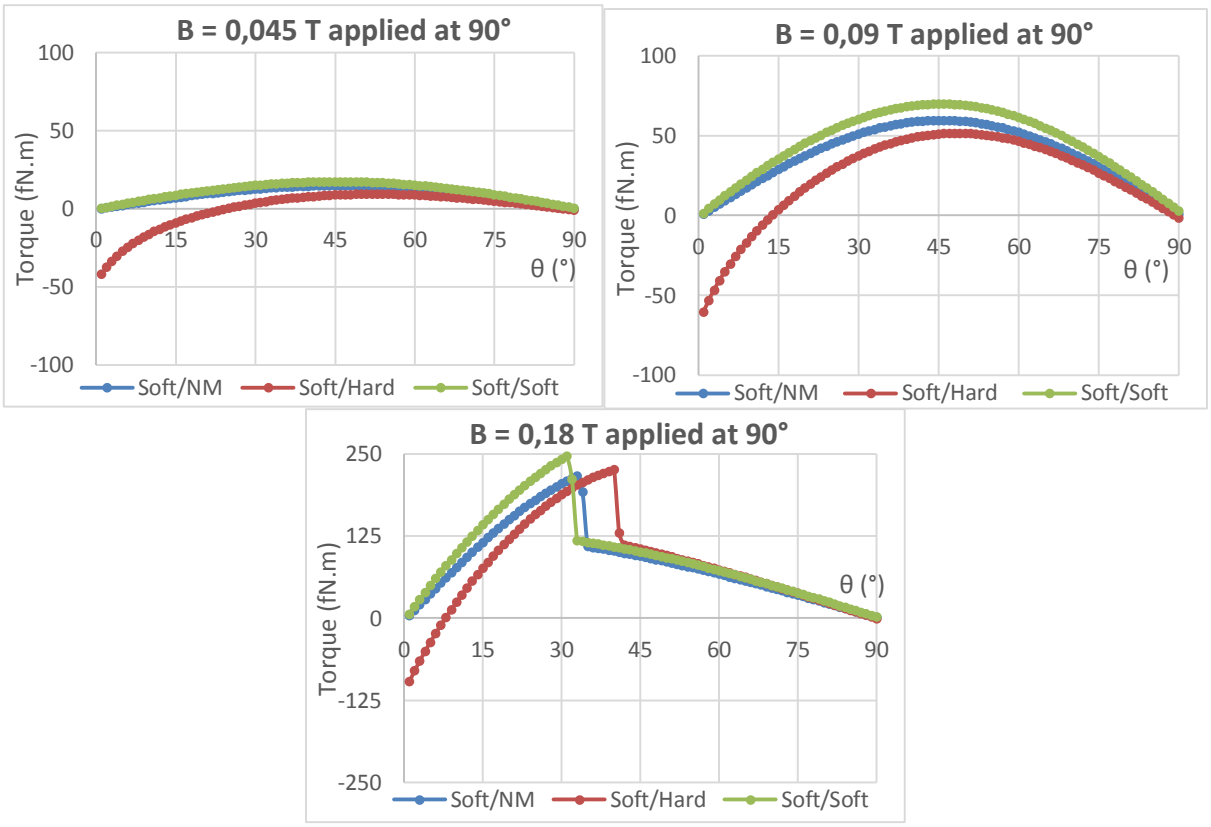

***Figure 30**: Magnetic torque exerted on the upper soft jaw versus θ under the application of increasing field applied at 90° for the three types of tweezers.*

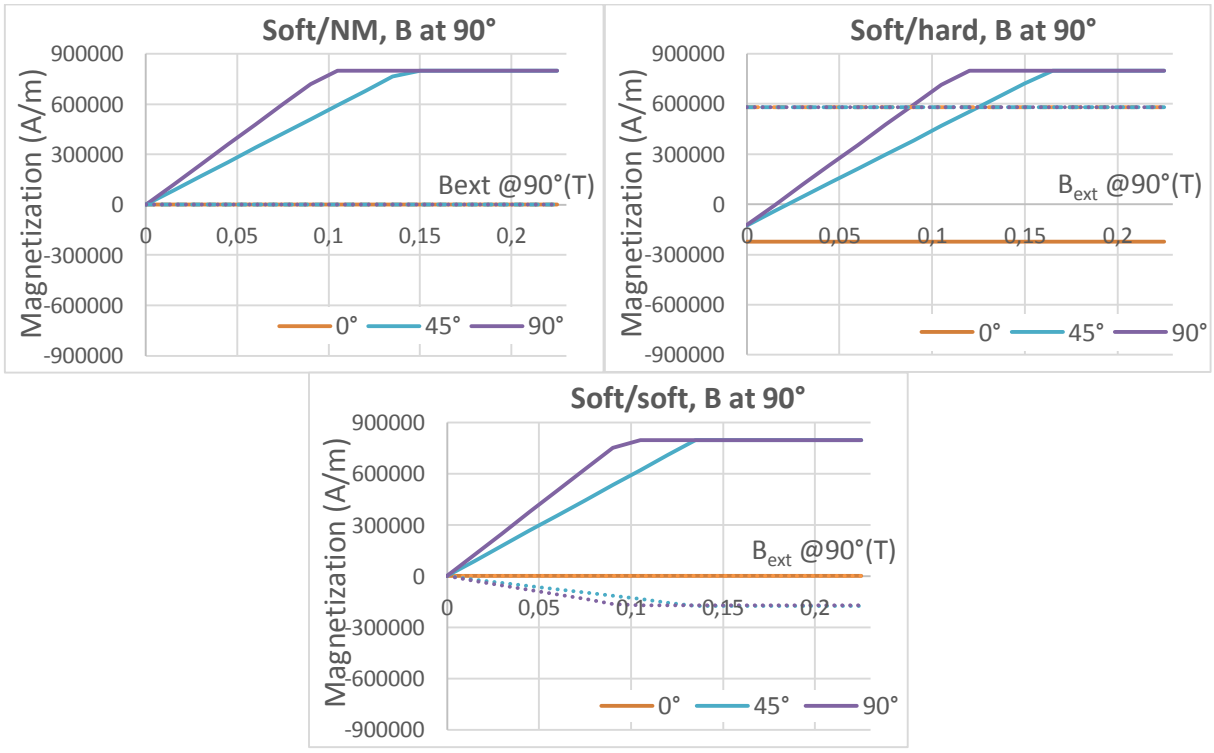

***Figure 31**: Magnetization (longitudinal component) of a soft/non-magnetic tweezer jaws (left), soft/hard tweezer (right) and soft/soft tweezer (bottom) for three different opening*

angles under the application of an increasing magnetic field applied at 90° (upper jaws in full lines and lower jaws in dotted lines).

The influence of the jaws thickness was also studied and ***Figure 32*** shows how it affects the torque, depending on the tweezer opening. As expected, the thicker the jaw, the stronger the torque. To study the influence of the thickness on soft jaws, we took into account the variation of the in-plane susceptibility of the vortex configuration as a function of the jaw aspect ratio (thickness/lateral dimension). This was carried out using Guglienskо's expression for the variation of susceptibility of a vortex [1] presented in chapter 1, equation (1): $\chi^{-1} = 2\beta[\ln 8/\beta - 1/2]$, where $\beta = \text{thickness}/width$. Although this expression was established for a cylindrical nanostructure, we used it here for a nanostructure of square shape. Such approximation stays valid in the frame of this semi-quantitative discussion.

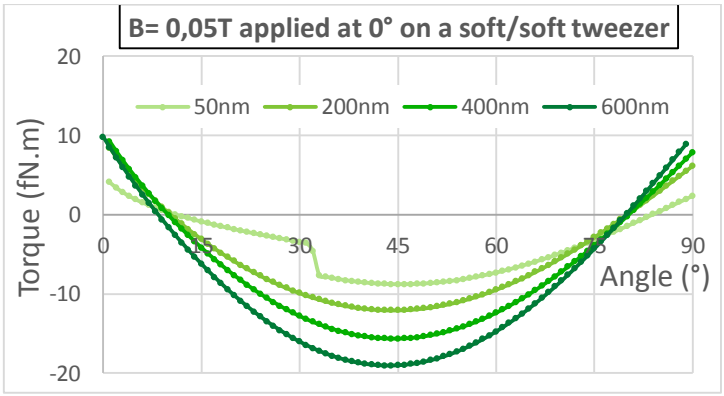

Figure 32*: Magnetic torque applied on the upper jaw of a soft-soft tweezer submitted to a uniform in-plane magnetic field of 0.05 T, plotted according to the opening angle of the tweezer for several examples of thickness for the jaws.*

In this example, the field is too low for jaws thicker than 50 nm to reach in-plane magnetic saturation. Indeed, according to Guslienko's susceptibility, the vortex susceptibility decreases with the vortex thickness. Therefore, tweezers with thicker jaws can avoid entering the saturation zone which leads to a drop in the torque intensity.

In the paragraphs above, the magnetic torque was discussed as a function of the opening angle, which was assumed to be a variable parameter. Now, in practical tweezers, the magnetic torque due to the applied field and coupling between the jaws is balanced by

the elastic mechanical torque from the hinge. The balance between these two torques determines the opening angle which can be measured experimentally. The purpose of the next section is therefore to calculate the elastic torque from the hinge as a function of the hinge characteristic parameters and opening angle.

3.2 Hinge mechanical response

The upper jaw motion under the magnetic torque application induces the hinge bending. As mentioned in chapter 2, section **2.2.2**, the angular amplitude θ of the tweezer opening is directly linked to the hinge stiffness K through the Euler-Bernoulli expression of the rigidity of an elastic end-loaded beam [2]:

$$\Gamma = K\,\theta \tag{16}$$

The stiffness constant K is a function of the hinge Young Modulus E, width w, length L and depends particularly on its thickness t. More precisely, the hinge stiffness is expected to vary as:

$$\mathrm{K} = \frac{E\,w}{12\,L}t^3 \tag{17}$$

For a gold hinge of 2 µm in width, 350 nm long and with a Young Modulus of 59 GPa, the relation (16) was plotted for several hinge thickness in *Figure 33*.

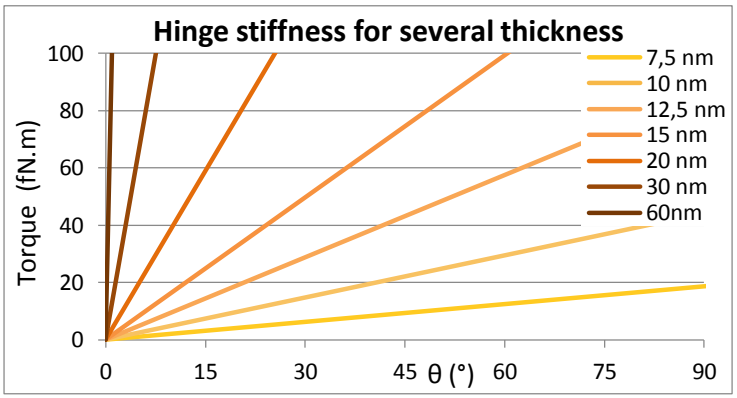

***Figure 33**: Elastic torque plotted according to the tweezer opening angle θ for several hinge thicknesses. The slope of each line corresponds to the stiffness of a given hinge.*

However, this relation is only valid for the elastic regime, limited to small deformations and angles. Even though gold is very ductile, there is a maximum force, the

yielding strength, above which plastic deformations occur. According to reference [3], this threshold has been measured between 260 MPa to 300 MPa for gold.

To see if the magnetic torque applied on the upper jaw can induce irreversible deformations in the gold hinge, the stress experienced by the latter was calculated by finite elements, using a numerical model of a tweezer built with COMSOL Multiphysics 4.2.a (**Annexes**). The Von Mises stress (MPa) is plotted versus the applied torque for various thicknesses of the hinge in *Figure 34*.

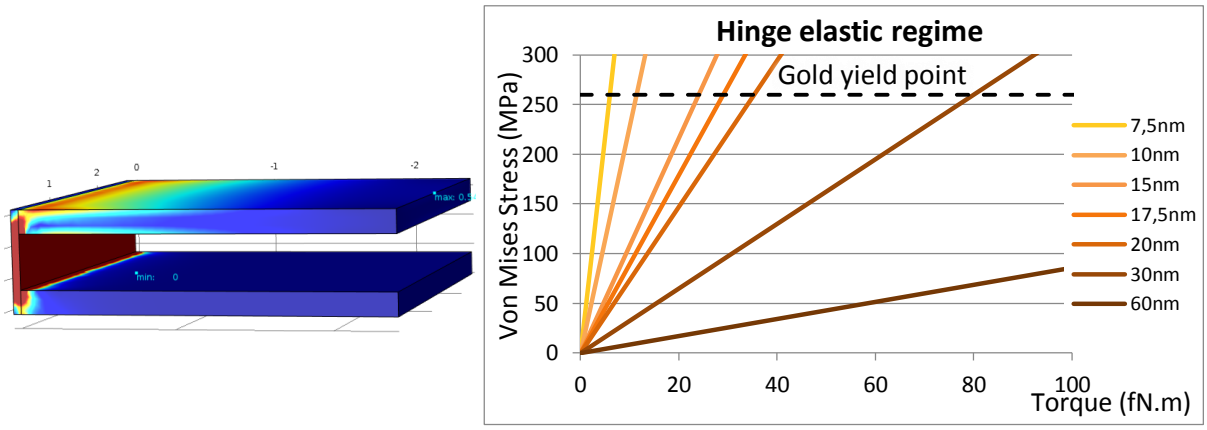

***Figure 34**: Determination of the elastic regime validity for the gold hinge. Left: Stress distribution in a tweezer with a gold hinge of 60 nm in thickness and 350 nm in height, a fixed lower jaw (2x2x0.2 µm^3) and an upper jaw with Permalloy mechanical properties (2x2x0.2 µm^3) submitted to an upward force. Right: Stress experienced by hinges of various thicknesses (from 7.5 nm to 60 nm) plotted versus applied torque. The dashed line shows the gold yielding strength, delimiting the elastic regime.*

The graph right above indicates that hinges of 17.5 nm and thinner would not withstand the magnetic torque due to magnetostatic interaction between a hard jaw and a soft one (~30 fN.m) as they would leave the elastic regime and be subjected to irreversible deformation. Even thicker hinges could experience plastic deformation and ultimately break under the application of strong magnetic fields.

For now, the best compromise between flexibility and elasticity would be for hinge thickness to be around 20 nm, which is the value used in our experiments.

3.3 Opening angle at equilibrium for the three types of tweezers

The actual measured opening angle is reached when the hinge mechanical restoring torque balances the magnetic opening torque. The determination of the equilibrium position is achieved graphically, by spotting the intersection between both torques when plotted on the same graph versus opening angle θ (***Figure 35***). The abscissa of their intersection is the expected angle at equilibrium for a given combination of mechanical and magnetic parameters (external field, hinge and jaws thicknesses).

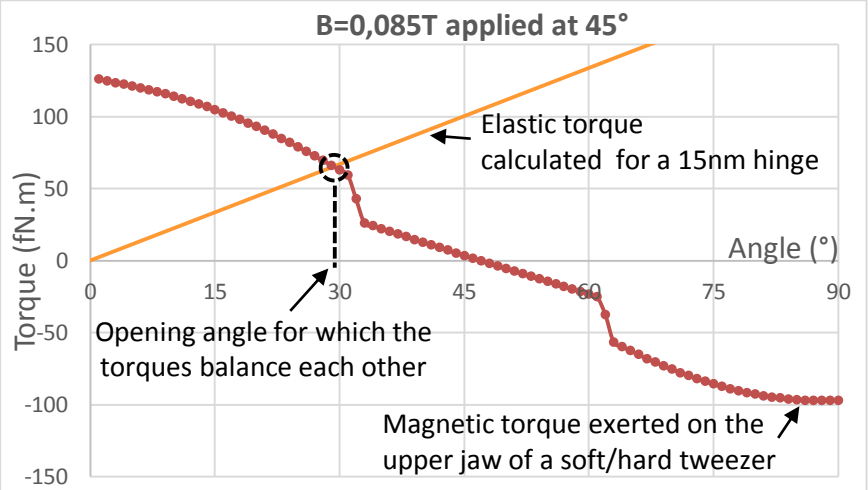

Figure 35*: Determination of the expected opening angle for a soft/hard tweezer with 2 µm x 2 µm x 200 nm jaws and 15 nm thick hinge submitted to an 85 mT external field applied at 45° with respect to the tweezer substrate. The intersection between the magnetic torque curve (red) and the elastic torque straight line (orange) indicates a position of equilibrium which balances both torques. In this example, the tweezer can open at 29° before the hinge restoring force balances the magnetic torque responsible for the opening.*

Using this method, the opening angle at equilibrium of the three types of tweezers were compared under the application of a magnetic field applied in-plane, at 45° and out-of-plane ***Figure 36***.

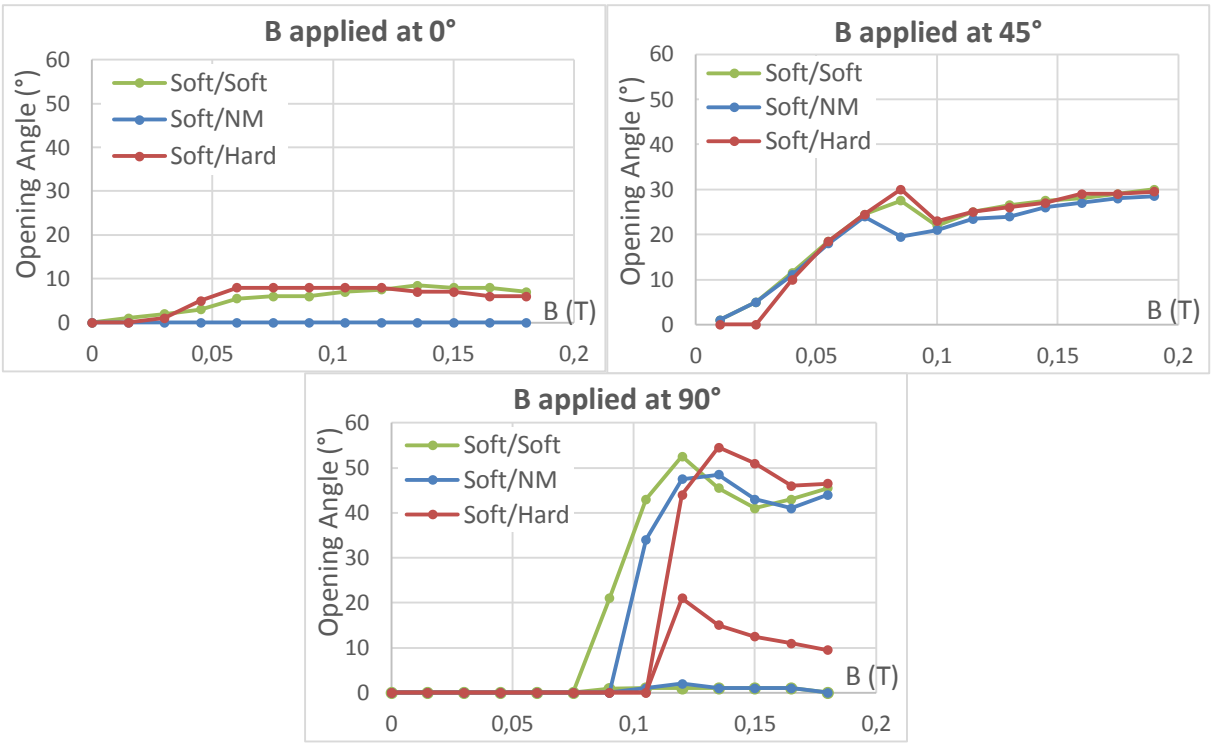

***Figure 36**: Opening angle of the three types of tweezers taking into account both the magnetic torques and the hinge stiffness. Each graph corresponds to a given orientation of the applied field.*

As a consequence to the dominance of the Zeeman coupling upon the magnetostatic interaction between two magnetic jaws, the application of an in-plane magnetic field is not very efficient at opening the tweezers. Therefore, in these particular conditions, it would be difficult to control the tweezers opening/closing if the tweezers were to be released in solution. This actuation of released tweezers would require an increase of the amplitude of the magnetostatic interactions between jaws for instance by increasing their thickness, length and magnetization.

The largest angles are obtained under the application of an out-of-plane field, whatever the type of tweezers. However, it is interesting to note that two stable positions exist under such conditions, separated by an energy barrier. This would certainly yield hysteresis in the opening/closing of such tweezer. It is actually hard to tell if the tweezers will continue to open after reaching the first stable state at narrower angles. In our experiments, we have not observed such double stable states, but we may not have gathered the proper conditions for this.

Overall, the application of the magnetic field at 45° seems the best option to control the opening/closing of the tweezers with large enough opening angles. Even though soft/hard tweezers resist to the opening at very low fields, they open at 30° at 0.085 T, which is wider than soft/soft and soft/non-magnetic tweezers. Plus, this could be improved by choosing a hard material with a higher saturation magnetization. Soft/soft tweezers also yield a promising behavior with 27.5° at 0,085 T and 30° at 0.19 T. Soft/non-magnetic tweezers reach these angles only for fields stronger than 0.145 T but are still well suited for applications which require the tweezers to be fixed on a substrate.

In this chapter, the behavior of the three types of tweezers (soft/soft, soft/non-magnetic and soft/hard) was modeled according to various parameters such as the magnetic field application, the jaws materials and their dimensions. The technological development of the tweezers will be reported in the next chapter (chapter **4**), before using these theoretical results to support the interpretation of the tweezers experimental characterization presented in chapter **5**.

3.4 References

[1] K. Y. Guslienko, V. Novosad, Y. Otani et H. Shima, «Field evolution of magnetic vortex state in ferromagnetic disks», Applied Physics Letters 78, p. 3848, 2001.

[2] «Engineering Vibrations», 2013. [Available Online]: http://ruina.tam.cornell.edu/Courses/ME4730%20Fall%202013/Rand4770Vibrations/BeamFormulas.pdf.

[3] H. Kahn et B. Bhushan (ed.), «Nanotribology and Nanomechanics II, Nanotribology, Biomimetics, and Industrial Applications», Chapter 24, Berlin Heidelberg: Springer-Verlag, 2011.

4 Technological elaboration

The technological elaboration of the magnetic micro/nano-tweezers has finally represented the main effort of this thesis. The fabrication process was developed from scratch, following the objectives determined in chapter **2**, so to say producing tweezers composed of two jaws made of evaporated metal layers (magnetic or not) separated by a sacrificial layer removed at the end of the process, bound together by a thin gold layer standing for the hinge. The prospect of being able to release the tweezers in solution kept orienting the development of the fabrication process although this objective was not reached in the frame of this work.

The fabrication methods were inspired from the microelectronic technics mastered by Spintec and the PTA for magnetic memories. Thus, a wafer-scale process was developed to be time-effective and to allow carrying out experiments of actuation on assemblies of tweezers, the latter remaining attached to the wafer.

The development of each step of the process is described below in **4.1** and the fabrication of tweezers with various materials and dimensions is presented in section **4.2**.

4.1 Fabrication process

A fabrication process was elaborated step by step in the PTA cleanroom, following a top-down approach based on microelectronic fabrication techniques (***Figure 37***).

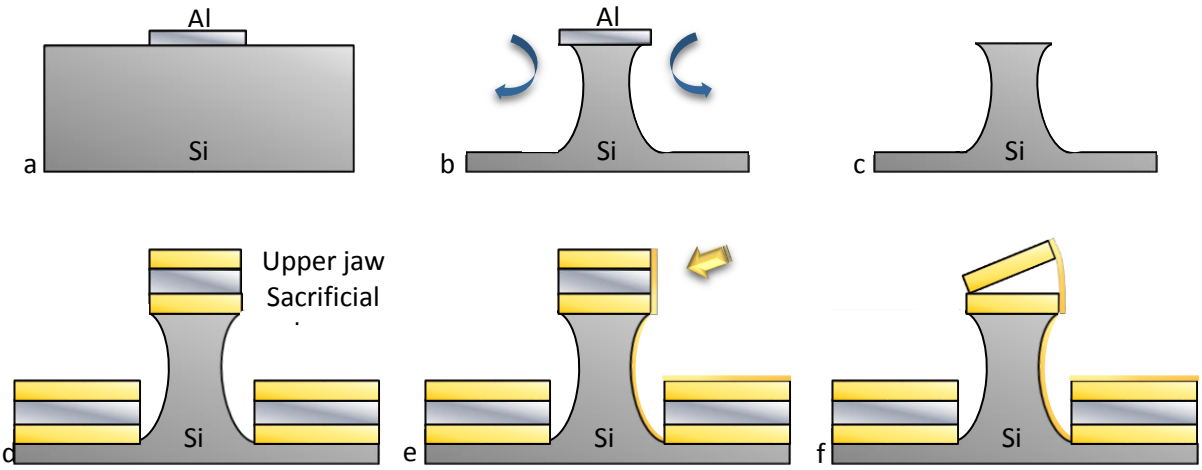

***Figure 37**: Illustration of the six main steps of the tweezers fabrication process. **(a)**: Aluminum hard-mask realization by UV-lithography. **(b)**: Silicon pillars patterning by isotropic reactive ion etching through the Al mask. **(c)**: Al mask removal by chemical etching. **(d)**: Stack deposition: two magnetic layers separated by an Al sacrificial layer. **(e)**: Gold hinge elaboration by evaporation of gold at oblique incidence on one side and soft etching of the 3 other sides. The yellow arrow indicates the evaporated gold incidence. **(f, vi)**: Jaws release by chemical etching of the Al sacrificial layer.*

Usually, the metallic stack of interest is deposited into an array of resist holes, and the resist dissolved afterwards (a fabrication process of this kind is proposed in Annexes). Here, the tweezers are deposited on a previously patterned silicon substrate. The first motivation to apply this original method was to avoid the possibility that the hinge bounds the jaws to the substrate, which would have prevented their subsequent release in solution. The additional advantage of this method is that the size of the pillars can be adjusted while using the same lithography mask (see **4.2.2**). This versatility proved to be very useful to start the development of the tweezers since it allowed the fabrication of tweezers of various sizes with only one pre-existing lithography mask. Indeed, the design and production of a new mask is a rather long and expensive process whose permanent nature is quite incompatible with the explorative nature of this work. Finally, the same mask was used during the entire thesis.

Each step of the process is detailed below.

4.1.1 Aluminum mask realization

The first step of the process consists in patterning the silicon wafer in the form of a regular array determining the silicon pillars location. This is achieved by UV-lithography (Ultra-Violet). This process described in ***Figure 38*** results in an array of aluminum square slabs, of lateral dimension 10 µm, thickness 20 nm on the silicon substrate. The pitch of this array is 15 µm.

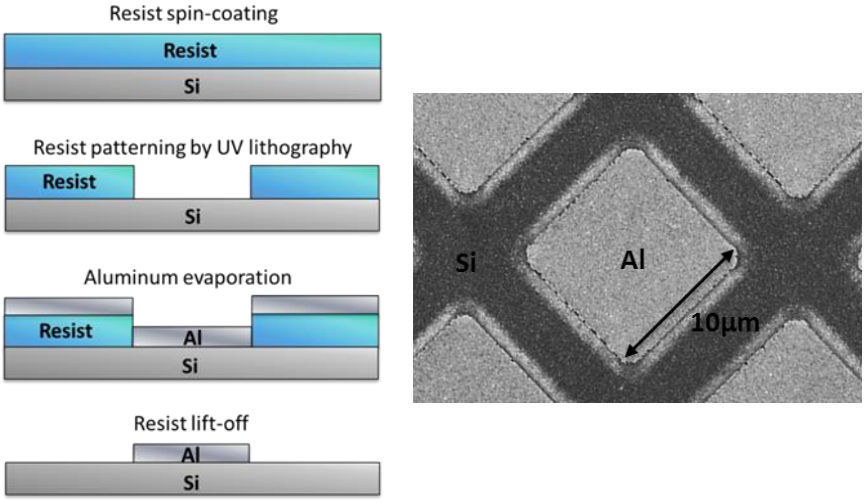

Figure 38*: Description of the lithography process used to pattern aluminum slabs (20nmx10µmx10µm) on a Si wafer illustrated by a Scanning Electron Microscopy (SEM) image.*

4.1.2 Silicon pillars fabrication

The silicon bulk is etched through the Al mask using a silicon isotropic Reactive Ion Etching (RIE) process. This dry etching technique consists in bombarding the sample with ions of a particular species. The chemical reactivity between the etching gas and the silicon creates some volatile chemical species which are pumped away during the etching process.

In this process, SF_6 (sulfur hexafluoride) (accompanied with argon) is used to etch silicon only. Isotropic etching has been preferred to anisotropic (vertical) etching because it enables creating undercuts under the mask (***Figure 39***).

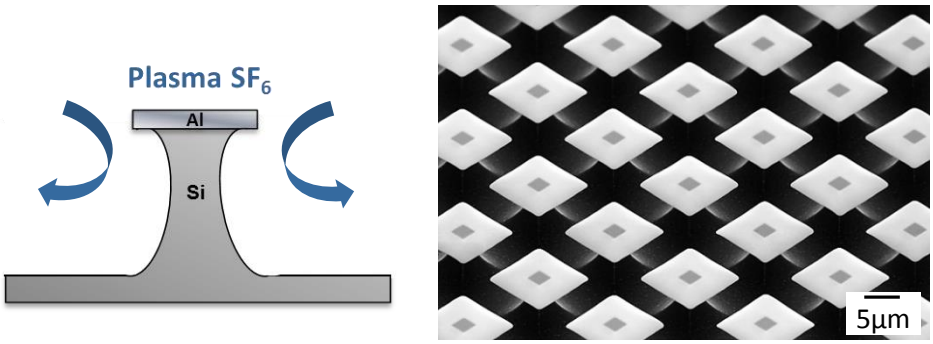

***Figure 39**: Reactive ion etching of silicon pillars through Al mask illustration illustrated by SEM image of Si micro-pillars (2.4 µm side) capped with Al slabs of 10 µm side.*

By adjusting the etching time, it is possible to get wider or narrower pillar sections (***Figure* 40**) and thus *in-fine* control the tweezers size, since they are deposited on top of the pillars.

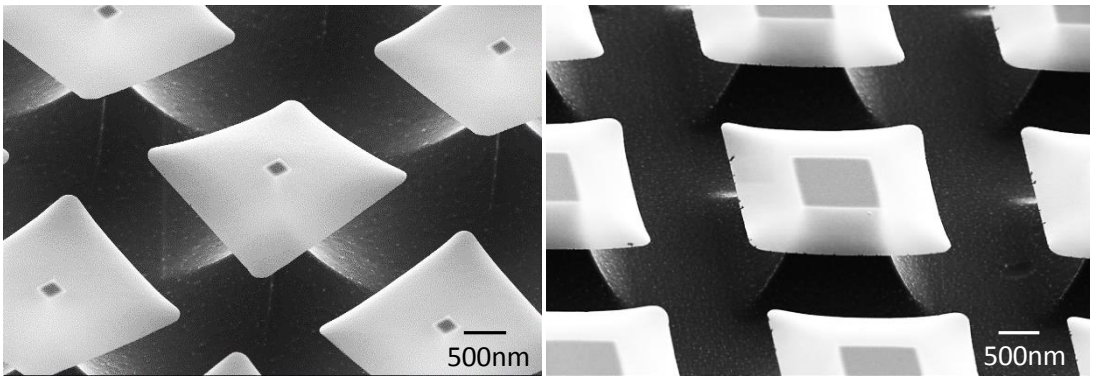

***Figure 40**: Demonstration of the etching process versatility to get diverse tweezers dimensions with the same initial lithography mask. The pillars top section measures 0.75 µm side on the right image and 4 µm side on the left.*

This method allowed decreasing the pillars top section from 10µm down to 500 nm. Tweezers of various sizes were fabricated by this method and are presented at the end of this chapter (section **4.2.2**).

4.1.3 Aluminum mask removal

The Al slabs are then removed by chemical etching with an acid solution (the recipe of *AluEtch 1960* is given in Annexes). Uncapped pillars are shown in ***Figure 41***.

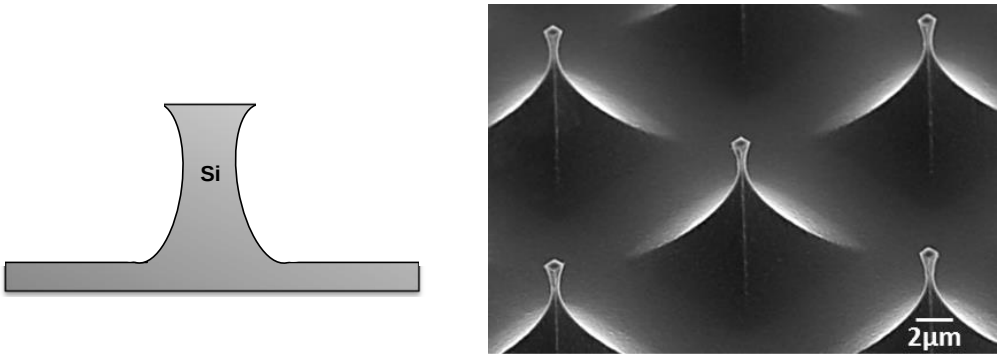

Figure 41*: Sketch and SEM image of silicon micro-pillars after Al slabs chemical etching.*

At this stage, the substrate is finally ready for the tweezers deposition.

4.1.4 Stack deposition

The tweezers consist in metal layers deposited by electron-beam evaporation. Although the deposit covers the full wafer (the top of the pillars and the trenches between them), only the stacks on top of the pillars constitute the tweezers.

The tweezers stack is made of three main layers (***Figure 42***):

- A first layer, magnetic or not, constituting the bottom jaw and being covered by a thin gold layer intended for subsequent functionalization,
- A sacrificial layer in aluminum whose thickness determines the future hinge height and thus its flexibility,
- A second magnetic layer constituting the second jaw and being deposited on top of another thin gold layer.

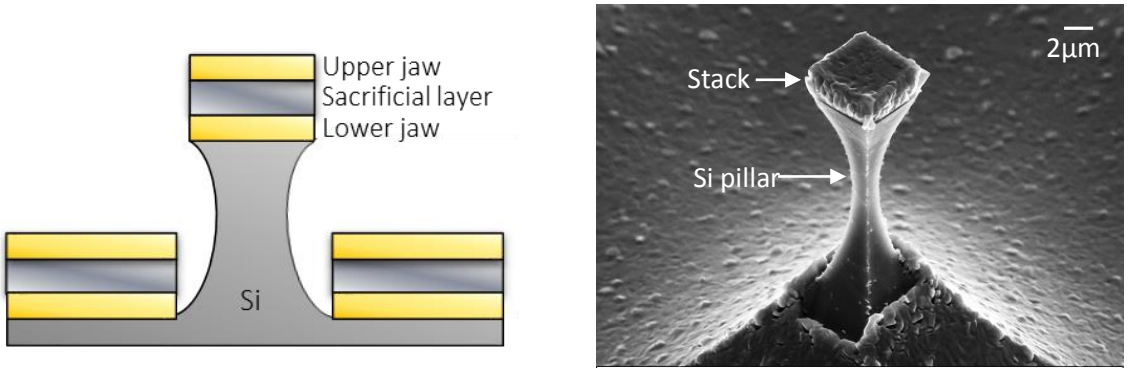

***Figure 42**: Example of stack with an upper jaw magnetically "soft" on top of a "hard" lower jaw, both separated by an Al sacrificial layer. The tweezers are located on top of the Si pillars.*

The typical stack is NiFe 200 nm, Au 15 nm, Al 350 nm, Au 15 nm, NiFe 200 nm. The study aiming at replacing NiFe by other materials to fabricate soft/non-magnetic and soft/hard tweezers is presented later in section **4.2.1**.

4.1.5 Hinge evaporation

The hinge consists in a gold layer deposited at oblique incidence on only one side of the tweezers, as pictured in ***Figure 43***. The deposition was performed by electron-beam evaporation rather than sputtering because it yields a better directionality (according to comparative experiments) and thus, limits the amount of gold deposited over the other lateral sides of the tweezers which may lock the tweezers in closed configuration.

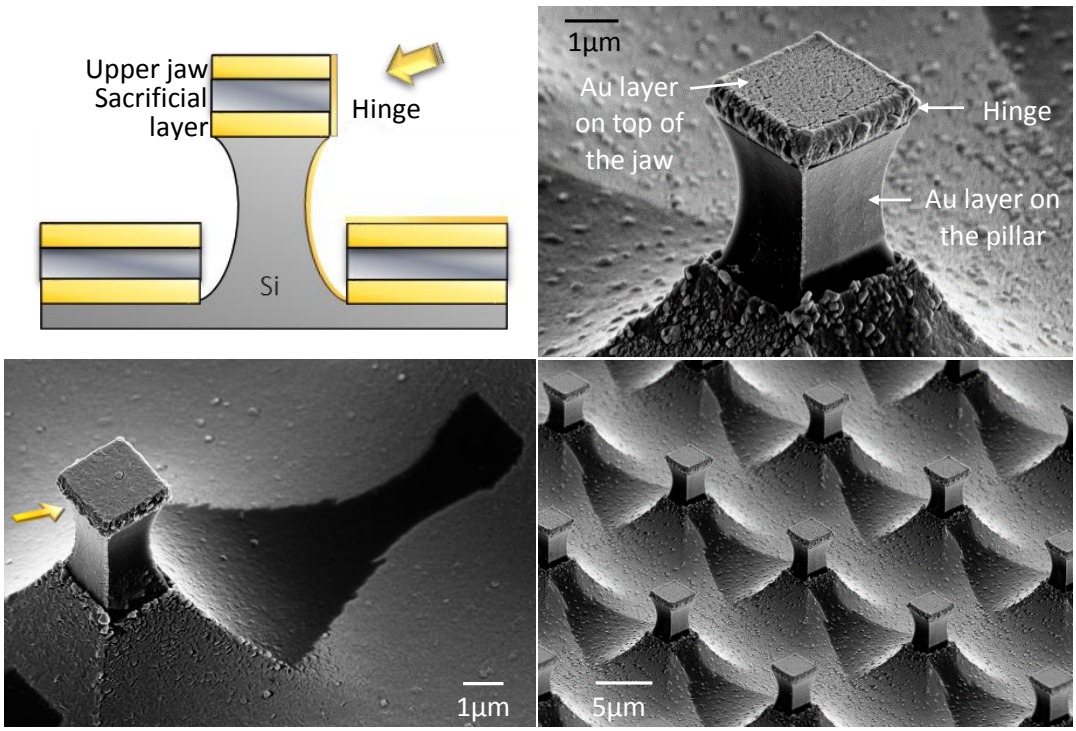

***Figure 43**: Evaporation of the hinge at oblique incidence on one side of the tweezers. Bottom: the pillars shade in the gold layer appears clearly on SEM images. The sharpness of the shade is a confirmation of the Au beam directivity (left: single tweezer after hinge evaporation; the lower jaw is in Co laminated with Ta and the upper jaw in NiFe laminated with Ta. Right: collection of tweezers after the hinge deposition from the right).*

The alignment of the sample in the evaporation chamber is carefully adjusted by hand (***Figure 44***). The vertical incidence of the deposition is then controlled by the motorized rotation of the sample holder. Finally, the speed and duration of the evaporation determines the hinge thickness and may impact its atomic structure. Its height is predetermined by the thickness of the jaws and the sacrificial layer deposited previously.

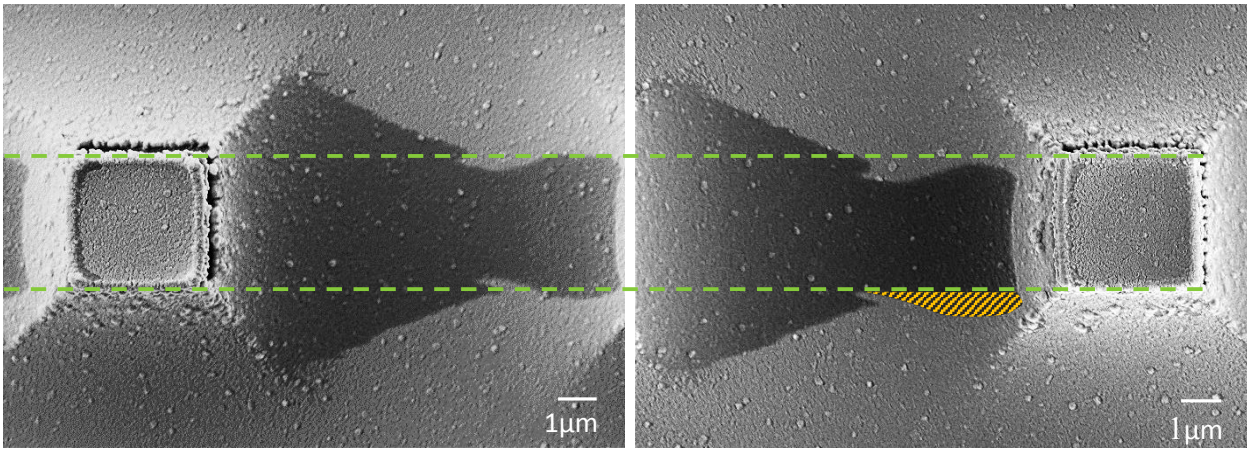

***Figure 44**: After hinge deposition, the Si pillars shadow in the gold layer informs on the quality of the alignment.*

To explore the hinge constitution and mechanical properties, hinges from 60 nm to 5nm thick were produced and compared in section **4.2.3**. Interestingly, when thinner than 30 nm, the gold layer was found to be no longer continuous but to present holes (***Figure 45***). Although this was first considered as a technological limit, very encouraging results were obtained with hinges 20 nm thick (see actuation trials in chapter **5**).

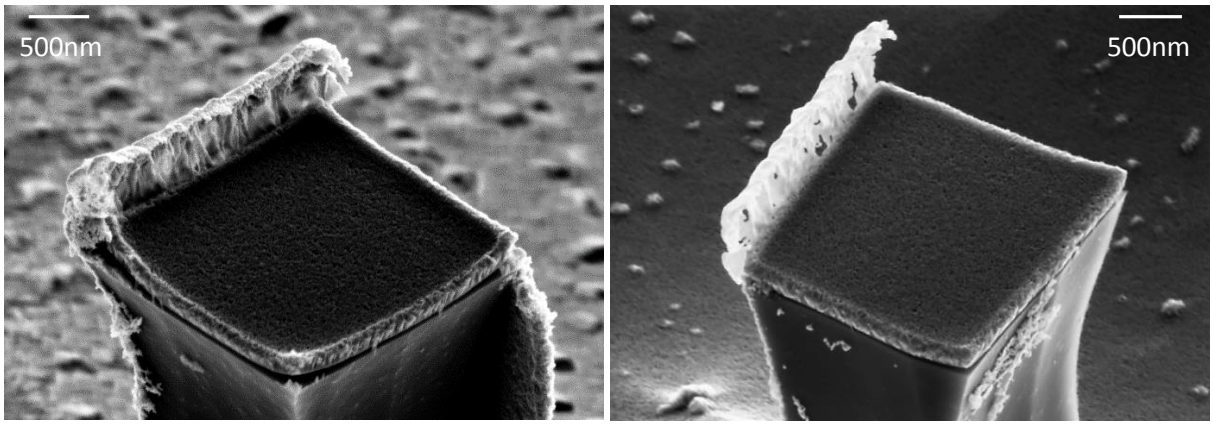

***Figure 45**: Tweezers which have lost their upper jaw offer an exclusive point of view on the hinge structure. Hinges look solid when their thickness is 60 nm (left), whereas they appear discontinuous (porous) at 30 nm (right). One can note the hinge wave-like curvature due to the sacrificial layer roughness.*

If the upper jaw is missing in the images right above, it is because the deposition angle of the hinge was too low (22° from the wafer plane, almost perpendicular to the tweezers targeted side). Indeed, this parameter is very important to make the hinge adhere

firmly to both jaws. Angles from 18° to 35° were tested. 30° was found to be the most suited for 2 µm side tweezers. The deposition angle needs to be adapted for each size of tweezers because mechanical strains within the tweezers can lift their edges (***Figure 46***) and modify significantly the slope of the tweezers sides. This phenomenon is stronger in tweezers comprising two jaws in Permalloy than in tweezers with only one jaw in Permalloy, while it is absent when the jaws are not in Permalloy. This suggests that the NiFe-Al interface is at the origin of this behavior.

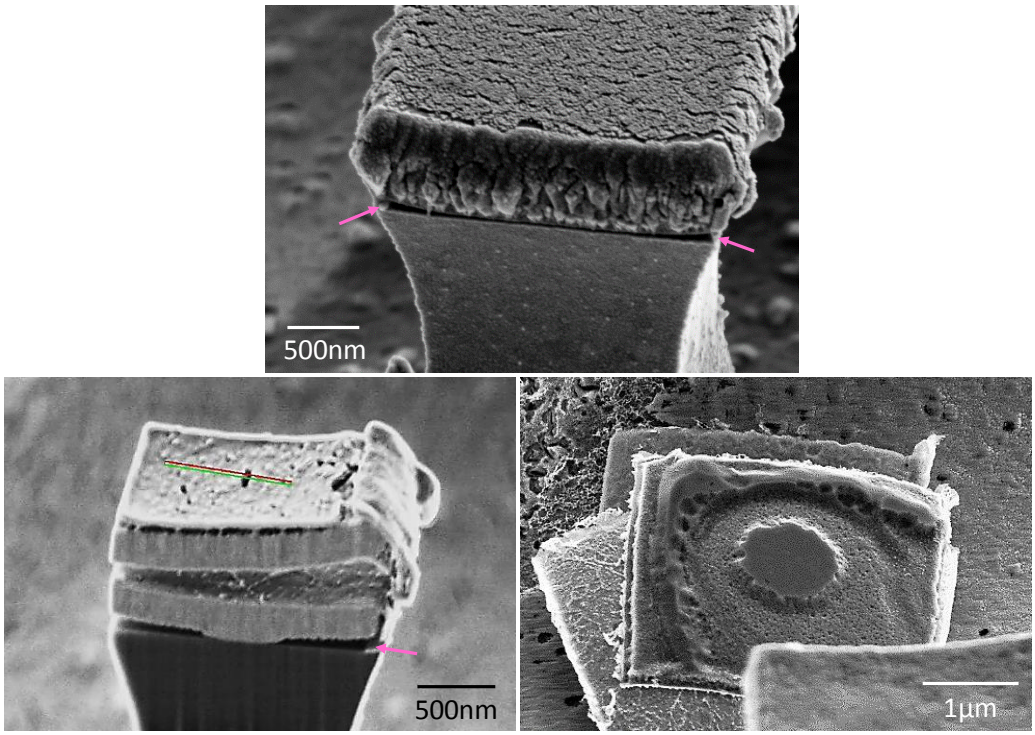

Figure 46*: Top: the strains between NiFe and Al layers lift the stack corners, providing an advantageous separation between the hinge and the rest of the gold layer on the pillar. Bottom left: side cut of a tweezer (by FIB) revealing the extent of the strains on the contact between the pillar and the lower jaw. Bottom right: A lower jaw found upside-down allows seeing the contact shape and surface state.*

Although the strains within the stack can hardly be controlled, the splitting of the gold layer between the tweezer and the pillar actually prevents the hinge from binding the tweezer to the substrate. Indeed, when the strains are not sufficient to separate the hinge from the rest of the gold layer, as it is the case for sub-micron tweezers (***Figure 47***), the latter can eventually get pulled down from their pillar.

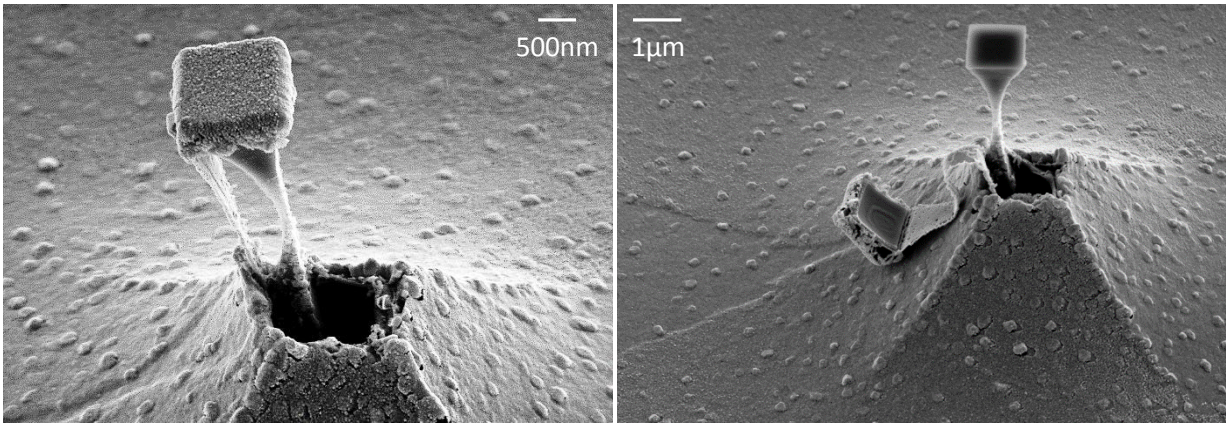

Figure 47*: Example of a tweezer (of 1.3 µm side with a lower jaw in Co/IrMn and an upper jaw in NiFe) with a hinge continuous to the ground. Left: The pillar is critically thin and bends under the hinge tension, realizing the first nano-catapult! Right: tweezers can eventually fall from the pillar.*

In the perspective of releasing the tweezers in solution, the tweezers bonding to the sample *via* the hinge will require particular attention.

4.1.6 Sides sharpening

Despite the efforts made on deposition directionality and sample alignment, a gold "muzzle" still forms and tends to lock the jaws together after the removal of the sacrificial layer (***Figure 48***). This may due to the fact that gold atoms can land on the Al layer imperfections or simply diffuse from the top of the upper jaw during the hinge evaporation.

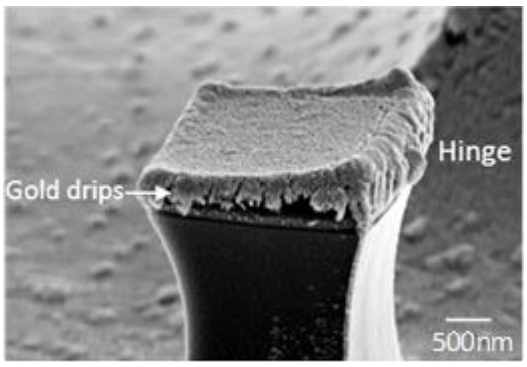

Figure 48*: SEM image of a tweezer after sacrificial layer removal showing the formation of a gold "muzzle" which prevents the tweezer opening.*

To evidence that this gold "muzzle" is keeping the tweezers closed, FIB (Focus Ion Beam) etching was used to clear the side walls of the tweezer. Thus, the three hinge-free sides of a collection of tweezers were milled with this technic, as shown in *Figure 49*.

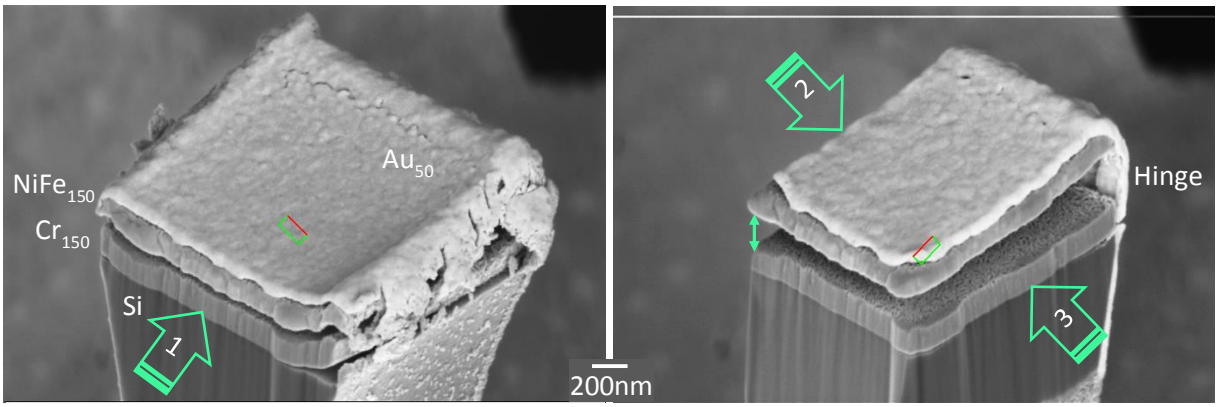

***Figure 49**: FIB etching procedure to clear the tweezer sides: first, the front side is etched until the jaws are no longer in contact, then gold is etched from left and right sides. Once freed, the upper jaw suddenly rises up due to the hinge restoring force.*

Once a tweezer got its sides cleared from gold drips, the upper jaw raised back to its idle position, parallel to the lower one. So besides confirming that the gold muzzle was indeed responsible for the jaws locking, this experiment also revealed the hinge solidity and restoring force.

Although this achievement enabled experimental characterization of the tweezers actuation (chapter **5**), FIB milling can be operated efficiently on only one tweezer at a time and is a rather slow operation. To allow collective actuation of an assembly of tweezers, it appeared necessary to develop a method to clean the sides of a whole sample at a time. Therefore, a step of Ion Beam Etching (IBE) was added after the hinge evaporation and before the sacrificial layer removal. Conveniently, an ion gun was available in the evaporator, allowing to deposit the hinge and subsequently carve the lateral sides of the tweezers (***Figure 50***).

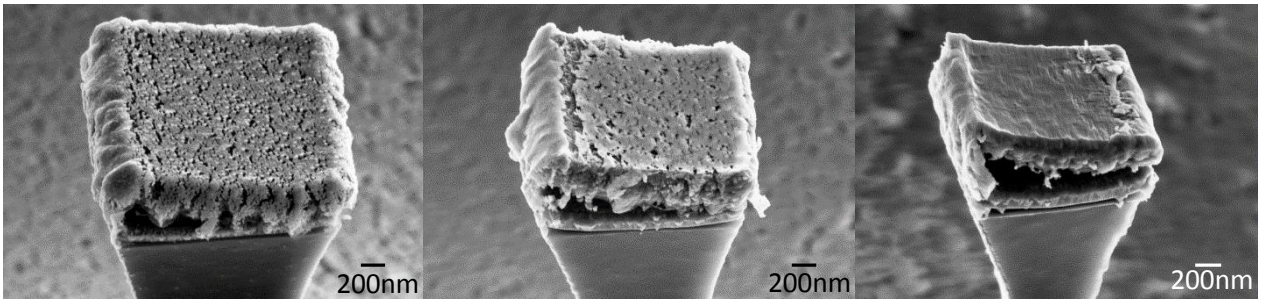

***Figure 50**: Examples of tweezers before (left), after one (middle) and after two (right) ion beam etching of their sides.*

4.1.7 Jaws release

Finally, the sacrificial layer (Al) is removed by chemical etching with *AluEtch 1960*, like in step **4.1.3**, and the upper jaw is ready for actuation (***Figure 51***).

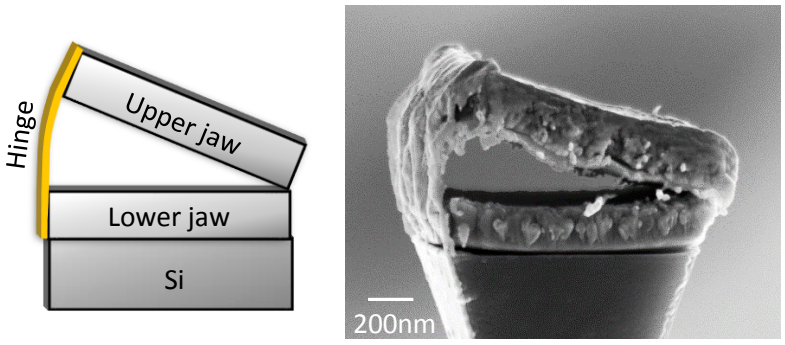

***Figure 51**: Side view of a tweezer after sacrificial layer removal by chemical etching.*

The incubation time in the acid solution depends on the tweezers lateral size: 20 min for 2 µm side tweezers and smaller, rather 1 h for 3 µm (at room temperature). The Al layer present in the trenches between pillars is also dissolved without altering the sample (***Figure 52***).

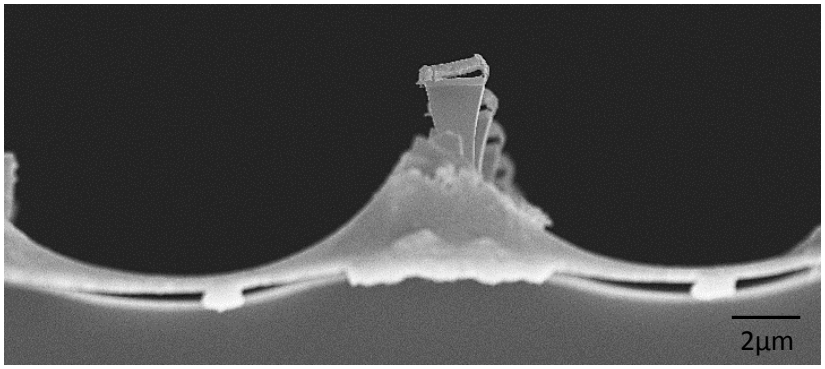

***Figure 52**: This SEM image acquired in chemical contrast mode shows that the Al sacrificial layer present in the deposit in the trenches between pillars is also dissolved during the process.*

The jaws release is a delicate operation because it can damage the sample. In particular, during the sample drying, the capillary forces due to the liquid removal pull on the jaws and can eventually break the bound between the hinge and the jaws. In most of the case, it only closes the tweezers (***Figure 53***). Unfortunately, once closed the capillary forces added to van der Waals interactions and the Casimir effect become significant and maintain the tweezer closed unless the contact area is cut by FIB milling.

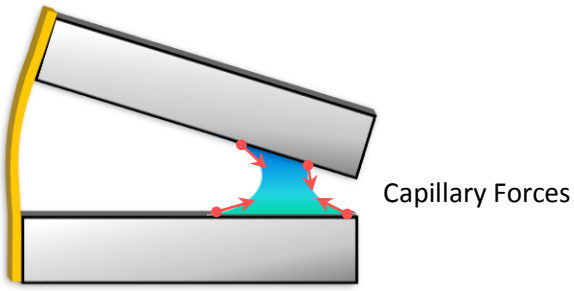

***Figure 53**: Representation of a liquid meniscus pulling on the jaws, leading to the tweezer closing.*

To avoid this as much as possible, the liquid removal should be made as quick as possible so that water meniscus does not form between the jaws. A set-up, the super critical drier or "MEMs Drier", is intended to dry sensitive samples by immersing them in liquid CO which is then brought at its triple point and evaporated instantaneously.

However, the transfer of the samples from one clean room to another in liquid conditioning and the flux of the CO replacing the initial alcoholic solution in which they are

immersed contribute to damage the sample. Therefore, simpler methods with comparable results were preferred. Indeed, heating the samples at more than 100°C on a hot plate for a few minutes yielded satisfying results. Another method consisted to replace water by ethanol, which has a lower surface tension than water; the results were also good but the simpler the better.

4.2 Exploration of various physical parameters

The fabrication of the three types of tweezers presented in the introduction was tested: soft/soft tweezers (two magnetic soft jaws), soft/non-magnetic tweezers (with a non-magnetic lower jaw) and soft/hard tweezers (with a hard magnetic lower jaw). While soft/non-magnetic and soft/soft tweezers could be successfully produced, adhesion problems were encountered in the making of soft/hard tweezers. These trials are presented below in section **4.2.1**.

To further explore the versatility and limitations of the fabrication process, tweezers with varying dimensions were fabricated. The samples obtained with jaws measuring from ~800 nm to 10 µm lateral dimension and hinges of 5 to 60 nm thick are succinctly listed at the end of this chapter, in sections **4.2.2** and **4.2.3**.

4.2.1 Jaws materials

4.2.1.1 Soft/non-magnetic tweezers

Soft/non-magnetic tweezers are made of a lower jaw in chromium and a top jaw in Permalloy (***Figure 54***). No particular problems related to the materials were encountered during the fabrication.

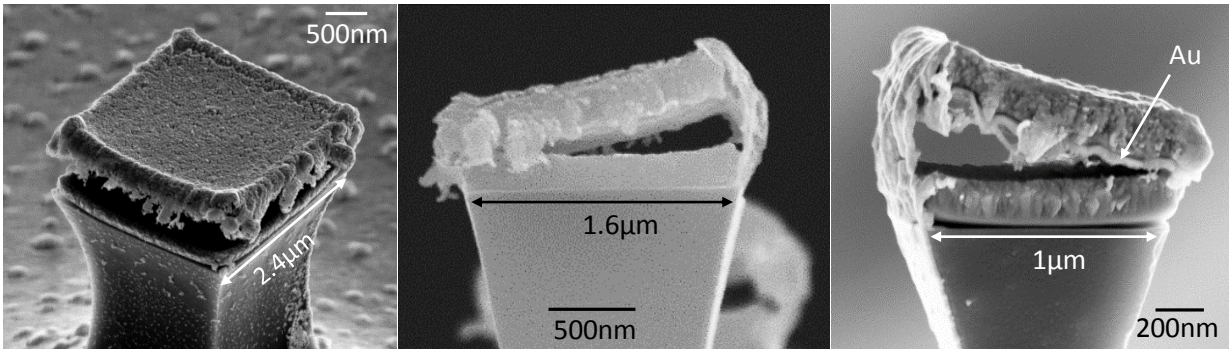

***Figure 54**: Soft/non-magnetic tweezers with a lower jaw in Cr (150 nm) at the end of the process. Left: Upper jaw in NiFe (150 nm), Au hinge of 65nm deposited at 22° plus 50 nm deposited with normal incidence on the top of the tweezer. Middle: Upper jaw in NiFe (250 nm), Au hinge of 23 nm deposited at 30°. Right: Same parameters except that the tweezer is only 1 µm wide and that gold layers were added inside the jaws.*

4.2.1.2 Soft/soft tweezers

Soft/soft tweezers are composed of two jaws in Permalloy measuring 250 nm thick (***Figure 55***). This kind of tweezers exhibits more strains and their edges are often more bended than soft/non-magnetic tweezers.

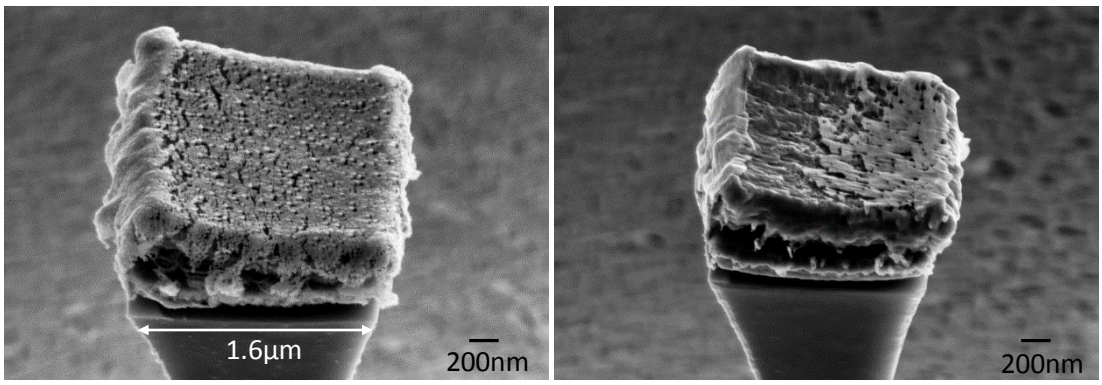

***Figure 55**: Left: soft/soft tweezer after jaw release, with a hinge of 23 nm deposited at 30° on the left. Right: same sample but with a 35 nm thick hinge and after IBE etching.*

4.2.1.3 Soft/hard tweezers

To make the "hard" lower jaw of soft/hard tweezers, the magnetic material with a coercivity higher than NiFe and CoFe selected for trials was exchange-biased cobalt/IrMn based multilayers. Indeed, permanent magnet materials such as NdFeB or $SmCo_5$ have a larger coercivity but were not directly available for preliminary tests. The coercivity of cobalt was purposely enhanced by biasing its magnetization using the exchange interaction

through the interface between an antiferromagnetic (AF) layer (IrMn) and the Co ferromagnetic (F) layer [1]. This F/AF pinning scheme, so-called exchange bias, is frequently used in spintronics devices to pin the magnetization of a reference layer and thereby define a reference direction for the spin of the electrons. Here, we use this pinning scheme to maintain the magnetization of the bottom jaw in a fixed direction. To maximize the proportion of interfaces in the volume of the jaw and more strongly pin the Co magnetization in the plane of the bottom jaw, thin antiferromagnetic layers of iridium-manganese alloy (20 % of Ir and 80 % of Mn) of 5nm were stacked with thin Co layers of 6nm. This stack was repeated 15 times, resulting in a jaw 165 nm thick. To avoid oxidization on one side and promote adhesion to the substrate on the other side, the stack was sandwiched between two layers of tantalum (3 nm). Once the magnetization of IrMn is set by annealing (30 min at 250°) under the application of an in-plane magnetic field, the hysteresis loop of the stack is shifted. This results in the magnetization remaining in a fixed direction up to the exchange bias field defined by the field shift of the hysteresis loop (~25 mT in ***Figure 56***).

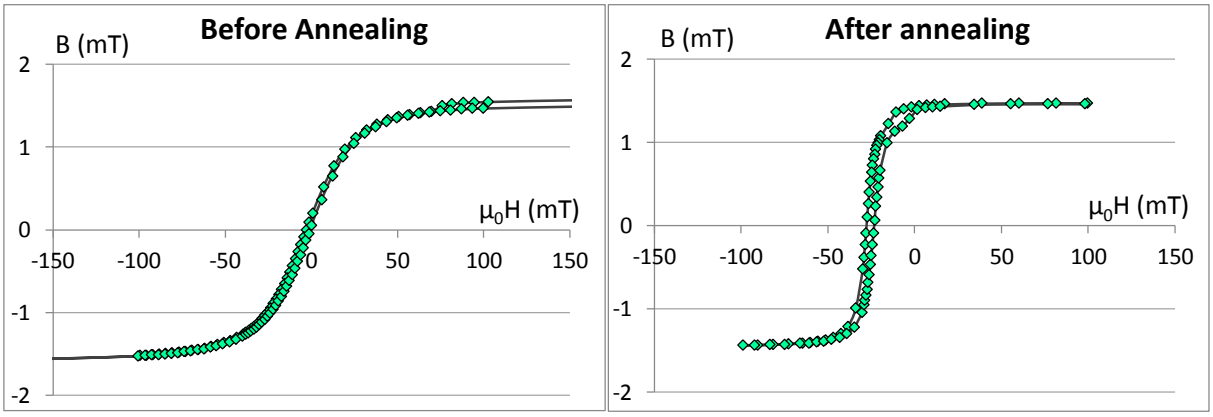

***Figure 56**: Vibrating Sample Magnetometer (VSM) measurements before and after annealing of a stack of $Ta_{(3nm)}/IrMn_{(5nm)}/\{Co_{(6nm)}/IrMn_{(5nm)}\}_{x15}/Ta_{(3nm)}$. The shift corresponds to the exchange bias field.*

Using this stack for the lower jaw, soft/hard tweezers were fabricated with an upper jaw in Co (150 or 200 nm) and NiFe (150 nm). The sacrificial layer in aluminum was 350nm thick and was surrounded by two $Ti_{(4nm)}/Au_{(16nm)}$ layers.

However, these samples completely pilled-off the substrate before the end of the fabrication process due to internal stress and poor adhesion on the Si substrate (***Figure 57***).

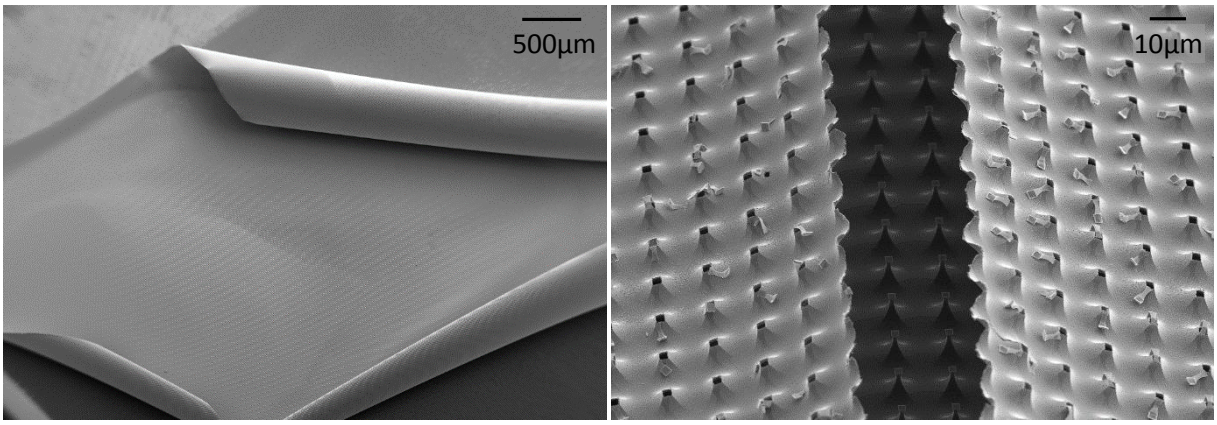

Figure 57*: Pilling-off of the sample from the silicon wafer (lower jaw in Co/IrMn, upper jaw in NiFe). Left: macroscopic view of a curled sample; right: zoom on a fracture of the ground layer revealing stripped silicon pillars underneath.*

Similarly, jaws in pure Co did not adhere properly to silicon (so the tweezers fell from their pillar at the end of the process) and neither to gold since the hinges tended to detach from the tweezers (illustrated in ***Figure 58***). Tweezers made of two jaws in pure cobalt were too unstable to reach the end of the fabrication process. The same observation was made for two jaws in laminated Co.

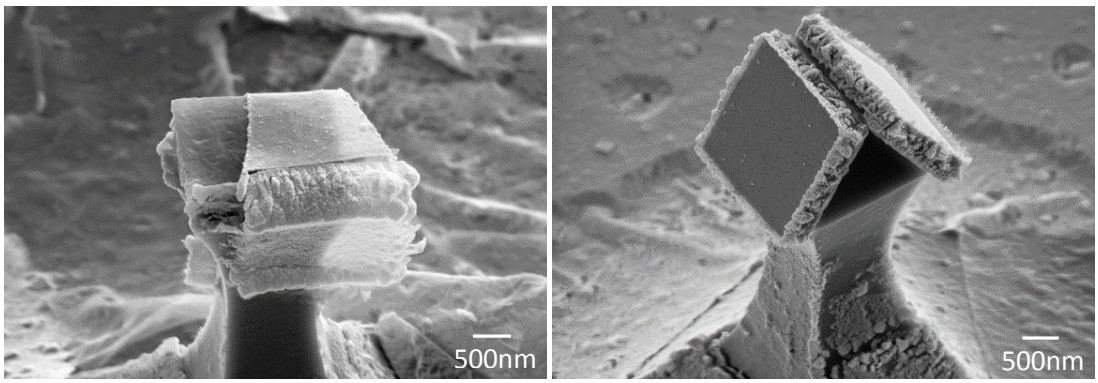

Figure 58*: Examples of tweezers comprising at least one jaw in 200 nm of cobalt. Left: gold hinge detached from the top jaw in Co (lower jaw in Cr, 150 nm). Right: two tweezers (both jaws in Co capped by a Ta layer) in an unexpected position on top of a Si pillar.*

Therefore, the adhesion of Co on SiO_x was successfully improved by the addition of a Ta underlayer known for its good adhesiveness on oxides (thanks to Ta-O bonding). On the other hand, the adhesion of the Au hinge on Co was improved by the addition of a titanium layer known to form alloys with Au and Co (6nm also deposited at oblique incidence).

The cohesion within Co layers was itself improved by adding tantalum thin layers (Co/Ta). Indeed, Ta is known to break the grain growth during the Co layer deposition, which reduces the internal stress in the layer and therefore the tendency to pill-off. In particular, tweezers with a lower jaw in Co/Ta and an upper jaw in NiFe, also laminated with Ta, were successfully produced (***Figure 59***). The same lower jaw put with a top jaw in CoFe exhibited a weaker adhesion to the silicon pillars.

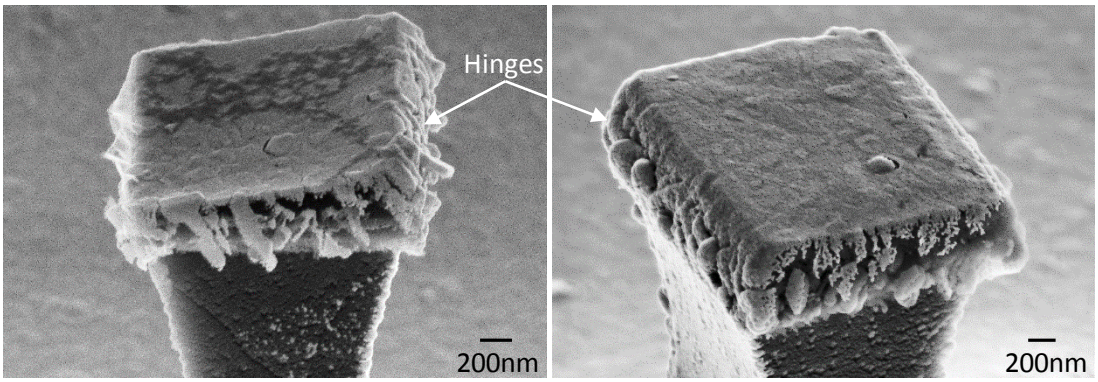

Figure 59*: Soft/hard tweezers comprising a lower jaw in Co laminated with Ta after chemical etching of the sacrificial layer. Left: tweezer with a top jaw in NiFe laminated with Ta yielded good results. Right: tweezer with an upper jaw in CoFe (200 nm) were more prone to detach from their pillars.*

Tweezers with an upper jaw in Co/Ta (tested with a lower jaw in Cr) adhered properly to the substrate. However, due to time constrain, the efforts in the following of the thesis were focused on the characterization of the actuation of two functional tweezers prototypes (a ferromagnetic/non-magnetic tweezer: NiFe on top of Cr and a ferromagnetic/ferromagnetic tweezer with two jaws in NiFe).

4.2.2 Jaws dimensions

The tweezers fabrication process was designed to allow the fabrication of tweezers with a variety of size in order to adapt them to the objects that they are supposed to grab. Since biological objects cover a wide range of dimensions comprised between tens of nanometers for viruses and antibodies to several microns for the smallest human cells [2], tweezers from ~800 nm to 10 µm side were fabricated (***Figure 60***). Since the jaws thickness cannot be increased due to adhesion issues, only the lateral size was varied in this exploratory study.

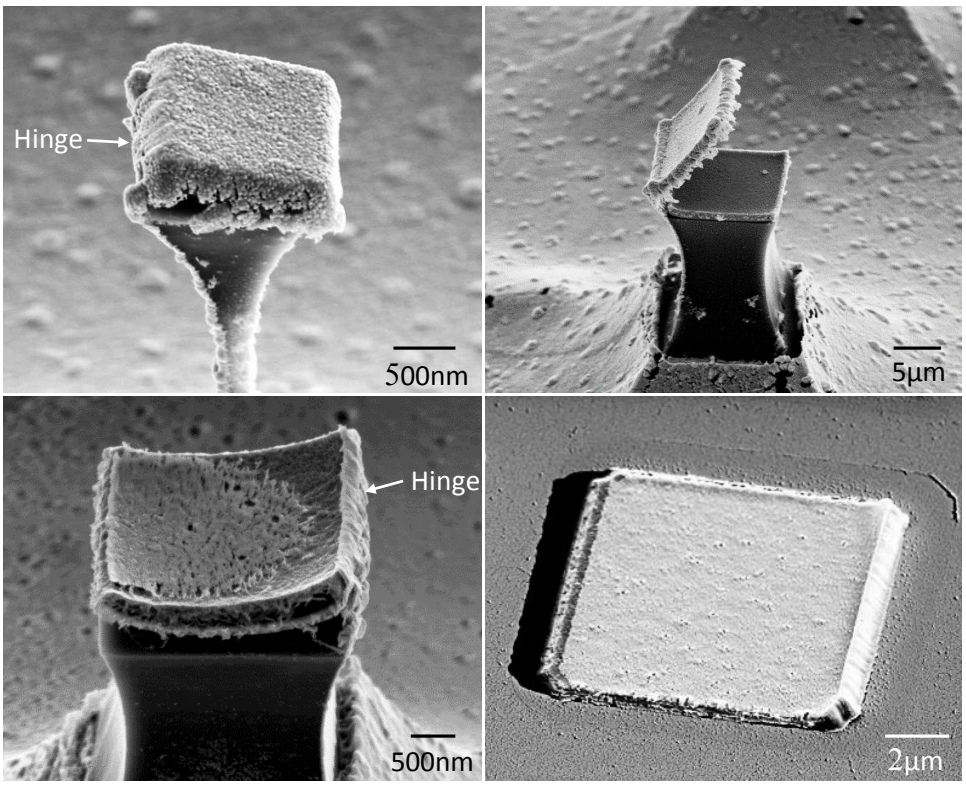

Figure 60*: a) 1.3 µm side soft/hard tweezer. b) 2.4 µm large soft/non-magnetic tweezer opened due to internal strains within the hinge. c) Soft/soft tweezer of ~3 µm in size. d) 10 µm large soft/soft tweezer fabricated with a resist-based process (no silicon pillars) due to their size. At this scale, the upper jaw collapses, most likely due to van der Waals and Casimir attraction with the lower jaw.*

Since the fabrication process was developed for tweezers of ~2 µm wide, this dimension is the one yielding the best results. If a significant modification of the tweezers

size was required, the strains within the jaws should be released and the sacrificial layer thickness should be adapted.

4.2.3 Hinge thickness

During the development of the fabrication process, the hinge was the object of a short study to determine its optimal thickness in the perspective of actuation experiments. Therefore, hinges with varying thicknesses (from 5 nm to 60 nm) were fabricated.

The tests started with rather thick and robust hinges of 60 nm (65 nm of gold evaporated with 22° incidence). SEM observations were encouraging (***Figure 61***) but mechanical actuation showed that they were too stiff to allow the tweezers wide opening (see chapter **4**).

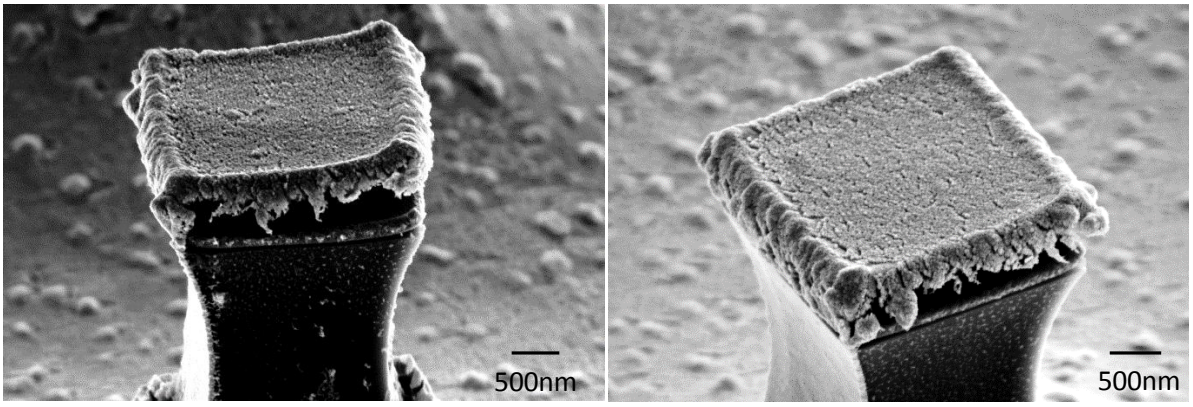

Figure 61*: Soft/non-magnetic tweezers of 2.4 µm wide and a 60 nm thick hinge (on the tweezers left side).*

On the other hand, these tests revealed that hinges of 5 nm and 10 nm were too fragile to be reproducibly produced and actuated, at least with the current fabrication process (***Figure 62***).

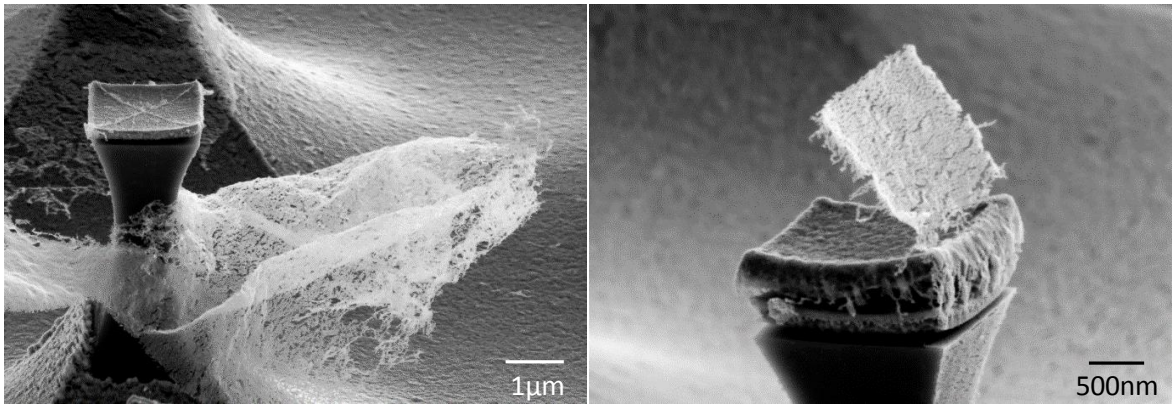

***Figure 62**: Examples of soft/soft tweezers with extra-thin hinges deposited at 30°. At 5 nm (left), the hinge is too fragile to withstand the final wet step and the thin gold layer deposited on the ground of the sample detaches from the rest of the stack. At 10 nm (right), the hinge is able to keep two jaws together but breaks too easily.*

After optimization, hinges with intermediate thickness such as 15, 20 and 30 nm yielded the best results (***Figure 63***). Their robustness makes them easier to reproduce while their porous aspect indicates a good potential flexibility.

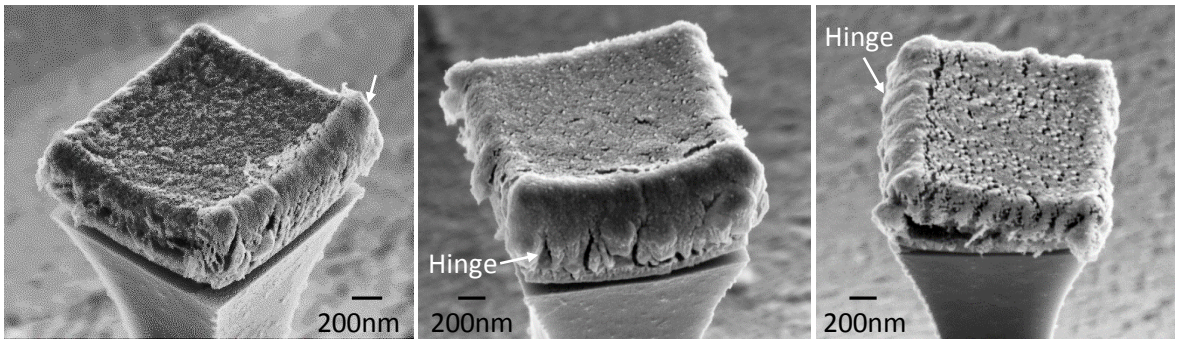

***Figure 63**: Examples of hinges of 15, 20 and 30 nm thick (from left to right) at the end of the fabrication process (evaporation incidence: 30°). The thinner, the more porous.*

4.3 Conclusion

The technological elaboration of micro/nano-tweezers was one of the main goals of this thesis work and was successfully carried out. Difficulties were encountered at each stage of the process, which was elaborated step by step from the silicon wafer preparation to the sacrificial layer removal at the PTA's cleanroom.

Soft/non-magnetic tweezers comprising a lower jaw in chromium and an upper jaw in Permalloy and soft/soft tweezers (both jaws in Permalloy) were fabricated. The elaboration of functional soft/hard tweezers would require additional work and could not be achieved in the frame of this thesis.

Various dimensions were tested for the jaws width (from less than 1 µm to 10 µm) and for the hinge thickness (5 to 60 nm). Finally, tweezers with jaws 2 µm wide and a hinge 20 nm thick were selected to perform the magnetic actuation experiments presented in the next chapter (**5**).

4.4 References

[1] M. M. Ali, C. H. Marrows, M. Al-Jawad, B. J. Hickey, A. Misra, U. Nowak and K. D. Usadel, "Antiferromagnetic layer thickness dependence of the IrMn/Co exchange bias system", *Phys. Rev. B,* vol. 68, no. 21, 2003.

[2] G. S. L. Center, «Cell Size and Scale» 22 June 2014. [Available Online: http://learn.genetics.utah.edu/content/cells/scale/.

5 Tweezers actuation: experimental characterization and modeling

This chapter reports the experimental demonstration of the tweezers magnetic actuation and the characterization of the hinge mechanical behavior. First, the experimental setup used in these experiments will be presented. It allows to test the hinge flexibility by applying a mechanical pressure and to approach a local micro-source of magnetic field in the proximity of an individual tweezer.

Then, the movies acquired during magnetic actuation will be analyzed using the theoretical model described in chapter 3. The motion of the upper jaw will be interpreted in terms of torques due to the external magnetic field on the upper jaw magnetization and, when applicable (*i.e.* when the two jaws are magnetic), to the magnetostatic interactions between the two jaws. These driving torques are counterbalanced by the elastic torque associated with the hinge stiffness. Through these experiments and their interpretation, a qualitative description of the hinge structure is proposed.

5.1 Experimental setup

The characterization of the tweezers magneto-elastic behavior were performed at the *Plateforme de Nano-caractérisation* (PFNC) inside a SEM (Scanning Electron Microscope) equipped with a FIB (Focused Ion Beam) with Eric Gautier's help from SPINTEC. The setup, shown in ***Figure 64***, comprises an electron gun, a Gallium ion gun (Ga^+) and a probe joined together with the ion gun. This probe has a rather large end and can only be moved back and forth along the ion gun axis. Therefore, another probe more suited to the needs of our experiment was added by Eric Gautier on the platform carrying the sample.

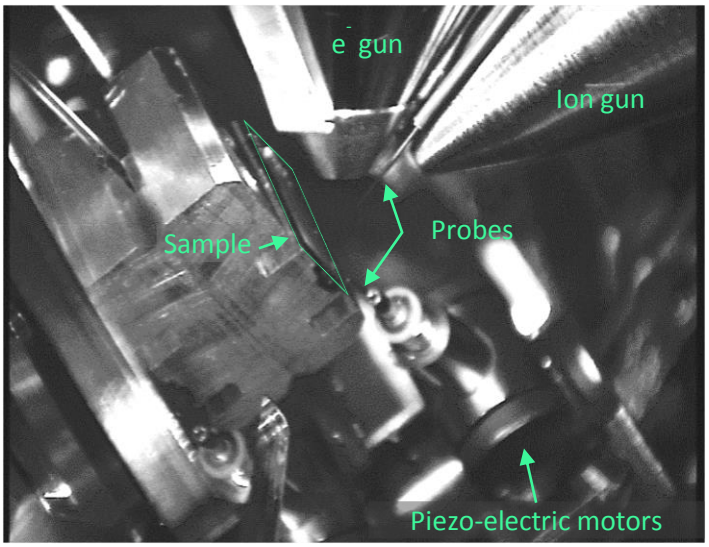

***Figure 64**: Setup in the SEM: the sample is under an electron gun, an ion gun and a micro-manipulated probe. An additional probe with three degrees of freedom was added to the setup, to which AFM or MFM tips can be attached to address the tweezers individually.*

The additional probe is commanded by piezo-electric motors and can be moved with three degrees of freedom: backward and forward, up and down and clockwise and counter-clockwise rotation. Besides offering more flexibility than the pre-existing probe, this one can easily be taken out of the SEM chamber and equipped with an AFM tip (***Figure 65***) to address single tweezers. To avoid electrostatic interactions between the tip and the sample, a thin coper wire was used to link the end of the probe (so the tip too) to the platform on which the sample was glued with a conductive carbon bond.

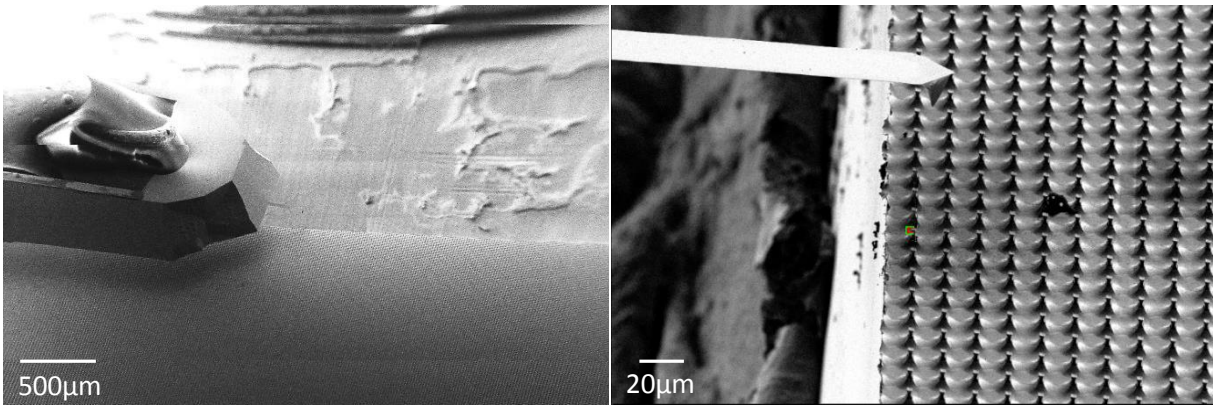

***Figure 65**: Left: SEM image of an MFM tip above an array of tweezers. Right: FIB image of the cantilever addressing a single tweezer.*

Positioning the tip on top of a given tweezer while having only a two dimensional feedback was a tricky operation. Therefore, the tip motion was controlled by using successively the two viewpoints offered by the electron and the ion guns, oriented at 54° from each other. However, ion imaging can damage the sample and in particular the gold layers (***Figure 66***).

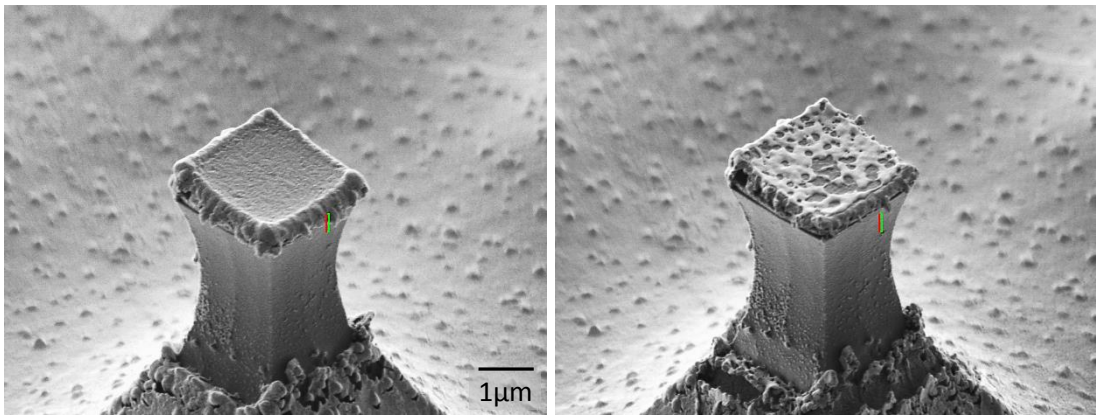

Figure 66*: Tweezer before and after extensive ion imaging: the gold layer exposed to ions has melt and coalesced. The red and green boxes are used to delimit the area etched by FIB and are not related to the image acquired by SEM, although it appears on it.*

When the tweezer edges have been cleaned from gold drips, a prolonged exposure to the ion beam can even trigger the tweezer opening, due to stress in the hinge associated with Au diffusion (***Figure 67***).

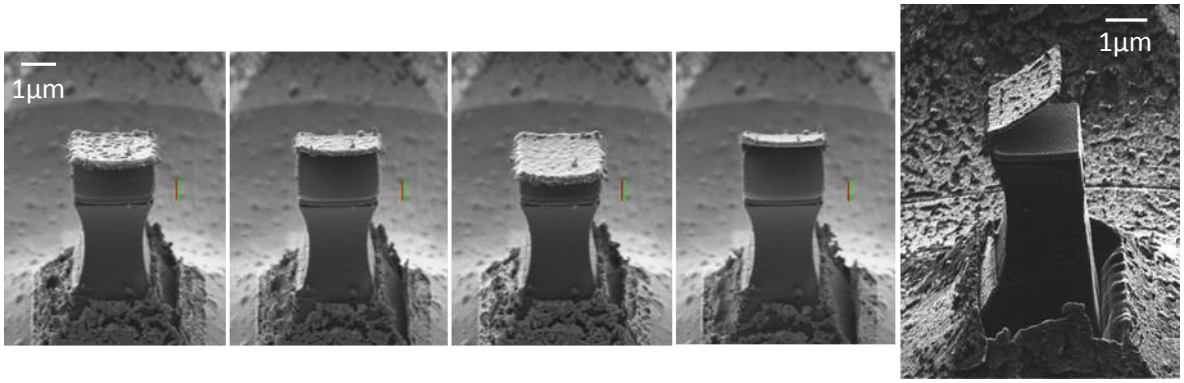

Figure 67*: Tweezer exposed to ions and imaged by SEM over a 1 min period: the melting of the gold hinge causes the tweezer opening.*

Consequently, ion beam imaging was used only parsimoniously to position the tip in order to prevent the hinge from melting.

5.2 Mechanical actuation and check of the elasticity of the hinge

Using the setup described above, a mechanical pressure was exerted repeatedly on the upper jaw of a tweezer with an AFM tip (***Figure 68***). The tweezer response was monitored in real time by SEM imaging.

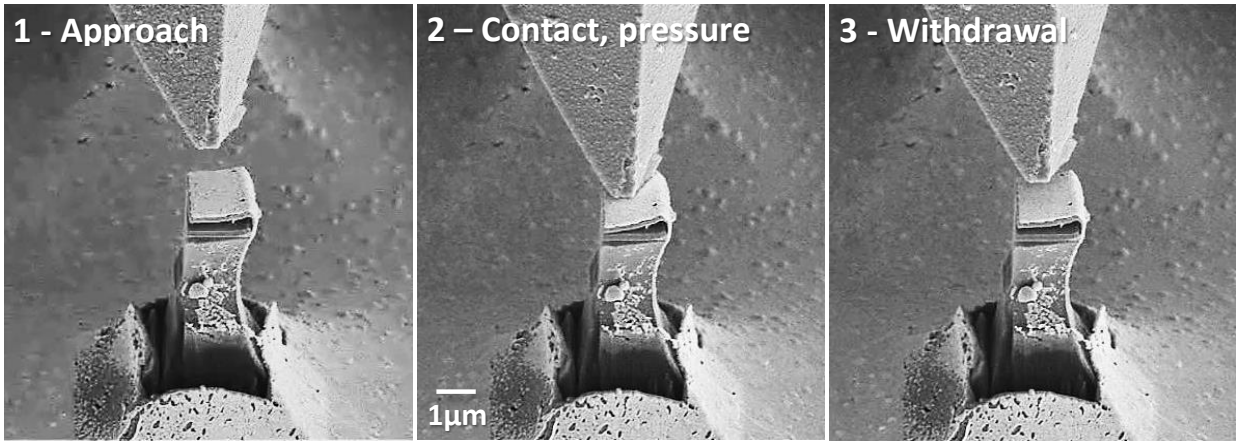

Figure 68*: An AFM tip attached to a micro-manipulated tip is approached from a tweezer inside a SEM (hinge thickness = 60 nm). The tweezer closes under the tip pressure and comes back to its rest position when the tip is drawn back, demonstrating the resistance and flexibility of the gold hinge.*

The tweezer, with initially parallel jaws, closes under the pressure and opens back when the tip is lifted back up. In a few cases, the tweezer remained closed, probably due to van der Waals or Casimir forces but could be re-opened by pulling on the side of the upper jaw with the tip.

This behavior demonstrates that a hinge of 60 nm thick allows small bending without breaking and moreover, that it yields a restoring force able to hold the upper jaw horizontally. However, magnetic actuation trials showed that hinges of this thickness were too stiff to allow a significant opening of the tweezer. A better compromise between robustness and flexibility was found for hinges of 20 nm. This could be noticed straightaway

as that the upper jaw did not lift back up once released from the gold muzzle by FIB. Magnetic actuation of tweezers with a 20 nm thick hinge confirmed this observation and yielded wider openings. These results are presented in the next section.

5.3 Magnetic actuation with a micro-magnet inside a SEM

The purpose of this experiment was to evidence the response of a tweezer to a magnetic field. The size of the tweezer (800 nm to 2 µm wide) does not allow observing the upper jaw motion with an optical microscope. Therefore the experiment was performed inside a SEM. However, the generation of a magnetic field inside a SEM can disturb the electrons path and thus, the image acquisition.

The solution presented here is to generate an extremely local magnetic field with a microscopic source in the vicinity of a single tweezer.

The first trials were performed with MFM-LM tips (Magnetic Force Microscopy tip with a Low Moment). The tweezers reacted to the tip approach but the amplitude of the upper jaw motion was too small to be clearly observed and quantified. Therefore, micromagnets were attached at the end of the tip to increase the magnetic field amplitude. In a first phase, a fragment of NdFeB magnet was attached to the tip but it emitted a strong and strongly anisotropic magnetic field which heavily deformed the SEM images (***Figure 69***). Despite cautious adjustments, the tweezer beneath the magnet could not be imaged properly.

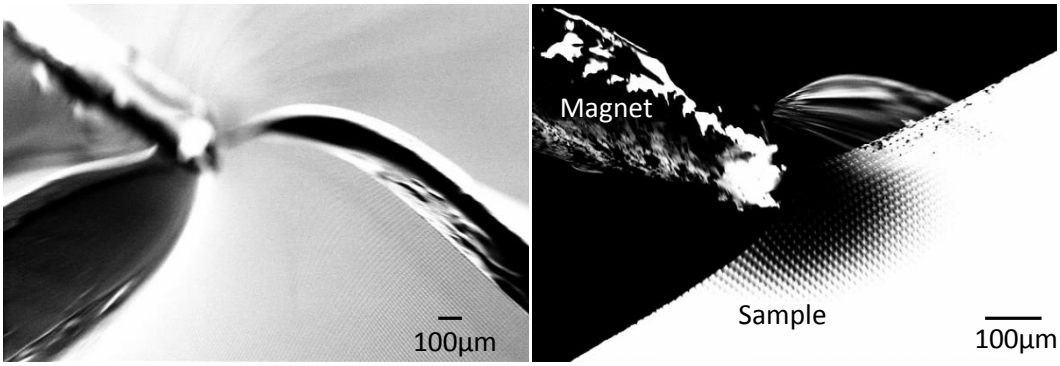

***Figure 69**: SEM images of the NdFeB fragment near the sample illustrating the large deflection of electrons in the vicinity of the magnet. Left: with settings adjusted before the approach of the magnet, right: best setting possible.*

Ion imaging could help in such situation, since ions are less deflected than electrons by the magnetic field due to their mass. However, prolonged exposure of the sample to ion beam leads to the tweezers melting. Therefore, a smaller source of magnetic field with a controlled shape is preferable. In particular, NdFeB microspheres (provided by Nora Dempsey from Néel Institute) yielded good results (***Figure 70***) and were therefore chosen to carry out the magnetic actuation trials.

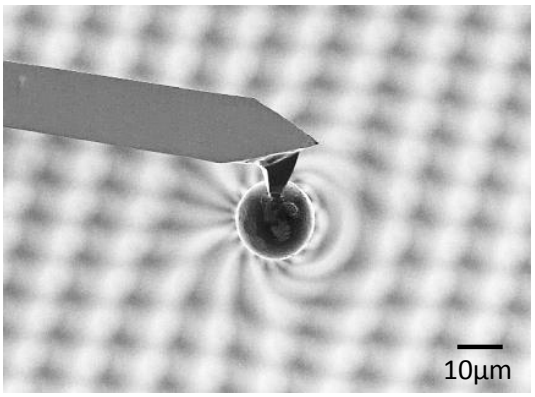

***Figure 70**: NdFeB sphere of 12 µm in diameter soldered to an MFM tip above an array of tweezers (out of focus). The deflection the image is more local and isotropic and thus easier to compensate with proper settings.*

5.3.1 Magnetic microsphere preparation

Bringing a magnetic microsphere in the vicinity of a single tweezer implies various preparation steps from the sphere selection from a powder to the careful three-dimensional approach to the sample, including soldering the microsphere to an AFM or MFM tip.

The NdFeB spheres are available in the form of a powder with a rather high dispersion in size, with a mean diameter of 50 µm. To select one sphere of proper diameter among such dispersed sample, the powder is diluted in water and a drop of this suspension is deposited on a small wafer for spreading and drying. The dispersed spheres can then be imaged by SEM and one of them selected with an accurate measurement of its diameter (***Figure 71***).

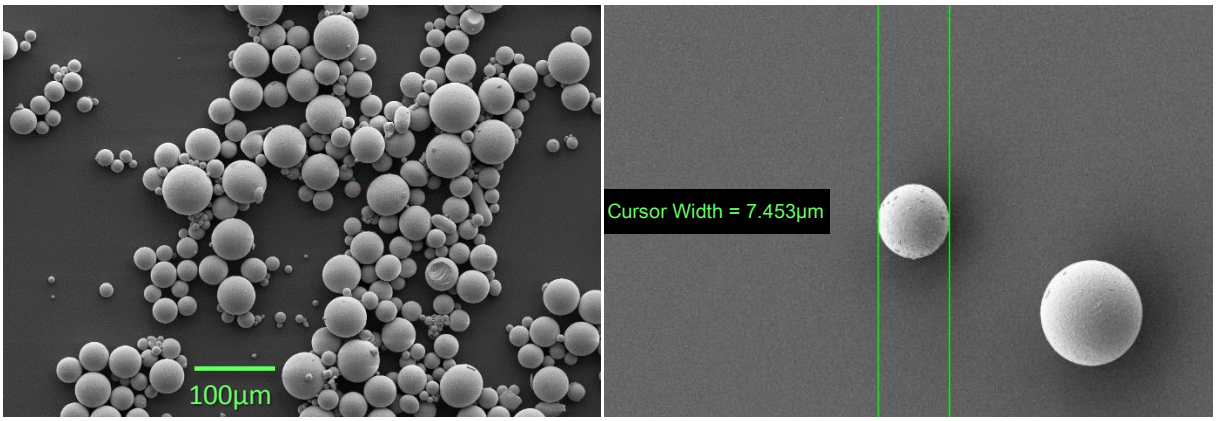

Figure 71*: Selection of a NdFeB sphere among a powder dispersed on a Si wafer.*

The probe joined to the ion gun is carefully approached to the selected sphere. Once in soft contact (too much pressure can make the sphere leap away), the probe and the sphere can be soldered together with a Tungsten bond. This bond is created by gas-assisted deposition. First a precursor gas of tungsten: hexacarbonyl ($W(CO)_6$) is sent and adsorbed on the surface. Then, the targeted area is scanned with the Ga^+ ion beam to dissociate the molecules into volatile (organic) and non-volatile (tungsten) components. The latter remain on the surface.

The sphere is then moved toward the AFM tip whose apex was previously flattened by FIB etching (***Figure 72***). The sphere and the AFM tip are soldered together before releasing the sphere from its first bond with the probe by FIB etching.

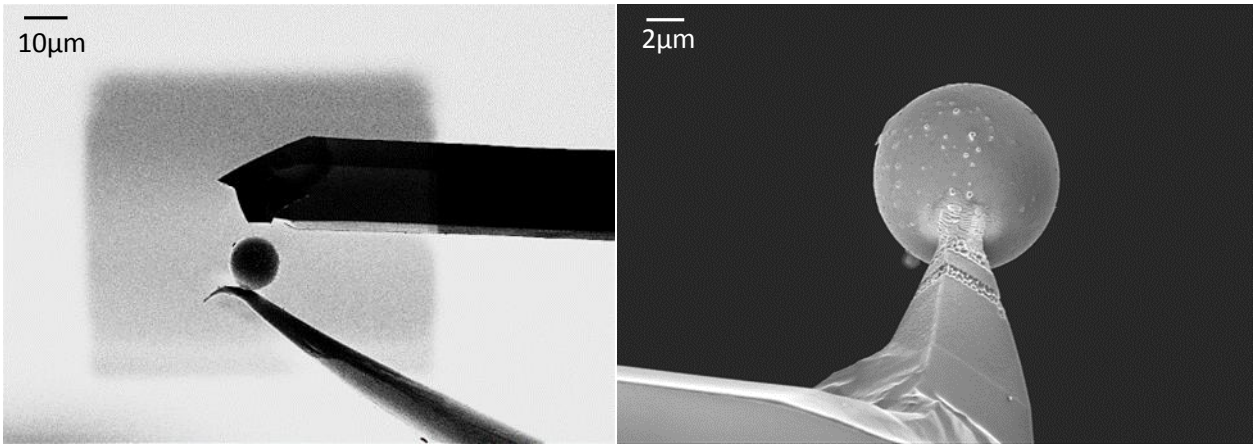

Figure 72*: Sphere fixation on an AFM tip apex by FIB soldering and etching. Left: the sphere is approached to the flattened tip after being soldered to a micro-manipulated probe. Right: the sphere has been successfully transferred from the probe to the AFM tip.*

Once the NdFeB microsphere has successfully mounted on the AFM tip, this assembly can be removed from the SEM chamber to get the sphere properly magnetized. To do so, the modified tip is brought between the poles of a vibrating sample magnetometer (VSM) electromagnet and submitted to a 1.7 T magnetic field.

Finally, this assembly can be attached to the apex of the 3D micro-manipulator inside the SEM and approached to the tweezers (***Figure 73***) to magnetically actuate individual tweezers.

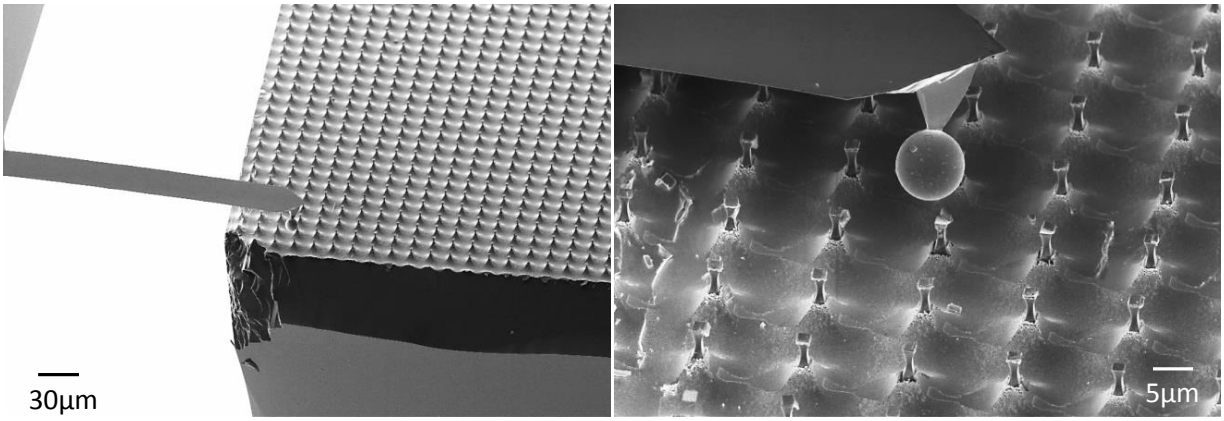

Figure 73*: SEM images of the NdFeB sphere attached to a MFM tip and approached to the sample's surface (left) and to a single tweezer (right).*

5.3.2 Observations

The sequence of action required to perform this experiment is quite long and requires lot of care. Nevertheless, the magnetic actuation of the tweezers could be observed by SEM imaging and recorded for subsequent analysis for a few of them.

Two sequences, one with a soft/non-magnetic tweezer and one with a soft/soft tweezer, were selected and analyzed with the software ImageJ (***Figure 74***).

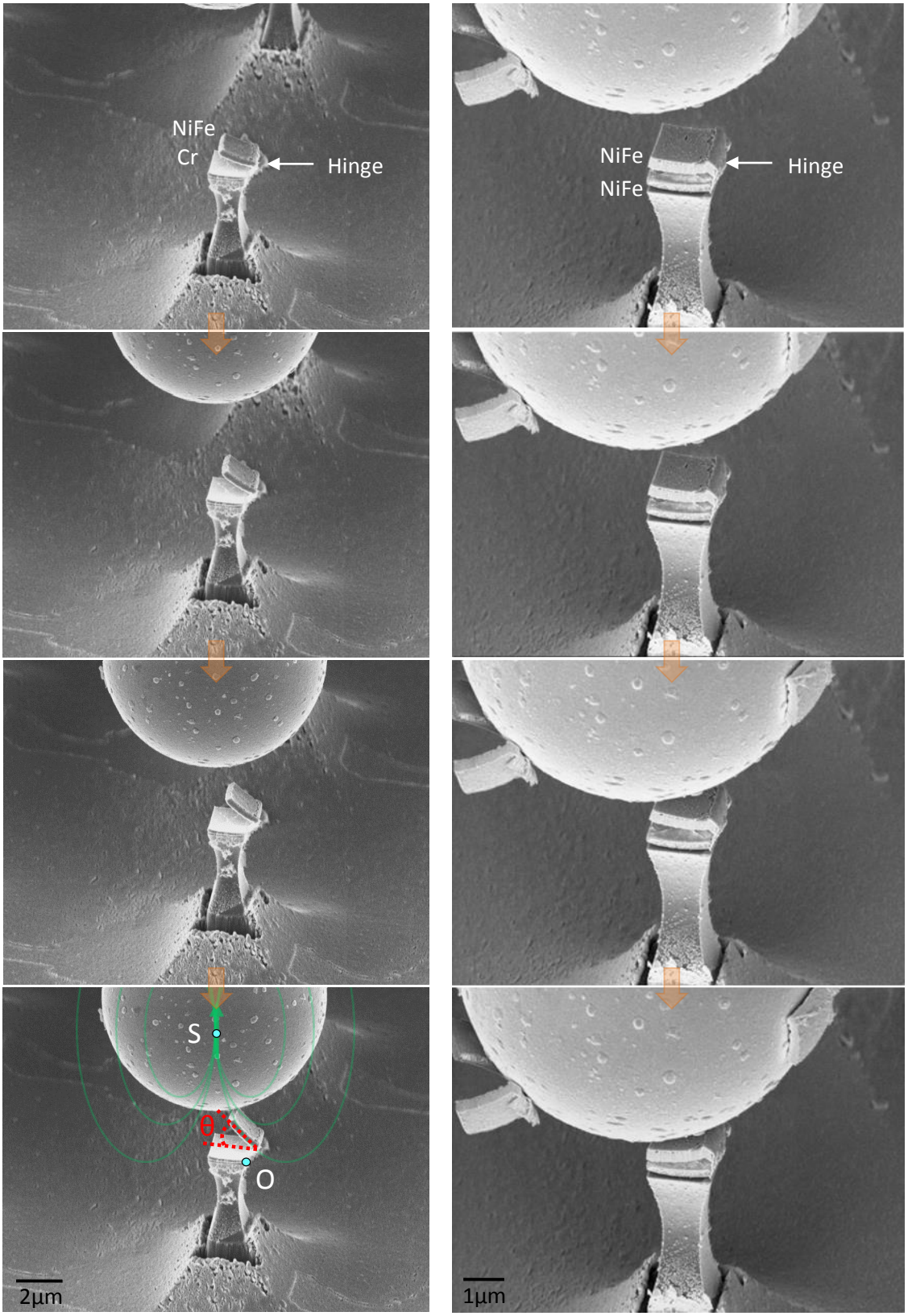

***Figure 74**: Magnetic actuation of magnetic micro/nano-tweezers by approaching a magnetic microsphere from above. Left: soft/non-magnetic tweezer of 1760 nm long and 1600 nm wide with an upper jaw in NiFe of 250 nm thick and a lower jaw in Cr (150 nm thick). Right: soft/soft tweezer of 1560 nm long and 1540 nm wide with two jaws of 250 nm of NiFe.*

The position of the center of the sphere S and the opening angle of the tweezer were acquired for a series of images. The SEM images were acquired from a tilted perspective as the sample was oriented at 54° to face the ion gun. Moreover, the tweezers do not exactly present their side to the electron gun. Therefore, the opening angle was not measured directly on the images but calculated from the jaws coordinates (O, P, C, M) after they were processed to avoid perspective distortion.

To do so, the coordinates (x', y') of the points O, P, C, M and S provided by ImageJ were changed into the three dimensional coordinates (x, y, z) (***Figure 75***). This basis was already used in the model presented in chapter **3**, used to calculate the torque exerted by the sphere on the tweezer upper jaw (see right after in **5.3.3**).

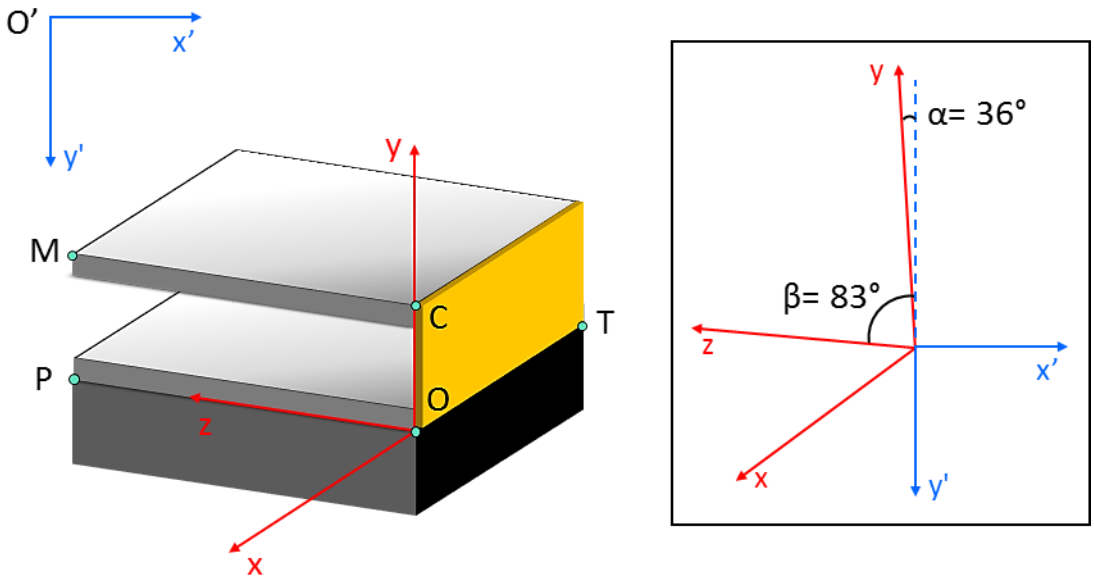

Figure 75*: The coordinates (x', y') provided by ImageJ needed to be processed to obtain the (x, y, z) coordinates of the sphere center S and the points O, P, C and M. The frame on the right clarifies the mismatch between the two bases after translating O' in O and operating a slight rotation to evidence the angle between y and y'.*

The expression of (x, y, z) coordinates of an undetermined point in the tweezer basis is obtained by projecting the (x, y, z) axes in the (x', y') basis of the images, after an origin shift $\overrightarrow{OO'}$. Therefore, by setting x'_0 and y'_0 as the coordinates of O in the (x', y') basis, α=36° the angle between the axes Oy and $-Oy'$, and β=83° the angle measured between the axes Oz and $-Oy'$ (***Figure 75***), one can write:

$$y = -(y' - y'_0)\cos\alpha$$

$$z = -(x' - x'_0)\sin\beta - (y' - y'_0)\cos\beta$$

The depth *x* cannot be known from these two dimensional images. Therefore, the widths of each tweezer were measured on additional images acquired from above with the ion gun. Similarly, the position of the sphere along the *x* direction was deduced from images where it enters in contact with the actuated tweezer.

After this transformation, the scalar product between the vectors $\overrightarrow{OP}$ and $\overrightarrow{CM}$, gives an estimation of the opening angle $\theta = Acos(\frac{CM_x.OP_x+CM_y.OP_y+CM_z.OP_z}{\|\overrightarrow{CM}\|.\|\overrightarrow{OP}\|})$.

The opening angle varies quasi-linearly with the sphere center position, as shown by the curves presented in ***Figure 76*** for a soft/non-magnetic tweezer and in ***Figure 78*** for two soft/soft tweezers.

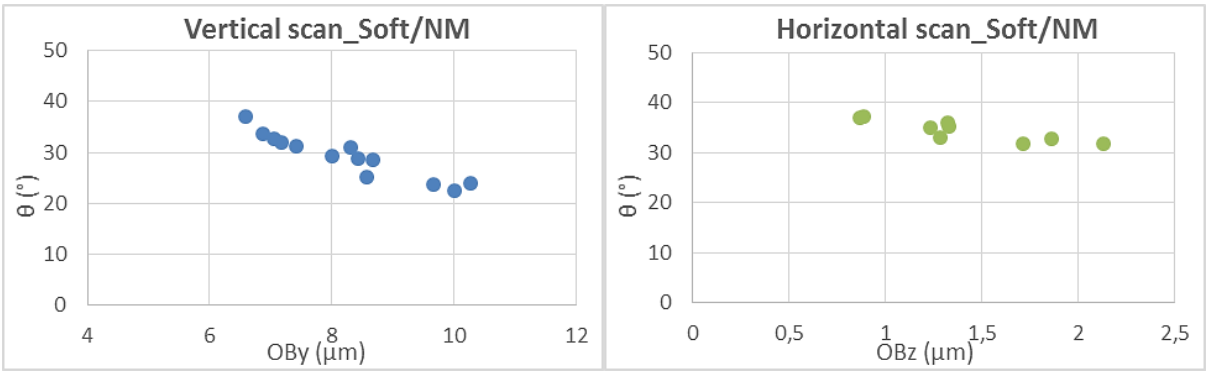

Figure 76*: Relation between the angle θ and the sphere center coordinates for the soft/non-magnetic tweezer. Left: the position of the sphere was moved along the y (vertical) direction at x= 1200 nm and z= 1500 to 2000 nm. Right: the position of the sphere varied along the z direction, laterally on the images, for x= 1200 nm and y= 7500 to 7600 nm. An offset of 13.8° should be subtracted to the opening angle θ to yield the angular displacement of the jaw.*

To get open, this tweezer and a few others needed initially to be gently knocked by the NdFeB sphere to break surface adhesion forces like van der Waals interactions and Casimir effect. Due to internal stress arising during the tweezer fabrication and potential subsequent damage within the hinge due for instance to partial melting associated with ion-beam imaging, the tweezers sometimes opened spontaneously at some angle (***Figure 77***). For instance, the studied tweezer of ***Figure 76*** had a spontaneous opening angle of 13.8°. In this situation, this initial angle will be subtracted from θ when calculating the actual

angular amplitude of the jaw opening which is used to estimate the elastic torque from the hinge. In the experiments of ***Figure 76***, the amplitude of the change of opening angle due to magnetic actuation reached approximately a maximum of 23°.

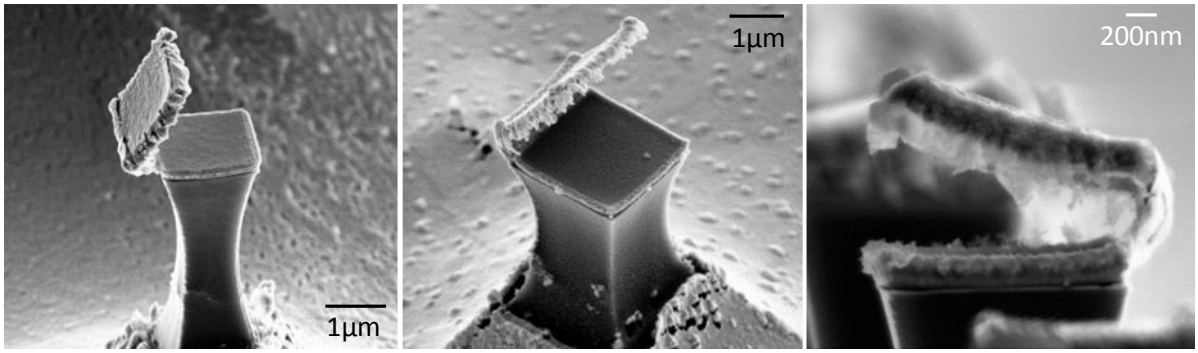

Figure 77*: Tweezers opened spontaneously, betraying the presence of stress within the hinge probably due to its deposition conditions (oblique incidence).*

The results from the experiments carried out on soft/soft tweezers were analyzed in the same way. The relation between the opening angle and the vertical position of the sphere is given in ***Figure 78***. The graph displays two vertical approaches of the sphere at two distinct lateral positions above the tweezer.

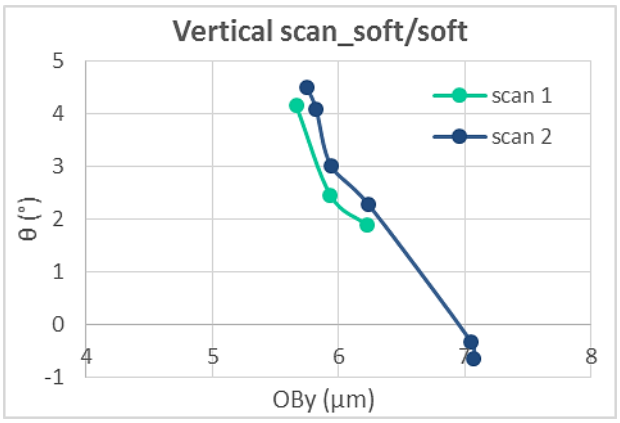

Figure 78*: Relation between the angle θ and the sphere center coordinates for soft/soft tweezers for two vertical scans, along the y axis, performed with the sphere at two distinct lateral positions above a soft/soft tweezer: y_1=2400 nm and y_2=1800 to 1900 nm, x=770 nm.*

The first striking result is the difference between the two types of tweezers. Indeed, the angle θ varies in a range of roughly 20° around the mean value of 18° for the soft/non-magnetic tweezer whereas it varies only over a 5° range (2.5° on average) for the soft/soft tweezer.

According to the theoretical study presented in chapter **3**, the magnetostatic interactions between two magnetic jaws is not significant enough to induce a difference in this range between the two types of tweezers. Therefore, the difference between the two cases can be due to important variation in the hinge mechanical properties.

To determine the hinge stiffness in both experiments, the theoretical model described in chapter **3**, was adapted to calculate the magnetic torque exerted by the sphere on the tweezers mobile jaw. Since at equilibrium the opening angle is determined by a balance between the elastic torque from the hinge (which varies linearly with the opening angle) and the magnetic torque exerted on the upper jaw, one expects a linear relationship between the calculated magnetic torque exerted on the upper jaw in the equilibrium position and the measured opening angle. The slope of this relationship should be equal to the hinge stiffness constant as defined in chapter 3, given by equation (17): $\mathrm{K} = \frac{E\,w}{12\,L}t^3$.

5.3.3 Determination of the hinge effective stiffness constant

To model the experiments, the magnetic field generated by the sphere was calculated and implemented in the model instead of the uniform magnetic field used before.

The sphere was assimilated to a magnetic dipole and its magnetic moment at remanence $\mathfrak{m}$ was obtained from the remanent induction provided by the technical data of the NdFeB powder: B_r =730-760 mT. The sphere remanent magnetization is $M_r = \frac{B_r}{\mu_0}$ =5.8x10^5 A.m^{-1} and its magnetic moment is $\overrightarrow{\mathfrak{m}} = -\frac{4}{3}\pi R^3 M_r \,.\, \hat{e}_y$, (R radius of the sphere) oriented along the *y* axis along the down direction.

This value of remanent magnetization is approximately half of the saturation magnetization of NdFeB (1.6T=12.7x10^5 A.m^{-1}). This is consistent with the model describing the sphere as being polycrystalline, made of independent grains of randomly oriented anisotropy. At remanence, the magnetization of each individual grain is pointing along its easy axis of magnetization in the hemisphere of the saturation field (***Figure 79***).

According to this picture, the remanent magnetization is proportional to the saturation magnetization, with a reduction factor due to the fact that the moments are orientated randomly over the half-sphere: $M_R = \langle \cos\theta \rangle_{1/2\ sphere} . M_{sat}$, which yields $M_R = \frac{1}{2} M_{sat}$.

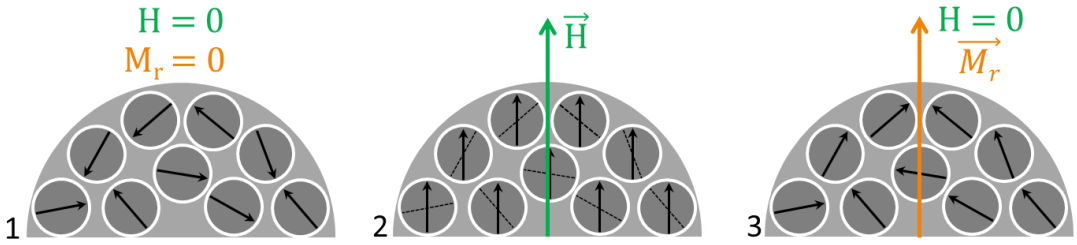

***Figure 79**: Half-view of the first magnetization curve of a NdFeB sphere decomposed in individual magnetic moments. 1: The magnetic moments are originally randomly oriented and compensate each other, resulting in a zero magnetization. 2: Then, the application of a saturation magnetic field brings all the moments along the same direction. 3: Once the field has been switched off, the moments come back to their easy axis in the direction lying in the saturation field hemisphere. Unlike the initial situation, they all point in directions comprised in the same hemisphere; thus, they no longer compensate each other and a remanent magnetization corresponding to half of the saturation magnetization appears in the same direction as the saturation applied field.*

The dipolar magnetic field emitted by the sphere and calculated at a given point within the mobile jaw (at a distance $\vec{r}$ from the sphere center) is $B_{dip} = \frac{\mu_0}{4\pi\, r^3}(3(\vec{\mathfrak{m}}.\vec{r})\vec{r} - \vec{\mathfrak{m}})$. This expression is then integrated on the jaw volume to calculate the torque exerted on the whole jaw by the field. This torque was calculated for each image of the two series and plotted according to the opening angle observed on the same image (***Figure 80***).

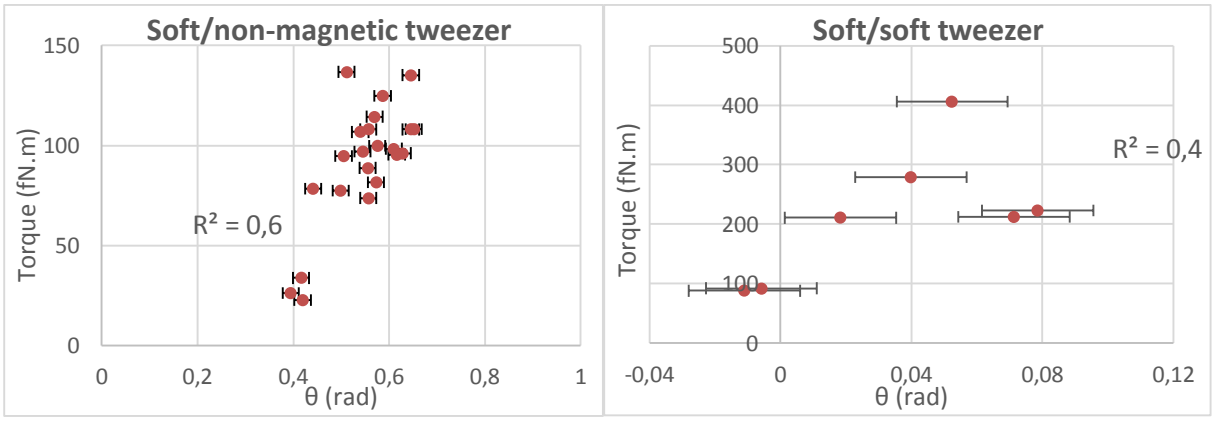

***Figure 80**: Relation between the torque calculated for a given position of the sphere and the angles acquired experimentally for a soft/non-magnetic tweezer (left, with the offset of 13.8° mentioned earlier) and a soft/soft tweezer (right) with a hinge of 20 nm nominal*

thickness. The error bars are 1° large and R² is the coefficient of determination of the data linear regression. Note that the scales differ between the two graphs.

The experimental thickness of these two hinges can be deduced from slope of the line fitting each set of data on the graphs of ***Figure 80***. Indeed, the stiffness is the proportionality factor between the torque and the angle θ (equation (16) in chapter 3, section **3.2**). Thus, the effective stiffness for the soft/NM tweezer is $K_{soft/NM} = 3.0 \pm 0.4 \times 10^{-13}$ N.m and it is $K_{soft/soft} = 20 \pm 9 \times 10^{-13}$ N.m for the soft/soft tweezer.

From these results, one can derive the effective thickness of the hinge of each tweezer using the relationship (equation (17), section **3.2**) between the stiffness constant K (in N.m) and the hinge dimensions (1.76 µm in width for the soft/non-magnetic tweezer and 1.56 µm for the soft/soft tweezer, 350 nm in length) and Young Modulus (59 GPa for evaporated gold [1]). Hence, the hinge of the soft/non-magnetic tweezer has an effective thickness of 22 ± 1 nm, while it is 41 ± 5 nm for the soft/soft tweezer.

The hinges of two tweezers were supposed to be similar as they both result from the same e-beam evaporation of 23 nm of gold at a 60° incidence with respect to the tweezers side. Thus, the expected thickness was 20 nm, from which these results are very close. This good agreement between our theoretical predictions and our experimental measurements is very encouraging as it not only validates the hypotheses used in our analytical model, but also confirms the feasibility and functionality of our first prototype of tweezers.

Nevertheless, the soft/soft tweezer exhibits a stiffer behavior than the soft/non-magnetic one. This variation between the two types of tweezers cannot be explained by the presence of magnetic interactions between the two soft jaws because the dimensions and materials used in this experiment do not allow these interactions to compete with the effect of the applied field. Therefore, the explanation should lie in the mechanical behavior of the hinge, most probably due to its heterogeneous structure.

Indeed, the gold layer is obliquely deposited on the aluminum sacrificial layer which has a large roughness (***Figure 81***). The random character of this roughness leads to several

consequences on the hinge structure and stiffness, and could explain the variability from one tweezer to another.

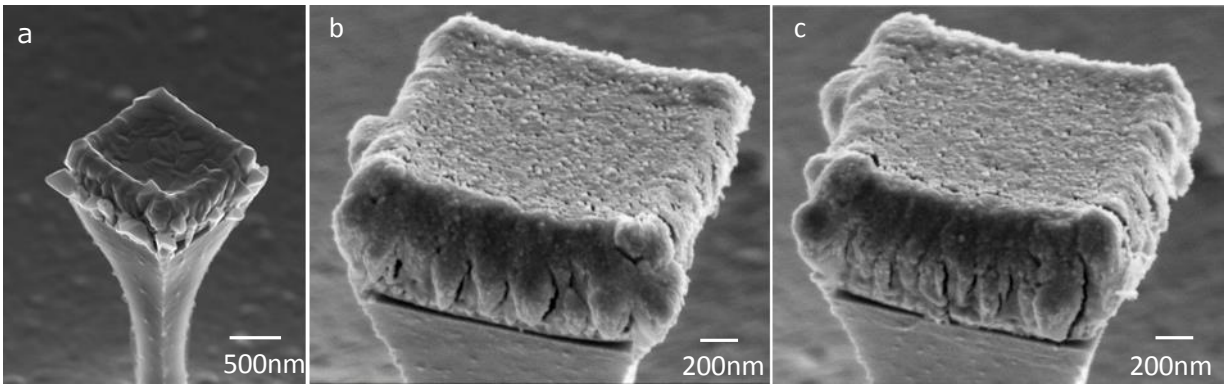

Figure 81*: The roughness of the aluminum sacrificial layer leads a random distribution of the hinge thickness. a) Example of a particularly rough Al layer deposited on a Cr lower jaw (approximately 800 nm side). b and c) Two hinges of 30 nm thick (2 µm wide) from the same sample do not present the same nanostructure.*

First, the hinge deposition at an oblique incidence favors self-shadowing at the nanometer scale (due to Au islands nucleation and growth), which can induce a nanometer scale porosity. Such porosity is known to induce magnetic, electrical and mechanical anisotropies within deposited films [2]. In particular, the Young modulus can decrease with the density of the material as the deposition angle increases [3]. The amplitude of this variation is exacerbated by the roughness of the surface on which the material is deposited.

Besides, the random character of the aluminum roughness also affects the thickness distribution within the gold layer. Actually, the larger stiffness observed for the soft/soft tweezer can be explained by describing the hinge thickness by a Gaussian law.

The effective thickness t_{eff} deduced from the experiments can be expressed according to a Gaussian distribution centered at t_{nom}, the nominal thickness (20 nm), with a dispersion standard deviation to be determined. Since the hinge stiffness varies as t^3, the effective thickness resulting from the Au thickness variations can be written as:

$$t_{eff}^3 = \frac{1}{\sigma\sqrt{2\pi}} \int_0^{+\infty} t^3 \exp\left(-\frac{(t - t_{nom})^2}{2\sigma^2}\right) dt$$

Defining $\lambda = \frac{t_{nom}}{\sigma}$ and $x = \frac{t}{t_{nom}}$, this yields:

$$\left(\frac{t_{eff}}{t_{nom}}\right)^3 = \frac{\lambda}{\sqrt{2\pi}}\int_0^{+\infty} x^3 \exp(-\frac{\lambda^2}{2}(x-1)^2)dx$$

which yields the following expression plotted versus σ in ***Figure 82***:

$$\left(\frac{t_{eff}}{t_{nom}}\right)^3 = \frac{e^{-\frac{\lambda^2}{2}}(2+\lambda^2)}{\lambda^3\sqrt{2\pi}} + \frac{(3+\lambda^2)(1+Erf\left(\frac{\lambda}{\sqrt{2}}\right))}{2\lambda^2}$$

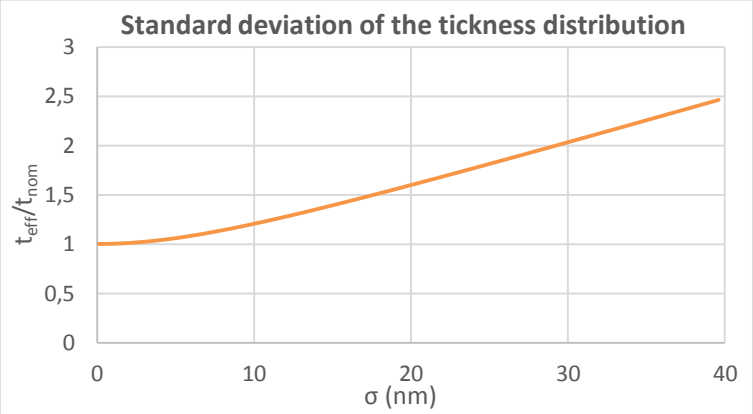

Figure 82*: Estimation of the hinge effective thickness following the hypothesis that it is distributed according to a Gaussian distribution with t_{nom} as mean value and σ as standard deviation. The ratio t_{eff}/t_{nom} plotted versus σ is strictly superior to 1, meaning that the roughness indeed yields an effective thickness larger than the nominal thickness. Our experimental results yielded σ=6.6 nm the soft/NM tweezer and σ=30.4 nm for the soft/soft tweezer.*

Given our experimental results, a Gaussian distribution with a standard deviation of ~30 nm could be used to describe qualitatively the heterogeneous thickness of the hinge (a quantitative description would require more statistical data). Such distribution implies that t_{eff} is always larger than t_{nom}, which is consistent with our observations. This can simply be understood by considering that if the hinge presents thinner regions, this implies that other regions are thicker, to keep the gold volume constant.

Let's assume as an extreme picture a hinge of width w_0 and thickness t_0, comprising a proportion a of randomly distributed voids and a proportion $(1-a)$ of gold, as illustrated in ***Figure 83***. This hinge can be assimilated to a homogeneous hinge with a shorter width $w_{eff} = (1-a)\,w_0$ and a larger thickness $t_{eff} = t_0\,(\frac{1}{1-a})$. With this assumption, the total volume is preserved.

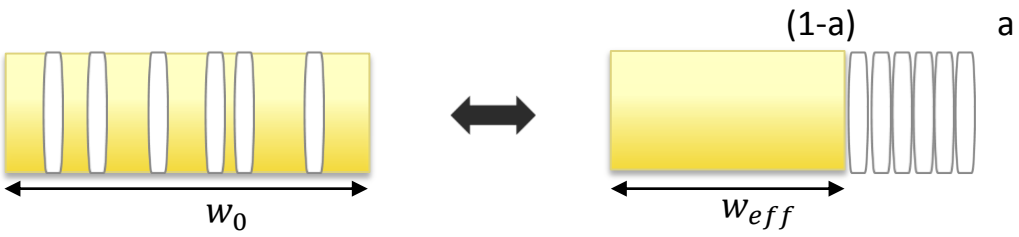

***Figure 83**: A porous gold hinge (of width w_0 and thickness t_0) with a proportion a of randomly distributed voids is mechanically equivalent to a homogeneous hinge of the same volume, with a shorter width w_{eff} and a larger thickness t_{eff}.*

One can express the effective thickness K_{eff} of such hinge as a function of the nominal dimensions w_0 and t_0, using Euler-Bernoulli linear relation (equation (17), section **3.2**):

$$K_{eff} = \frac{E\, w_{eff}\, {t_{eff}}^3}{12\, L} = \frac{E\, w_0\, {t_0}^3}{12\, L} \frac{1}{(1-a)^2} = \frac{K_0}{(1-a)^2}$$

This yields the relationship between K_{eff}, measured experimentally, and K_0, the theoretical stiffness of a non-porous hinge with the nominal dimensions. The porosity a can therefore be expressed as:

$$a = 1 - \sqrt{\frac{K_0}{K_{eff}}}$$

The porosities of the hinges studied experimentally were determined according to this simple model. The value of K_{eff} was set as either $K_{Soft/NM}$ or $K_{Soft/Soft}$ (***Figure 80***) and $K_0 = \frac{E\, w_0\, {t_0}^3}{12\, L}$ was calculated with t_0 = 20 nm, L = 350 nm, E = 59 GPa and w_0 = 1.6 µm for the soft/non-magnetic tweezer and 1.54 µm for the soft/soft one. Hence, the hinge of the soft/non-magnetic tweezer would exhibit a porosity of 25%, while the hinge of the soft/soft tweezer would be 70% porous.

This qualitative result indicates a substantial variation in the hinge porosity from a type of tweezer to another. The structural difference between soft/NM and soft/soft tweezers is the composition of their lower jaw: Cr or NiFe. The roughness of the aluminum sacrificial layer is likely influenced by the composition of the layer on which it is grown. Therefore, given that the hinge structure results mainly from the roughness of the layer on which it is deposited (along with the self-shadowing occurring at oblique incidence deposition), this result suggests that the hinge structure can also be affected by the composition of the lower jaw.

5.4 Conclusion

In this study, the magnetic actuation of two types of tweezers (soft/non-magnetic and soft/soft) by the generation of a local magnetic field inside a SEM chamber was reported. The repeated approach of a magnetized NdFeB microsphere in the vicinity of a single tweezer yielded a 23° (maximum) wide opening for the soft/non-magnetic tweezer and an opening of 5° maximum for the soft/soft tweezer without breaking the hinge. This achievement constitutes an encouraging proof of concept of the tweezers behavior.

The analysis of the images acquired during the experiments, combined with calculations performed with our analytical model (chapter **3**), allowed the quantitative interpretation of the interplay between the magnetic and elastic torques involved in the tweezers actuation. These results, in good agreement with our theoretical predictions, led to the qualitative description of the hinge heterogeneous structure due to its particular deposition conditions. Indeed, the evaporation at oblique incidence of the gold layer on a rough surface probably induces atomic-scale porosity and thickness variation whose random character can affect each single tweezer differently. In addition, it appears that the composition of the lower jaw can also affect the hinge structure, exacerbating the difference between soft/soft tweezers and soft/non-magnetic tweezers. In light of these phenomena, the mechanical behavior of the hinge is quite well described by the linear elastic beam model of Euler-Bernoulli.

To improve the reproducibility of the hinge behavior, the tweezers fabrication process can be adapted to yield a more homogeneous hinge structure. For instance, a preliminary ion beam etching of the tweezers sides could be added before the hinge evaporation. This would smoothen the aluminum surface on which the hinge is deposited and limit the influence of the lower jaw composition on the latter's structure. The aluminum sacrificial layer can also be grown at low temperature (Liquid N_2 temperature) to drastically decrease its granularity.

5.5 References

[1] L. Wang et B. C. Prorok, «The Influence of Deposition Technique on the Mechanical Properties of Freestanding Gold Films», chez *SEM Annual Conference & Exposition on Experimental and Applied Mechanics*, 2007.

[2] L. Abelmann et C. Lodder, «Oblique evaporation and surface diffusion», *Thin Solid Films,* pp. 1-21, 1997.

[3] R. B. Tokas, S. Jena, P. Sarkar, S. polaki, S. Thakur, S. Basu et N. K. Sahoo, «Oblique Angle Deposition of HfO2 Thin Films: Investigation of Elastic and Micro Structural Properties», *arXiv:1406.6858 [cond-mat.mtrl-sci],* 26 06 2014.

[4] J. G. W. Van der Waterbeemd et G. W. Van der Oosterhout, «Effect of the mobility of metal atoms on the structure of thin films deposited at oblique incidence», *Philips Res. Repts.,* pp. 375-387, 1967.

6 General conclusion and perspectives

6.1 General conclusion

The last two decades witnessed a growing interest in magnetic particles intended for bio-nanotechnologies and nanomedicine, which have now largely proved their potential in these fields, thanks to their ability to be remotely actuated in biological media by the application of magnetic fields. Nowadays, the optimization of the particles magnetic properties to better control their behavior is still the subject of intense investigations. In this context, the recent development of top-down fabrication approaches permitted the emergence of magnetic particles with an unprecedented control in size, shape and composition, and thus magnetic properties [1, 2, 3, 4].

These advances enabled considering the elaboration of complex structures such as magnetic micro/nano-tweezers, the object of this thesis. Indeed, the original idea of this project was to bind two magnetic particles together with a flexible hinge for the creation of micro/nano-tweezers which could be remotely actuated by the application of a magnetic field, similarly to magnetic micro/nanoparticles. Although the tweezers were kept attached to their substrate in this study to facilitate their manipulation and characterization, they can constitute reversibly actuable clamping devices once released in solution.

The main objectives of the thesis were: i) to model the tweezers magneto-elastic behavior in order to predict their response to an applied external magnetic field depending on various physical parameters, ii) to develop a fabrication process allowing collective production of tweezers on silicon wafers, following a top-down approach based on micro/nano-electronic fabrication technics at the PTA's cleanroom, iii) to demonstrate the magnetic actuation of such magnetic micro/nano-tweezers.

Firstly, an analytical model was elaborated to study quantitatively the tweezers magneto-elastic behavior under the application of a homogeneous external magnetic field. In particular, the calculations aimed at determining the opening angle of a tweezer

depending on various parameters such as the applied magnetic field amplitude and orientation, the jaws magnetic properties and the dimensions of the jaws and the hinge.

In this study, a tweezer with two square jaws bound by a flexible hinge was considered. The lower was assumed fixed on the substrate whereas the upper one was mobile. The latter was made of a soft ferromagnetic material and supposed to adopt a vortex-like magnetic structure, which was confirmed experimentally. Regarding the lower jaw, three types of material were tested: non-magnetic, magnetically “soft” and “hard”. To constitute the hinge, gold was chosen for its high ductility and its biocompatibility.

The calculations consisted in determining the magnetic torque exerted on the mobile upper jaw by the external field and, when applicable, by the magnetostatic interaction between the jaws in a first place. Then, the elastic deformation of the flexible gold hinge induced by the action of this magnetic torque was determined. The opening angle at equilibrium was determined by the balance between the magnetic torque exerted on the upper jaw by the applied field and elastic torque due to the hinge stiffness.

This opening angle can reach 30° for the three types of tweezers when submitted to a homogeneous magnetic field applied 45° with respect to the substrate. The comparison between soft/non-magnetic, soft/soft and soft/hard tweezers revealed that although the magnetostatic interactions between two magnetic jaws influenced the tweezers behavior as expected, this interaction appeared relatively weak compared to the action of the external field. Indeed, the torque due to magnetostatic interaction between the two magnetic jaws typically reaches ~30 fN.m, while the torque due to the external source can be up to ~250 fN.m.

In addition, when the jaws come into contact, micro-scale surface forces like the London dispersion and the Casimir effect may become significant (depending on the jaws roughness) compared to the magnetic force due to magnetostatic interactions between two magnetic jaws. Experimental observations actually confirmed the contribution of these forces to keep the tweezers in a closed configuration.

The technological elaboration of the magnetic micro/nano-tweezers was guided by these theoretical results. Therefore, to obtain a vortex-like structure within soft jaws, their dimensions were set at 2 x 2 μm^2 and 200 nm in thickness. Their separation distance,

350 nm, represents the height of the gold hinge. Regarding its thickness, our theoretical predictions stated that 20 nm was the thickness yielding the best flexibility while staying the gold elastic regime to avoid plastic deformations.

The tweezers fabrication process was elaborated in the PTA's cleanroom using microelectronics fabrication technics. The tweezers were prepared on silicon wafers through various steps which can be summarized as follows: i) surface micro-structuration of the wafer (including deep-UV photolithography and reactive ion etching); ii) e-beam evaporation of the jaws separated by a sacrificial layer; iii) e-beam evaporation of a thin gold layer (hinge) at oblique incidence on one of the tweezers side; iv) physical etching of the tweezers three other sides to remove the gold muzzle subsequent to the hinge deposition; v) chemical etching of the sacrificial layer and drying.

The development of such time-effective and rather simple fabrication process successfully enabled the production of functional magnetic micro/nano-tweezers. This enabled the first magnetic actuation of individual tweezers, directly observed inside a SEM. Indeed, the experimental setup was installed inside a SEM to study the tweezers actuation, since their size did not allow optical microscopy monitoring of their opening.

The magnetic actuation was achieved by approaching a micro-source of magnetic field from a tweezer: a magnetic microsphere in NdFeB (provided by Nora Dempsey, Néel Insitute) which had been soldered to an AFM-tip fixed at the apex of a micro-manipulated arm. The sphere was moved around the studied tweezer to explore the evolution of the tweezer opening depending on the sphere position.

The first remarkable result was that the gold hinge of 20 nm in thickness allowed a good tweezer opening and withstood repeated actuation. Thus, such dimension indeed represented a very good compromise between flexibility and robustness, as predicted by our theoretical model.

Using this method, the magnetic actuation of soft/soft and soft/non-magnetic tweezers was successfully recorded and analyzed. The theoretical model of the tweezers previously developed for uniform fields was modified to calculate the torque exerted on the tweezer's upper jaw as a result of the application of the non-uniform dipolar field created by

the NdFeB sphere. The distance between the sphere and the upper jaw was extracted on several images from the movies of the experiments, as well as the tweezer opening angle.

Thus, the relationship between the calculated magnetic torque for a given position of the sphere and the opening angle observed on the images was established and yielded the hinge effective stiffness, which was in very good agreement with theoretical predictions, in particular for the soft/non-magnetic tweezer. The stiffness of the soft/soft tweezer appeared a little larger than expected, most likely due to the high roughness of the gold layer (due to the sacrificial aluminum layer roughness) and related impact on the averaged hinge stiffness.

In conclusion, in this thesis, a fabrication process was elaborated to produce collections of remotely actuable magnetic micro/nano-tweezers. Magnetic actuation experiments proved their good functioning, the gold nano-hinge flexibility and resistance over repeated actuation in particular. In addition, the tweezers experimental magneto-elastic behavior and the theoretical prediction yielded by our analytical model were found in very good agreement. Besides, this analytical model yielded results in excellent agreement with finite element calculations (Flux 3D, COMSOL Multiphysics).

This thesis constituted the beginning of a 4-year project led in collaboration between Spintec, SPrAM and the LTM funded by the French National Agency of Research (Nanoshark, ANR-11-NANO-001). During the remaining year, the tweezers technological elaboration could be brought further by optimizing the fabrication process and performing more characterizations of their mechanical and magnetic behavior (**6.2**).

Since these tweezers are intended for biotechnological applications and more precisely, the capture of biological micro/nano-objects, the biochemical functionalization of their surfaces to tailor their interaction with biological species constituted the main objective of the 4th year of the Nanoshark project (**6.3**). Other perspectives of applications which could also be considered are proposed at the end of this chapter (**6.4**).

6.2 Perspectives of further characterizations and technological optimizations

After demonstrating the magnetic actuation of individual tweezers, the next objective is to achieve their collective actuation by the application of a macroscopic magnetic field. The experimental setup and technological optimizations implemented in this purpose are presented in section **6.2.1**. Further optimization and characterization of the hinge mechanical properties are addressed in section **6.2.2**.

6.2.1 Magnetic actuation: toward collective actuation

One of the tweezers main asset, when fixed on a substrate, is to be collectively actuable by the application of a macroscopic field. This is desirable in the perspective of various applications, as well as for further characterization of the tweezers magnetic response. For quantitative characterization of the latter, an innovative experiment was set inside a SEM to allow direct observation of the jaws motion. Indeed, at the considered dimensions (~1 - 2 µm), optical microscopy would not provide a sufficient resolution.

The setup, developed by the company NewTec, consists in a platform including an electromagnet able to generate a well-controlled magnetic field across the sample. To operate inside a SEM chamber, the electromagnet is shielded from the electron beam by a mu-metal plate with a gap intended to let the beam reach the sample located in the air gap (***Figure 84***).

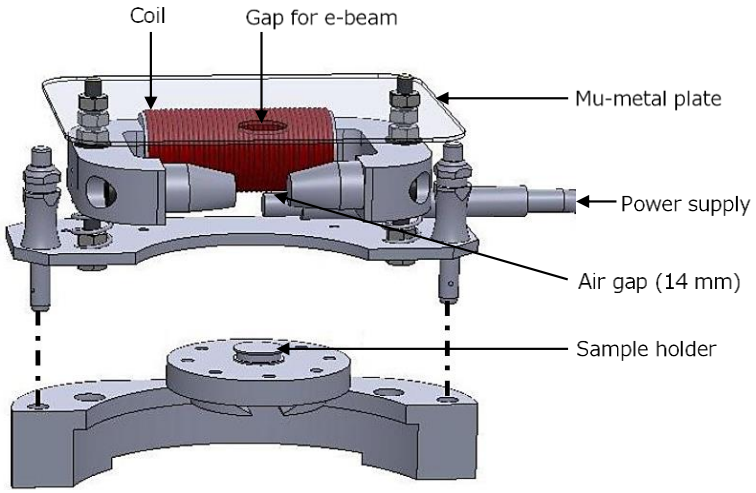

***Figure 84**: Setup to generate a magnetic field with an electromagnet inside a SEM. Sketch from NewTec.*

This setup should enable the characterization of the magnetic actuation of a collection of tweezers by the application of a magnetic field at various angles. Indeed, the sample holder can be adapted to tilt the sample with respect to the field direction. In particular, theoretical prediction of a double equilibrium position of the upper jaw under the application of a magnetic field at 90° with respect to the substrate could be investigated.

Most of all, highly-parallel magnetic actuation would promote the characterization of the influence of dimensional parameters on the tweezers behavior. Varying the ratio between the jaws magnetic volume and the hinge stiffness should provide more information on the balance between the magnetic torque and the elastic torque exerted on the tweezers mobile jaw. This could be achieved by fabricating tweezers with various length-to-width ratios. Indeed, for the same width, and thus the same hinge dimensions (and stiffness), an increase in the jaws length increases the magnetic torque which can be exerted on the mobile jaw (by increasing both the magnetic volume and the lever arm).

To make this study, a solid lithography mask was elaborated during the redaction of this manuscript by G. T. Ortiz. This mask is intended to produce tweezers with various sizes and shapes on the same wafer.

Besides, such a mask allows skipping the first step of the fabrication which consisted in forming micro-pillars in the silicon substrate to isolate the tweezers from the rest of the wafer surface. This step was useful at the beginning of the study to allow varying the size of

the tweezers during the development of the fabrication process, to explore the tweezers physical properties, but is no longer needed if the size variation is already integrated in the new mask design. Instead, the stack could be directly deposited at the bottom of resist holes.

6.2.2 Hinge mechanical properties

The hinge mechanical behavior is the second key feature of the tweezers actuation. The results yielded by the magnetic actuation experiments performed in this thesis showed that the high roughness of the hinge can induce a significant uncontrolled variation of its properties. Therefore, the reproducibility of the hinge structure could be improved by etching the tweezers sides prior to the hinge evaporation (by ion beam etching). In this way, the gold layer would be deposited on a smoother surface, resulting in a smoother hinge. This could enable the fabrication of thinner hinges (down to 10 or 5 nm) by limiting the apparition of voids within the gold layer. The first trials led by Dr. Guillermo Tulio Ortiz, who took over the continuation of the elaboration of the tweezers at Spintec, yielded very promising results.

Besides, the characterization of the gold hinge stiffness for various dimensions and its resistance over time would be very interesting. In this purpose, AFM measurements of the opening angle as a function of the applied field could be performed by either immobilizing the tip on top of a tweezer while applying a sinusoidal magnetic field, either scanning a tweezer with and without field application. Sequential automatic measurements of the same kind could provide better knowledge of the hinge resistance to repeated actuation.

In this study, a thin layer of gold was selected to play the role of the hinge by binding the two jaws together and controlling their relative motion. Alternatively, using a polymeric hinge could also be interesting (***Figure 85***). Indeed, polymers can be more flexible and elastic than metals; for instance, PMMA (Poly(methyl methacrylate)) has a Young modulus between 1.8 and 3.1 GPa [7] (~60 GPa for e-beam evaporated gold [8]).

Besides, the use of polymers could also enhance the tweezers biocompatibility by embedding the micromagnets in a polymer matrix, as pictured in ***Figure 85***. Furthermore, the biochemical functionalization of some polymers, such as polystyrene [7], can be enabled by a simple exposure to O_2 plasma of the desired surfaces. This method activates surface charges on which electropositive groups like polylysine bound to alkane chains can be grafted in order to form self-assembled monolayers (see section **6.3.1**).

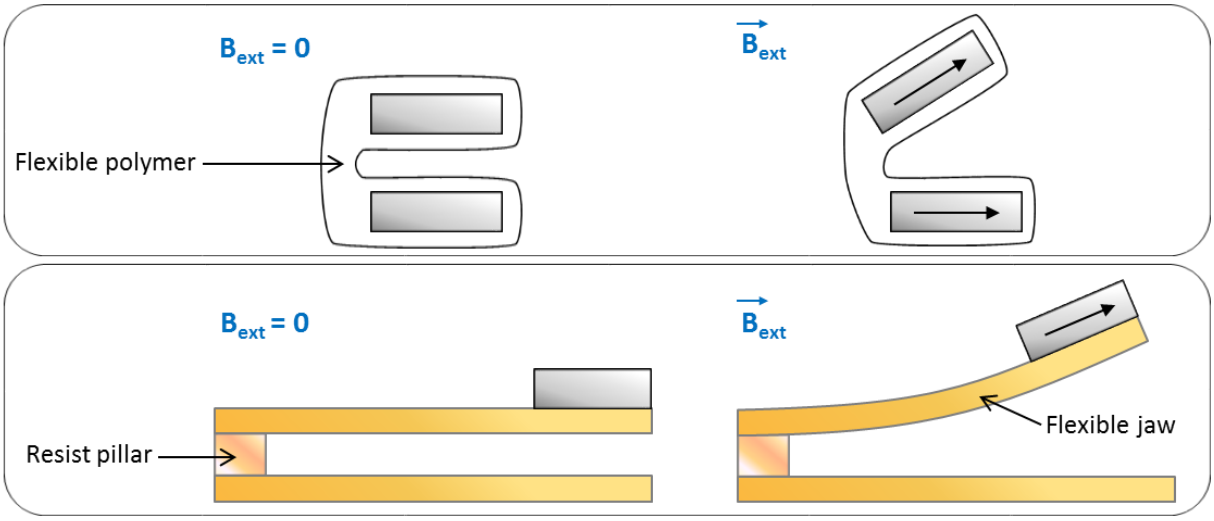

Figure 85*: Design of tweezers including a polymeric hinge. Top: tweezer made of two soft ferromagnetic layers embedded in an elastic and biocompatible polymer matrix. Bottom: tweezer with a hinge made of a resist pillar; to increase the lever arm of the magnetic torque, the jaws can be flexible (in gold for example) with the magnet positioned at their end (only one jaw is magnetic in this example).*

As mentioned above, the main objective of the 4th year of the Nanoshark project is to make the tweezers interact with specific biological objects using chemical functionalization of their jaws in the perspective of applications in biotechnologies and medicine.

The mechanical grabbing characteristic of the tweezers, combined to the ability to bind specifically to targeted samples promises exciting applications in microfluidics (magneto-optic biochip and biological complexes force measurements presented in the Introduction, section **1.2.2**) and maybe more at longer term (**6.4**).

6.3 Functionalization of tweezers for micro/nano-objects capture

The development of a strategy to functionalize the tweezers, exposed below in section **6.3.1**, was done in collaboration with the CREAB team from the SPrAM. The CREAB is involved in the development of micro-bioanalytical tools at the interface of physics, optics, chemistry and biology. They have expertise in surface functionalization particularly intended for biological applications.

The preliminary studies undertaken during this thesis and the continuation of this work at the SPrAM are reported in section **6.3.2**.

6.3.1 Tweezers functionalization strategy

The idea is to functionalize the tweezers in a selective manner so as to obtain chemically active surfaces only inside the jaws. The external surfaces can be functionalized differently in order to avoid interaction with biological media. This can be achieved using self-assembled monolayers (SAMs) to coat the tweezers surfaces in a local-selective manner [8].

SAMs are ordered molecular assemblies formed by the adsorption of an active surfactant on a solid surface. Molecules constituting SAMs are usually composed of a “head group” that can chemisorb on the substrate, a “chain” that enhances the stability of SAMs thanks to van des Waals interactions with neighboring chains, and a terminal functional group offering (***Figure 86***) the possibility for biomolecular targeting.

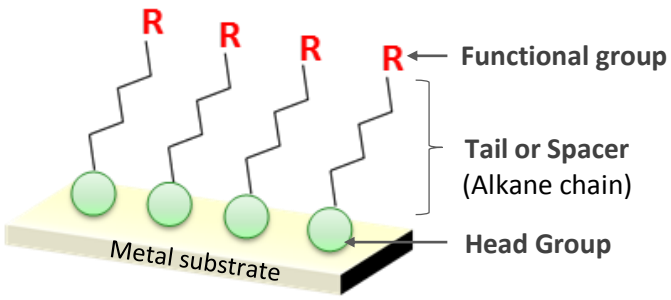

***Figure 86**: Scheme of a self-assembled monolayer grafted on a metal substrate by a head group and presenting a functional group for further reactions.*

In our case, the tweezers' inner surfaces were modified for specific binding to targeted samples, whereas the external surfaces were blocked with an inert polymer to avoid non-specific binding with biological entities. ***Figure 87*** illustrates the approach selected for this goal.

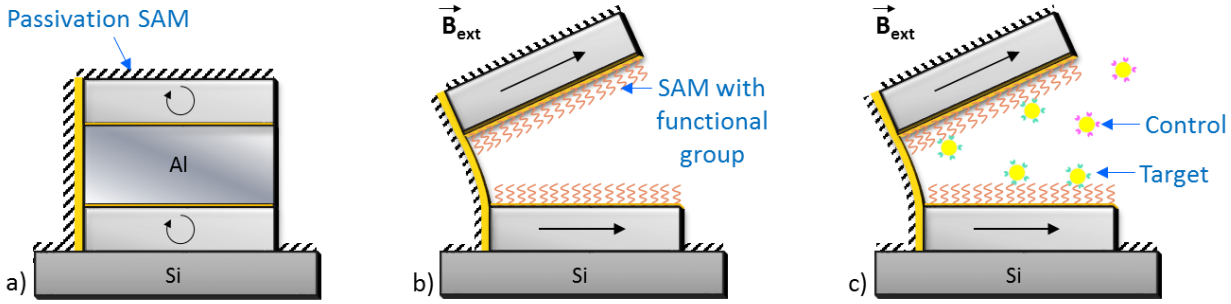

***Figure 87**: Chemical functionalization protocol: a) passivation of the tweezers external surfaces with a SAM of thiolated PEG chains. b) After the sacrificial layer removal by chemical etching, the gold surfaces inside the jaws can be functionalized with thiols possessing bioactive terminal entities. c) Exposure to analytes leading to specific binding with the targeted molecules inside the jaws, while unspecific adsorption outside the jaws is prevented by the SAM passivation. The interactions inside the jaws can be promoted by applying a magnetic field to widen the gap between the jaws.*

For the external passivation SAM, thiolated poly-(ethylene glycol), **HS-PEG** was used. They are widely used in biosensors to eliminate non-specific binding [10].

Regarding the jaws' inner surfaces, the SAM was constituted of **HS**-$(CH_2)_{11}$-**NH_2**: a thiol with an amine terminal functional group. Once the SAM is formed on the gold surface, the amine terminal was then activated by NHS-biotin. Afterwards, streptavidin can be

captured with good specificity *via* strong streptavidin-biotin bond with a dissociation constant (Kd) of the order of 10^{-15} mol/L.

6.3.2 Preliminary studies

In the perspective of biotechnological applications, some preliminary tests were performed during this thesis to check the feasibility for the functionalization of the tweezers. First, the chemical functionalization of the gold layers inside the jaws, which could be altered by the fabrication process, was confirmed. Second, a strategy for the jaws local-selective functionalization was validated by the preparation of gold Janus particles.

The surface state of the gold layers inside the jaws after chemical etching of the sacrificial layer was tested. Indeed, this etching step could damage the gold layers and prevent SAMs formation. Therefore, a simple test of functionalization using fluorescent probes (for easy observation) was performed with a sample of tweezers deprived of upper jaws. Thus, the unveiled lower jaws could be imaged by optical microscopy to check the formation of SAMs on top of them, with the help of the fluorescent probes.

As shown in ***Figure 88***, only the unveiled lower jaws exhibited high intensity of fluoresce, proving that they were successfully functionalized by SAMs.

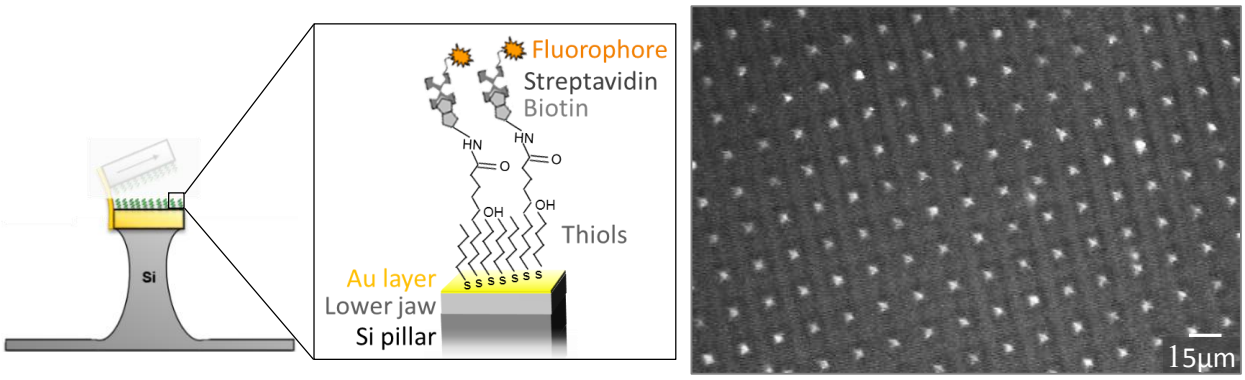

Figure 88*: Proof of the good surface state of the gold layers inside the jaws. Left: scheme of the ligand grafted on the lower jaw of tweezers deprived of upper jaws. Right: fluorescence image of a sample; the bright squares array indicate that the lower jaws top surfaces were successfully functionalized with the fluorescent tag.*

Moreover, some preliminary experiments were carried out to demonstrate the feasibility of local selective functionalization based on SAMs. Indeed, the tweezers chemical functionalization implies the grafting of two different SAMs on the tweezers surface (passive outside, active inside). For this, Janus particles, which exhibit different properties on each of their sides, were chosen as models (***Figure 89***).

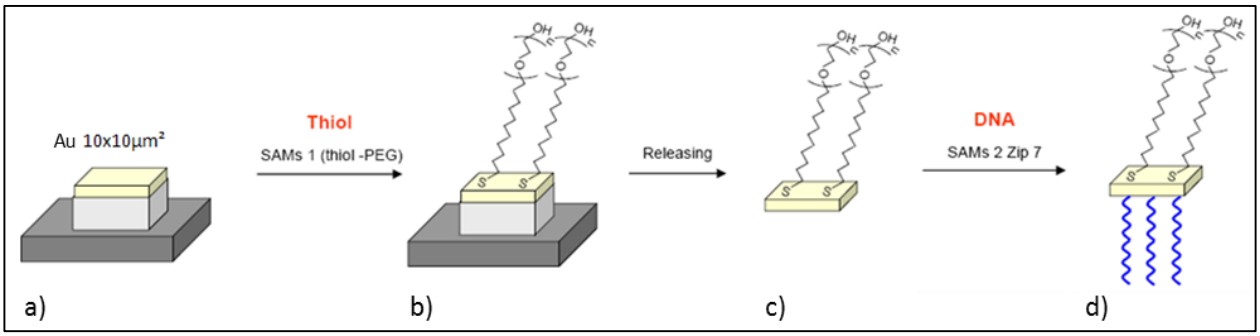

Figure 89*: Preparation of Janus particles. a) The gold particles (10 µm side) are initially fixed on a substrate. b) The top gold surface is passivated by grafting SAMs of thiolated-PEG chains to it. c) The particles are released in solution by dissolving the underlying resist in acetone. d) Thiolated-DNA strands are grafted on the newly exposed gold surface.*

In this study, the particles had one inert side (thiol-PEG) and one side covered with thiolated DNA (deoxyribonucleic acid) strands terminated by a biotin. Incubating such particles with a streptavidin-conjugated fluorophore, which binds specifically to biotin, allows demonstrating the success of the experiment by tagging fluorescently only one of the particles sides. The observation of the samples by fluorescence microscopy confirms the presence of one bright side and one dark side (***Figure 90***).

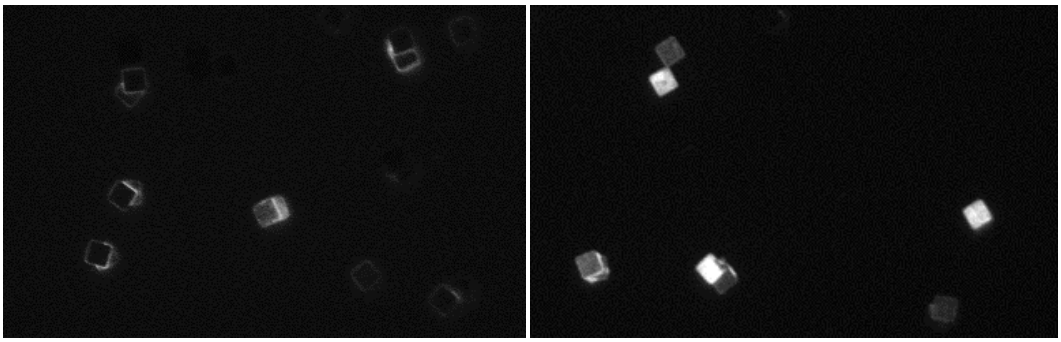

Figure 90*: Fluorescence microscopy images of Janus particles of 10x10 µm² exhibiting fluorescence on one out of their two sides. (Exposure: 0,12s, gain: x4, magnification: x40.)*

Regarding the follow-up of this project in the frame of the Nanoshark project, Nora Reinhardt (SPrAM) already obtained some encouraging results by the end of the redaction of this manuscript. Each step of the functionalization process were validated and are ready to be implemented on the magnetic micro/nano-tweezers. In particular, the pegylation of the tweezers external surfaces, prior to the chemical etching of the Al sacrificial layer, is not altered by the exposure to the acid solution. The capture of streptavidin-conjugated gold nanoparticles of 40 and 80 nm in diameter is currently under progress.

6.4 Other potential applications

Besides the applications considered in the frame of the Nanoshark project which were mentioned in the Introduction of this manuscript (magneto-optical biochip, micro-array for chemical bonding force measurements and mechanotransduction studies, micro-oven for extremely local hyperthermia or apoptosis induction by mechanical stimulation, non-invasive nano-biospy, etc...), the magnetic micro/nano-tweezers could also find applications in nanophysics.

For instance, the fact that they constitute a micro-array of reflective micro-surfaces (***Figure 91***) whose reflectivity can be modified by the application of a magnetic field could be exploited to detect and map magnetic fields with a high resolution which would depend on the pitch of the tweezers array. This concept was already set up at Spintec with magnetic micro-beams whose deflection under the application of a magnetic field could be detected as a change of surface reflectivity with bare eyes.

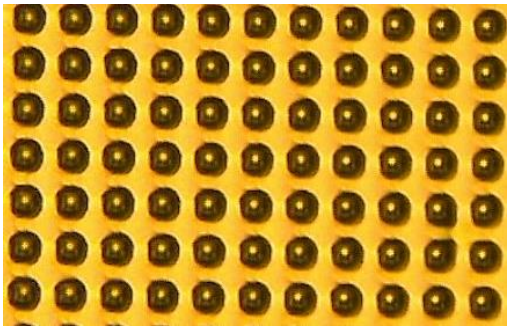

Figure 91*: Top view of tweezers (bright squares of 2.4 µm wide in the middle of darker ones) by optical microscopy. The change of reflectivity of the tweezers top surface can inform on the magnitude and spatial distribution of an applied field.*

Besides their magnetic properties, the tweezers also exhibit interesting mechanical behaviors. The upper jaw being fixed by one of its end to the flexible nano-hinge like a cantilever, it can behave as a micro-resonator. It could be coupled with a laser beam to measure its oscillation frequency, which could reach hundreds of MHz depending on the hinge stiffness.

6.5 References

[1] S. X. Wang, R. J. Wilson et W. Hu, «Synthetic antiferromagnetic nanoparticles». US Brevet 20080206891, 16 08 2007.

[2] H. Joisten, T. Courcier, P. Balint, P. Sabon, J. Faure-Vincent, S. Auffret et B. Dieny, «Self-polarization phenomenon and control of dispersion of synthetic antiferromagnetic nanoparticules for biological applications», *Applied Physics Letters,* vol. 97, n° 1253112, 2010.

[3] D.-H. Kim, E. A. Rozhkova, I. V. Ulasov, S. D. Bader, T. Rajh, M. S. Lesniak et V. Novosad, «Biofunctionnalized magnetic-vortex microdiscs for targeted cancer-cell destruction», *Nature Materials,* vol. 9, p. 165–171, 2010.

[4] S. Leulmi, H. Joisten, T. Dietsch, C. Iss, M. Morcrette, S. Auffret, P. Sabon et B. Dieny, «Comparison of dispersion and actuation properties of vortex and synthetic antiferromagnetic particles for biotechnological applications», *Appl. Phys. Lett.,* vol. 103, n° 1132412, 2013.

[5] P. C. L. a. J. Voldman, "MIT Material Property Database" 20 February 2004. [Online]. Available: http://www.mit.edu/~6.777/matprops/pmma.htm. [Accessed 13 April

2015].

[6] L. Wang et B. C. Prorok, «The Influence of Deposition Technique on the Mechanical Properties of Freestanding Gold Films», chez *SEM Annual Conference & Exposition on Experimental and Applied Mechanics*, 2007.

[7] K. Kuribayashi-Shigetomi, H. Onoe et S. Takeuchi, «Cell origami: self-folding of three-dimensional cell-laden miscostructures actuated by cell traction force», *Plos One,* vol. 7, n° 112, 2012.

[8] M. L. Immordino, F. Dosio et L. Cattel, «Stealth liposomes: review of the basic science, rationale, and clinical applications, existing and potential», *Interational Journal of Nanomedicine,* vol. 1, n° 13, p. 297–315, 2006.

[9] G. Oukhaled, A. Cebers, J.-C. Bacri, J.-M. Di Meglio et C. Py, «Twisting and buckling: A new undulation mechanism for artificial swimmers», *European Physical Journal E,* vol. 35, n° 1121, 2012.

[10] K. Y. Guslienko, V. Novosad, Y. Otani et H. Shima, «Field evolution of magnetic vortex state in ferromagnetic disks», *Applied Physics Letters 78,* p. 3848, 2001.

[11] K. L. M. a. Y. Lee, «Map of metastable states for thin circular magnetic nanocylinders», *Appl. Phys. Lett.,* vol. 92, n° 1112506, p. 112506, 2008.

7 Annexes

7.1 COMSOL model conception

A numerical model of a tweezer was built with COMSOL Multiphysics 4.2.a to calculate the stress experienced by the hinge when it bends under the action of the magnetic torque applied on the tweezer upper jaw.

The model tweezer was designed with a fixed, non-magnetic lower jaw (2 x 2x 0.2 μm^3), an upper jaw with Permalloy mechanical properties (2 x 2x 0.2 μm^3) and a hinge with gold mechanical properties and variable height and thickness.

A specific mesh was designed to fit with the tweezer high aspect ratio, since the jaws length is about 100 times larger than the hinge thickness. Further to the convergence analysis of this model, the best compromise between computation time and reliability of the results was found for meshes composed of 50 000 to 80 000 elements.

Surface mechanical forces in the range of picoNewtons to nanoNewtons were applied on the upper jaw surfaces (as sketched in ***Figure 92***) to mimic the application of magnetic forces on each of its magnetic surface poles by magnetic fields (calculated with the analytical model presented in chapter 3, section **3.1.1**).

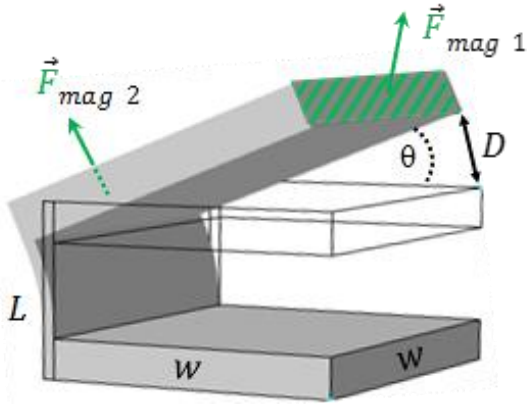

Figure 92*: Model tweezer with a fixed lower jaw and a mobile upper jaw submitted to mechanical surface forces corresponding to magnetic forces exerted on each magnetic pole of the jaw. The gold hinge linear deflection induces the tweezer opening of an angle θ.*

The hinge bending under the application of these forces induces the upper jaw's displacement D, calculated by the software. Likewise, the Von Mises stress (MPa) distribution in the structure was calculated and plotted for several hinge thicknesses (5 nm to 60 nm) in FIG (chapter 3, section **3.2**).

7.2 Magnetic actuation program

For a tweezer with two magnetically soft jaws (Permalloy) of same area, whose lower one is fixed on a substrate and put in the presence of a magnetic NdFeB microsphere, this program calculates the magnetic state (magnetization) of each of the two interacting jaws and the resulting torque acting on the mobile upper jaw due to the magnetic fields emitted by the microsphere and the lower jaw.

```
input "Jaws length (in nanometer)";long
input "Jaws width (in nanometer)"; larg
input "thickness bottom jaw (in nanometer)";e1
input "thickness top jaw (in nanometer)";e2
input "spacing between jaws (in nanometer)";d
print "origin of frame at the upper left front corner of the bottom
jaw"
input "x boulle (nm)";xb
input "y boulle (nm)";yb
input "z boulle (nm)";zb
pi=4*atn(1)
mu0=4*pi*1e-7

'Magnetization of bottom jaw
m1=800000
'Magnetization of top jaw
m2=800000
'Saturation field of both jaws (T)
Bsat=0.1

'Magnetic sphere characteristics
rayon=4.75e-6
aimnfb=581000
mnfb=4/3*pi*rayon*rayon*rayon*aimnfb
mdipx=0
mdipy=mnfb
mdipz=0

theta=0
'Number of integration steps in each integral
N=30

'Loop on theta
ltheta:
```

```
print "theta=",theta

'Calculation of the magnetic states of the two jaws'
m2var=m2
m1var=m1

'Calculation of average field b2 created by the sphere on upper jaw:
bx2av=0
by2av=0
bZ2av=0
for ix=0 to N
for iy=0 to N
for iz=0 to N
'variable point in the volume of the upper jaw in the lab frame
x=ix*larg/N
y=iy*e2/N
z=iz*long/N
xam=x
yam=sin(theta)*z+cos(theta)*(y+d)
zam=cos(theta)*z-sin(theta)*(y+d)

rx=xam-xb
ry=yam-yb
rz=zam-zb
r=sqr(rx*rx+ry*ry+rz*rz)
'local dipolar field b2 created by the magnetic sphere on the upper
jaw
bx2=1/r/r/r*(3*(mdipx*rx+mdipy*ry+mdipz*rz)/r/r*rx-mdipx)
by2=1/r/r/r*(3*(mdipx*rx+mdipy*ry+mdipz*rz)/r/r*ry-mdipy)
bz2=1/r/r/r*(3*(mdipx*rx+mdipy*ry+mdipz*rz)/r/r*rz-mdipz)
if ix=0 or ix=N then coefix=1/2 else coefix=1
if iy=0 or iy=N then coefiy=1/2 else coefiy=1
if iz=0 or iz=N then coefiz=1/2 else coefiz=1
bx2av=bx2av+coefix*coefiy*coefiz*bx2
by2av=by2av+coefix*coefiy*coefiz*by2
bz2av=bz2av+coefix*coefiy*coefiz*bz2
next iz
next iy
next ix
bx2av=bx2av/N/N/N*mu0/4/pi*1e27
by2av=by2av/N/N/N*mu0/4/pi*1e27
bz2av=bz2av/N/N/N*mu0/4/pi*1e27
'Calculation of the longitudinal component of field (along Z)
b2avl=cos(theta)*bz2av+sin(theta)*by2av

'Calculation of average field b1 created by the sphere on lower jaw:
bx1av=0
by1av=0
bZ1av=0
for ix=0 to N
for iy=0 to N
for iz=0 to N
'variable point in the volume of the lower jaw in the lab frame
x=ix*larg/N
y=iy*e1/N
z=iz*long/N
```

```
rx=x-xb
ry=y-yb-e1
rz=z-zb
r=sqr(rx*rx+ry*ry+rz*rz)
'Local dipolar field b1 created by the magnetic sphere on the lower
jaw
bx1=1/r/r/r*(3*(mdipx*rx+mdipy*ry+mdipz*rz)/r/r*rx-mdipx)
by1=1/r/r/r*(3*(mdipx*rx+mdipy*ry+mdipz*rz)/r/r*ry-mdipy)
bz1=1/r/r/r*(3*(mdipx*rx+mdipy*ry+mdipz*rz)/r/r*rz-mdipz)
if ix=0 or ix=N then coefix=1/2 else coefix=1
if iy=0 or iy=N then coefiy=1/2 else coefiy=1
if iz=0 or iz=N then coefiz=1/2 else coefiz=1
bx1av=bx1av+coefix*coefiy*coefiz*bx1
by1av=by1av+coefix*coefiy*coefiz*by1
bz1av=bz1av+coefix*coefiy*coefiz*bz1
next iz
next iy
next ix
bx1av=bx1av/N/N/N*mu0/4/pi*1e27
by1av=by1av/N/N/N*mu0/4/pi*1e27
bz1av=bz1av/N/N/N*mu0/4/pi*1e27
'Calculation of the longitudinal component of field (along Z1)
b1avZ=bz1av

'Calculation of the mutual susceptibility of the two jaws

'Calculation of the field created by the top jaw on the bottom jaw
assuming that the top jaw has a magnetization m2var
b21az=0
for ixp1=0 to N
for iyp1=0 to N
for izp1=0 to N
xp1=ixp1*larg/N
yp1=iyp1*e1/N
zp1=izp1*long/N
'Calculation of field at variable point P1 of the bottom jaw
'Variable point M at right edge surface of top jaw: Y2=long
b21x=0
b21y=0
b21z=0
for ix=0 to N
for iy=0 to N
x=ix*larg/N
y=iy*e2/N
xm=x
ym=e1+sin(theta)*long+cos(theta)*(y+d)
zm=cos(theta)*long-sin(theta)*(y+d)
mp1x=xp1-xm
mp1y=yp1-ym
mp1z=zp1-zm
rmp1=sqr(mp1x*mp1x+mp1y*mp1y+mp1z*mp1z)
if ix=0 or ix=N then coefix=1/2 else coefix=1
if iy=0 or iy=N then coefiy=1/2 else coefiy=1
b21x=b21x+coefix*coefiy/rmp1/rmp1/rmp1*mp1x
b21y=b21y+coefix*coefiy/rmp1/rmp1/rmp1*mp1y
b21z=b21z+coefix*coefiy/rmp1/rmp1/rmp1*mp1z
```

```
next iy
next ix
'Variable point M at left edge surface of top jaw: Y2=0
for ix=0 to N
for iy=0 to N
x=ix*larg/N
y=iy*e2/N
xm=x
ym=e1+cos(theta)*(y+d)
zm=-sin(theta)*(y+d)
mp1x=xp1-xm
mp1y=yp1-ym
mp1z=zp1-zm
rmp1=sqr(mp1x*mp1x+mp1y*mp1y+mp1z*mp1z)
if ix=0 or ix=N then coefix=1/2 else coefix=1
if iy=0 or iy=N then coefiy=1/2 else coefiy=1
b21x=b21x-coefix*coefiy/rmp1/rmp1/rmp1*mp1x
b21y=b21y-coefix*coefiy/rmp1/rmp1/rmp1*mp1y
b21z=b21z-coefix*coefiy/rmp1/rmp1/rmp1*mp1z
next iy
next ix
b21x=mu0/4/pi*m2var*larg*e2/N/N*b21x
b21y=mu0/4/pi*m2var*larg*e2/N/N*b21y
b21z=mu0/4/pi*m2var*larg*e2/N/N*b21z

'Calculation of the average longitudinal component (along Z1) of the
field created by upper jaw on lower jaw
if ixp1=0 or ixp1=N then coefix=1/2 else coefix=1
if iyp1=0 or iyp1=N then coefiy=1/2 else coefiy=1
if izp1=0 or izp1=N then coefiz=1/2 else coefiz=1
b21az=b21az+coefix*coefiy*coefiz*b21z
next izp1
next iyp1
next ixp1
b21az=b21az/N/N/N
ki21=b21az/m2var
print "ki21=ki12=",  ki21
'Criterion on magnetization m1 of the bottom jaw
if abs(b21az+b1avz)<bsat then m1var=(b21az+b1avz)/bsat*m1 else
m1var=m1*(b21az+b1avz)/abs(b21az+b1avz)
ki12=ki21
b12al=ki12*m1var
'Criterion on magnetization m2 of the top jaw
if abs(b12al+b2avl)<bsat then m2var=(b12al+b2avl)/bsat*m2 else
m2var=m2*(b12al+b2avl)/abs(b12al+b2avl)

'Convergence towards the magnetic equilibrium state
'Loop on m1var and m2var
m1m2:
b21az=ki21*m2var
if abs(b21az+b1avz)<bsat then m1van=(b21az+b1avz)/bsat*m1 else
m1van=m1*(b21az+b1avz)/abs(b21az+b1avz)
b12al=ki12*m1van
if abs(b12al+b2avl)<bsat then m2van=(b12al+b2avl)/bsat*m2 else
m2van=m2*(b12al+b2avl)/abs(b12al+b2avl)
print "magnetizations of the jaws", m1van, m2van
```

```
if abs(m1van-m1var)+abs(m2van-m2var)>1 then
m1var=m1van:m2var=m2van:goto m1m2
'Equilibrium magnetization of the two jaws given by m1van and m2van

'Calculation of magnetic energy of the top jaw for this angle theta
ener=-m2van*(b12al+b2avl)*long*larg*e2*1e-27
if theta=0 then write#1,theta*180/pi, m1van, m2van,
ener*1e15:enern=ener

'Calculation of torque as -dEnergy/d(theta)
if theta>0 then tor=-(ener-enern)*180/pi: write#1,theta*180/pi,
m1van, m2van, ener*1e15, tor*1e15:enern=ener:print "torque
(fN.m)",tor*1e15

theta=theta+pi/180
if theta>pi/2+0.0001 then goto fin else goto ltheta
end
```

7.3 Aluminum etching solution recipe

Aluminum Etch 1960, OLIN Microelectronic Materials: Aluminum etching solution ready for use between 50°C and 60°C.

Composition: H_3PO_4 à 85% 25 volumes, HNO_3 (d= 1.40) 1 volume, CH_3CO_2H 5 volumes, H_2O 2 volumes, AES surfactant (Alcohol Ethoxysulphates).

8 Résumés en français

8.1 Introduction

8.1.1 Situation du sujet dans le contexte global des biotechnologies

Manipulables à distance en milieu liquide par l'action de champs magnétiques, les micro/nano-particules magnétiques ont fait l'objet de nombreuses études scientifiques ces dix dernières années et sont déjà largement utilisées en biotechnologie et en médecine pour des applications variées allant du diagnostic (agents de contraste IRM, imagerie à particules magnétiques, tri cellulaire...) à la thérapie (vectorisation et délivrance ciblée de médicaments, hyperthermie...).

Le déplacement des particules magnétiques en milieu liquide est généralement obtenu à l'aide de gradients de champ magnétique. L'inconvénient de ces derniers est que leur intensité décroit rapidement avec la distance. Or il est important dans la plupart des applications de maximiser la force magnétique appliquée aux particules pour pouvoir les diriger efficacement au travers de milieux visqueux et de résister au flux sanguin dans le cas d'applications *in vivo*. Pour compenser la diminution du gradient de champ magnétique, il est possible d'augmenter le volume magnétique des particules. Néanmoins, cette solution est limitée car la taille des micro/nanoparticules importe beaucoup selon l'application visée. D'une autre façon, le gradient de champ peut être remplacé par un champ uniforme pour appliquer un couple magnétique sur des particules de forme anisotrope, donnant lieu à des comportements originaux. Cette approche nécessite un bon contrôle de la forme des particules magnétiques.

Pour les utiliser en milieu biologique, il est important que les particules magnétiques ne s'agglomèrent pas spontanément en solution, c'est-à-dire en l'absence de champ magnétique. Leur capacité à se disperser en solution après la coupure du champ appliqué dépend principalement de leur aimantation rémanente. Ainsi, les particules superparamagnétiques sont préférées aux particules ferromagnétiques car elles ne présentent pas de rémanence et ne s'agglomèrent donc pas spontanément en l'absence de champ magnétique. Les particules superparamagnétiques d'oxyde de fer (SPION) préparées

par voie chimique sont d'ailleurs devenues la référence dans le domaine, aussi bien en tant que sujet de recherche que produit commercial.

Néanmoins, le comportement superparamagnétique n'apparaît dans des matériaux ferromagnétiques que pour des particules de taille nanométrique (5-10 nm de diamètre en général). En effet, dans un ferro-aimant, l'aimantation est fixée dans une direction donnée par la barrière énergétique de l'anisotropie magnétocristalline, qui est proportionnelle au volume et intrinsèque au matériau. A des dimensions nanométriques, cette barrière est suffisamment basse pour être franchie avec l'apport énergétique des fluctuations thermiques. L'aimantation dans la particule devient alors aléatoire et apparait nulle lorsqu'elle est moyennée dans le temps (typiquement sur une période de 100 s). Ainsi, le comportement superparamagnétique permet d'éviter le phénomène d'agrégation des particules magnétiques en solution. En revanche, le faible volume de telles particules ne permet pas d'exercer sur elles des forces et couples magnétiques importants, notamment pour résister au flux sanguin.

Ainsi, l'idéal est de créer des particules capables de se redisperser en solution tout en présentant un volume micrométrique et anisotrope, permettant d'y exercer des forces magnétiques significatives par l'intermédiaire de champs magnétiques uniformes (qui ne décroissent donc pas avec la distance comme les gradients de champ). Les recherches poursuivant ce but ont récemment conduit à l'émergence d'une méthode de fabrication de particules innovante, inspirée des techniques de la micro/nano-électronique. Contrairement aux méthodes de synthèse conventionnelles par voie chimique, cette approche « top-down » permet de synthétiser des particules dont la composition, la taille et la forme sont parfaitement contrôlées. Par exemple, les particules antiferromagnétiques synthétiques (SAFs) et les particules vortex sont deux solutions très différentes qui présentent toutes deux un comportement pseudo-superparamagnétique pour un volume micrométrique (1 µm de côté ou de diamètre pour une centaine de nanomètres d'épaisseur) et anisotrope, permettant d'y appliquer des couples magnétiques efficacement.

Cette avancée technologique a ouvert la voie à la conception de particules plus complexes telles que les micro/nano-pinces magnétiques qui ont fait l'objet de cette thèse. Composées de deux microparticules magnétiques parallélépipédiques en vis-à-vis reliées par une nano-charnière en or, leur ouverture peut être commandée à distance par l'application d'un champ magnétique. A l'instar des particules magnétiques, ces pinces sont conçues dans la perspective d'être libérées en solution.

Ceci contraste avec la plupart des dispositifs existants capables de capturer mécaniquement des échantillons à l'échelle micro/nanométrique. En effet, ces derniers sont dépendants d'une alimentation électrique câblée ou d'une interaction mécanique avec le substrat et ne peuvent pas prétendre à des applications *in situ*. Seuls les dispositifs magnétiques peuvent être contrôlés à distance et permettent de s'affranchir de câbles. Les seules micro-pinces magnétiques déjà existantes font environ 500 µm de large et sont donc deux ordres de grandeur au-dessus des micro/nano-pinces magnétiques élaborées dans cette thèse. Ainsi, nos **micro/nano-pinces sont actuellement les seuls dispositifs magnétiques actionnables à distance pour capturer des objets d'un micron et moins et pouvant être libérés en solution comme des microparticules**.

Leur fabrication étant compatible avec la fonctionnalisation chimique, les micro/nano-pinces magnétiques peuvent voir leurs surfaces externes passivées pour améliorer leur biocompatibilité et leurs surfaces internes activées pour leur permettre d'interagir spécifiquement avec le(s) composant(s) ciblé(s). Ainsi, elles se situent à la croisée entre colloïdes magnétiques et bio-MEMS ou -NEMS magnétiques (micro et nano *Electro-Mechanical Systems*) et apparaissent particulièrement adaptées à des applications biotechnologiques et médicales.

8.1.2 Présentation de l'étude

L'idée innovante à l'origine de ce projet est de lier deux particules magnétiques par une nano-charnière flexible pour réaliser une micro/nano-pince magnétique capable de s'ouvrir et fermer sur commande par l'application d'un champ magnétique externe. Son actionnement est basé sur le principe fondamental d'attraction et répulsion entre deux corps aimantés. La nature répulsive ou attractive de leur interaction magnétostatique dépend de la direction de l'aimantation dans chacune des mâchoires.

En l'absence de champ appliqué, la pince apparaît fermée car les aimantations dans les deux mâchoires sont soit nulles (si elles sont toutes deux composées du même matériau ferromagnétique doux), soit en configuration antiparallèle et s'attirent mutuellement (si l'une d'elles au moins a une aimantation rémanente).

Lorsqu'un champ magnétique suffisant est appliqué, les mâchoires vont s'aimanter dans la direction du champ et atteindre une configuration parallèle, ce qui déclenche leur répulsion mutuelle et l'ouverture de la pince. Cette dernière peut être grandement augmentée si le champ est appliqué hors du plan des pinces. L'amplitude de cette ouverture est déterminée par l'équilibre entre le couple magnétique et le couple élastique dû à la force

de rappel de la charnière qui s'exercent sur la mâchoire mobile. La charnière doit donc être suffisamment flexible pour permettre une bonne ouverture de la pince sans être trop fragile.

Ce principe de fonctionnement requiert que l'aimantation de chaque mâchoire reste dans le plan de la couche magnétique. En effet, si l'aimantation pouvait pivoter hors du plan à l'intérieur du volume des mâchoires, le couple magnétique exercé par les champs appliqués ne serait pas traduit mécaniquement et aucun mouvement ne serait produit. Cette propriété est assurée par l'énergie d'anisotropie de forme, qui augmente lorsque l'épaisseur des mâchoires diminue.

Il est aussi essentiel que le retournement de l'aimantation d'au moins une des deux mâchoires puisse être obtenu par l'application d'un champ aussi faible que possible, pour passer aisément de la configuration antiparallèle à parallèle. Ceci implique l'utilisation d'un matériau magnétique de faible coercitivité.

Enfin, une aimantation à saturation élevée est souhaitable dans chacune des mâchoires magnétiques afin d'optimiser le fonctionnement des pinces car cela augmente le couple magnétique que l'on peut exercer sur elles, ainsi que le champ magnétique qu'elles génèrent.

Selon les applications visées, les pinces pourront être composées d'une seule mâchoire magnétique (l'autre étant non-magnétique) ou de deux mâchoires magnétiques dont les propriétés peuvent être identiques ou non. Le premier cas sera appelé « doux/non-magnétique » tout au long du manuscrit tandis que les pinces entièrement magnétiques seront nommées « doux/doux » et « doux/dur », faisant allusion à la coercitivité de chaque mâchoire magnétique. Une mâchoire dite dure sera faite d'un matériau dont la coercitivité est notablement supérieure à celle du matériau doux mais pas nécessairement un aimant permanent.

Les pinces «doux/non-magnétiques » seront particulièrement adaptées à des applications où les pinces restent fixées à un substrat (« lab-on-chips » à détection optique, mesure de forces au sein d'assemblages de biomolécules, ...). En effet, la mâchoire supérieure mobile peut être actionnée par un champ appliqué tandis que l'autre, non-magnétique, reste attachée au substrat. Les pinces avec deux mâchoires magnétiques pourront aussi être utilisées dans cette configuration.

En revanche, seules les pinces « doux/doux » ou « doux/dur » dont les mâchoires peuvent interagir pour s'attirer ou se repousser mutuellement sont adaptées à des applications où les pinces sont libérées en solution (tri d'échantillons biologiques, nano-

biopsie non-invasive, ...). Le mécanisme de déclenchement de l'ouverture des pinces est légèrement différent si les deux mâchoires sont en matériau doux ou si l'une d'elle est dure, ce qui pourra être mis à profit en fonction de l'application visée.

Cette thèse s'inscrit dans le cadre du projet Nanoshark financé par l'Agence Nationale de la Recherche (référence : ANR-11-NANO-001) mené en collaboration entre les laboratoires Spintec, SPrAM, tous deux membres de l'INAC (Institut Nanosciences et Cryogénie) et LTM du CNRS (Centre National de la Recherche Scientifique). La thèse couvre les 3 premières années du projet qui dure 4 ans au total et s'est principalement déroulée entre Spintec pour le développement théorique et technologique des pinces et le SPrAM (équipe CREAB) pour leur fonctionnalisation chimique.

Les principaux objectifs de la thèse étaient les suivants :

Dans un premier temps, construire un modèle analytique permettant de décrire et prédire le comportement des micro/nano-pinces magnétiques pour orienter leur fabrication et aider à l'interprétation de leur caractérisation expérimentale.

Dans un second temps, développer un procédé de fabrication permettant de réaliser des pinces de composition et dimensions permettant leur actionnement à distance par l'application d'un champ magnétique. Cette étude technologique a été menée dans la salle blanche de la Plateforme Technologique Amont (PTA) au CEA.

Finalement, démontrer et caractériser l'actionnement magnétique des pinces, l'objectif majeur de la thèse. Dans ce but, une expérience originale a été mise en place à la Plateforme de Nano-caractérisation (PFNC), où une microsphère magnétique attachée à un bras micro-manipulé a été utilisée comme micro-source locale de champ magnétique pour actionner des pinces individuellement.

8.1.3 Plan du manuscrit

Le premier chapitre de ce manuscrit (chapitre **2**) approfondit la description des pinces abordée dans l'introduction en expliquant le choix des matériaux, des dimensions et de la forme des éléments constitutifs des pinces : les mâchoires et la charnière. Une première estimation des diverses forces mises en jeu est aussi avancée afin de valider le concept du fonctionnement des pinces.

Un modèle analytique permettant de calculer les couples magnétiques et élastiques responsables de l'ouverture des pinces en fonction de différents paramètres (dimensions, composition, champ appliqué) a été élaboré et est présenté dans le chapitre **3**. L'analyse de

trois types de pinces différents enrichit notre compréhension du comportement magnéto-élastique des pinces.

Le développement de chaque étape du procédé de fabrication de ces micro/nano-pinces, du wafer en silicium à la pince complète, est présenté dans le chapitre **4**. L'exploration de certains paramètres physiques tels que la largeur des mâchoires et l'épaisseur de la charnière est traitée à la fin du chapitre.

La démonstration de l'actionnement mécanique et magnétique de pinces de 2 µm de côté et hautes de 500 nm constitue le résultat principal de la thèse. Le chapitre **5** décrit la mise en place de l'expérience utilisée pour y arriver et détaille l'analyse des résultats, ainsi que leur interprétation basée sur le modèle analytique construit précédemment.

Le chapitre **6** conclut sur le travail effectué au cours de ces 3 ans de thèse et discute des pistes visant à optimiser les micro/nano-pinces magnétiques et à poursuivre leur caractérisation, avant de proposer quelques idées d'applications à plus long terme.

8.2 Description générale des micro/nano-pinces magnétiques

Le projet de réalisation des micro/nano-pinces magnétiques étant tout à fait original, leur conception a démarré de zéro, en même temps que la thèse. Le premier objectif de ce travail fut donc de définir la forme, les dimensions et les matériaux qui constitueront les pinces pour qu'elles soient fonctionnelles (**2**). Une première estimation des forces mises en jeu dans l'actuation des pinces permettra d'en valider le concept.

Pour faciliter les calculs théoriques et la caractérisation expérimentale, ce travail de thèse se concentrera uniquement sur des pinces dont la mâchoire inférieure reste fixée au substrat. Les trois types de pinces envisagés dans l'introduction seront tout de même étudiés : doux/non-magnétique, doux/doux et doux/dur.

Dans un souci d'efficacité, un modèle aussi simple que possible a été élaboré pour établir une première preuve de concept, c'est-à-dire la démonstration de leur actuation par l'action d'un champ magnétique. L'expérience acquise au cours de ce travail permettra ensuite d'affiner la structure des pinces de façon plus optimale.

Ainsi, l'étude a démarré avec des pinces composées de deux particules métalliques (magnétiques ou non) déposées par évaporation et qui constituent les mâchoires et qui sont séparées par une couche sacrificielle éliminée à la fin du procédé de fabrication. Une charnière flexible établit le lien entre les deux mâchoires. Celle-ci doit être suffisamment flexible pour permettre leur ouverture répétée et assez rigide pour exercer une force de rappel qui referme la pince en champ nul et éviter que les deux mâchoires ne restent collées l'une à l'autre.

La charnière sera constituée d'une fine couche d'or déposée par évaporation en incidence oblique sur un des flancs des pinces. L'or est un matériau noble, biocompatible et très ductile. Son module de Young estimé à 59 GPa (pour un film déposé par évaporation) est parmi les plus faibles des métaux évaporables sous vide.

Pour chaque type de pince, la mâchoire supérieure sera composée de Permalloy (80 % Nickel, 20 % Fer), le matériau ferromagnétique doux le plus utilisé actuellement en microélectronique et dont les propriétés magnétiques constituent un bon compromis pour assurer le fonctionnement correct des pinces.

La mâchoire inférieure peut être soit non-magnétique (composée de chrome dont les propriétés de croissance sont bien maîtrisées), soit magnétique douce (en NiFe comme la mâchoire supérieure), soir magnétique dure, auquel cas elle peut être composée de néodyme-fer-bore (NdFeB) qui a une coercitivité bien supérieure à celle du NiFe (670 à 750 kA.m-1).

L'épaisseur des deux mâchoires est fixée à 200 nm, bon compromis entre la maximisation du volume magnétique et les contraintes technologiques (adhésion de la couche métallique). Dans un premier temps, elles seront de forme carrée pour permettre l'apparition de la configuration magnétique en vortex dans les mâchoires douces (en Permalloy).

Cette configuration magnétique apparaît typiquement dans des disques ferromagnétiques mais un équivalent peut être observé dans les particules carrées qui ont l'avantage de présenter des bords droits pour y déposer une charnière métallique plus proprement que sur des flancs courbes. Les propriétés magnétiques de telles structures sont bien quantifiées (Guslienko et al., Metlov and Lee), ce qui permet d'établir des hypothèses simples utilisées ensuite dans le modèle théorique analytique visant à calculer les couples magnétiques qu'elles peuvent subir sous l'application d'un champ magnétique (développé dans le chapitre **3**). Les hypothèses faites sur l'aimantation des mâchoires douces sont :

- Une réponse linéaire et réversible au champ magnétique appliqué jusqu'à saturation, atteinte pour un champ de 0,1 T (cohérent avec nos mesures expérimentales au VSM (magnétomètre à échantillon vibrant)
- Le confinement de l'aimantation dans le plan de la mâchoire.

Pour savoir si de telles pinces peuvent effectivement s'ouvrir sous l'action d'un champ magnétique externe, une première estimation des couples mis en jeu dans ce processus a été réalisée. L'ouverture d'une pince est déclenchée par l'application de couples magnétiques sur la mâchoire supérieure, la mâchoire inférieure étant fixée au substrat.

On distinguera le couple magnétique dû au champ magnétique externe, pouvant atteindre 300 fN.m, de celui résultant du champ magnétique émis par la mâchoire inférieure lorsqu'elle est magnétique, qui n'atteint que 30 fN.m pour les matériaux et dimensions choisis. Ainsi, le couple exercé par le champ magnétique externe semble être dominant dans le mécanisme d'ouverture d'une pince. Un calcul plus approfondi de ces couples et l'analyse des résultats pour divers cas de figures sont présentés dans le chapitre **3**.

La position d'équilibre de la mâchoire supérieure est atteinte lorsque ces couples magnétiques sont compensés par le couple élastique exercé par la charnière. Bien qu'il soit difficile d'appréhender les propriétés élastiques d'un film d'or à ces dimensions et déposé sous de telles conditions (évaporation électronique sous incidence rasante), un calcul simple dans la limite élastique indique qu'une charnière de 20 nm d'épaisseur devrait permettre une ouverture large de 70°. La confirmation d'un tel résultat, notamment la détermination de la limite du régime élastique, nécessite une analyse plus fine présentée dans le chapitre **3**.

Les micro-forces de surface comme l'effet Casimir et les forces de van der Waals apparaissent négligeables entre les mâchoires, sauf lorsque ces dernières entrent en contact. Ces forces sont alors susceptibles d'atteindre l'ordre du nanoNewton et d'entrer en compétition avec les couples magnéto-élastiques qui gouvernent l'actionnement des pinces. Cet effet a été observé expérimentalement.

8.3 Modélisation de l'actionnement magnétique d'une pince

Pour décrire plus précisément les mécanismes en jeu lors de l'actuation des pinces et en prédire le comportement en fonction de divers paramètres, un modèle théorique a été construit (**3.1.1**). Ce dernier permet de calculer analytiquement les trois couples exercés sur la mâchoire supérieure mobile (la mâchoire inférieure étant fixe) lors de l'actuation des pinces : i) le couple magnétique dû au couplage Zeeman entre le moment magnétique de la mâchoire et le champ externe, ii) le couple magnétique dû à l'interaction magnétostatique avec la mâchoire inférieure lorsqu'elle est magnétique, iii) le couple élastique dû à la force de rappel de la charnière.

Le but de ces calculs est de déterminer l'angle d'ouverture d'une pince à l'équilibre de ces trois couples pour des paramètres physiques donnés tels que les matériaux qui composent chaque mâchoire et la charnière, les dimensions de chacun de ces éléments, ainsi que la valeur du champ magnétique externe et son orientation. Les résultats obtenus pourront ainsi guider la fabrication des pinces et l'interprétation des expériences de caractérisation (présentées dans les chapitres **4** et **5** respectivement).

Dans ce modèle, les mâchoires sont assimilées à des parallélépipèdes ferromagnétiques dont l'aimantation prend différentes propriétés en fonction du matériau qui les compose (ferromagnétique doux, ferromagnétique dur ou aimant permanent, non-magnétique). D'un type de pince à l'autre, c'est le matériau qui compose la mâchoire inférieure qui varie, tandis que la mâchoire supérieure mobile est toujours en matériau doux.

La méthode utilisée consiste à déterminer l'aimantation de la mâchoire mobile, qui est proportionnelle au champ magnétique total appliqué (jusqu'à saturation à 0.1 T). Ce dernier vaut la somme du champ uniforme externe et du champ dipolaire rayonné par la mâchoire du bas (si elle est magnétique), tous deux intégrés sur le volume de la mâchoire supérieure et projetés sur son plan (lui aussi mobile). Ce calcul est trivial pour les pinces dont la mâchoire est non-magnétique ou dure. En revanche, lorsque les deux mâchoires sont douces, un calcul auto-consistant est nécessaire pour prendre en compte leur susceptibilité mutuelle.

L'énergie magnétique de la mâchoire est déduite de son aimantation. Finalement, le couple magnétique total exercé sur la mâchoire est obtenu en dérivant l'énergie par rapport à l'angle d'ouverture de la pince (orientation du plan de la mâchoire supérieure).

Ce couple magnétique est ensuite compensé par le couple élastique exercé par la charnière qui est assimilée à une poutre élastique chargée à une extrémité. Ainsi, dans la limite du régime élastique, le couple est donné par le produit de l'angle de déflection de la charnière (égal à l'angle d'ouverture de la pince) avec la constante raideur, ou rigidité, de la charnière. Cette dernière est proportionnelle au cube de l'épaisseur (Euler-Bernoulli) qui prend donc une importance particulière dans cette étude et que l'on tentera de réduire autant que possible expérimentalement (chap. **4**). Le respect de la limite du régime élastique pour des charnières d'au moins 17 nm d'épaisseur a été validé par des calculs numériques effectués avec COMSOL.

L'évolution des aimantations, du couple magnétique et de l'angle final d'ouverture (prenant en compte la rigidité de la charnière) a été analysée pour les trois types de pince (doux/doux, doux/dur et doux/non-magnétique) sous l'effet d'un champ magnétique uniforme croissant de 0 à 0.2 T par pas de 0.05 T, appliqué à 0°, 45° et 90° par rapport au plan de la mâchoire inférieure fixée au substrat.

L'angle d'ouverture des pinces peut atteindre environ 30° pour un champ appliqué à 45°, quel que soit le type de pince. Deux positions d'équilibre ont été trouvées lorsque que le champ est appliqué hors du plan, l'une d'elle correspondant à une ouverture de 50° environ!

La comparaison des trois types de pince a mis en évidence l'impact des propriétés magnétiques de la mâchoire inférieure sur l'évolution du couple lors de l'actuation magnétique. La contribution variable de l'interaction magnétostatique au couple magnétique total renseigne notamment sur sa nature attractive ou répulsive.

Cette interaction apparaît faible comparée au couple dû au champ uniforme externe (comme prédit dans la section **2.1.3**). En conséquence, l'application d'un champ magnétique dans le plan des pinces n'est pas la solution la plus efficace pour ouvrir celles-ci. L'actuation des pinces, une fois libérées en solution, nécessitera donc d'augmenter l'intensité de l'interaction magnétostatique entre mâchoires magnétiques. Pour cela, il est possible d'augmenter les volumes magnétiques des mâchoires et de les allonger, ainsi que d'utiliser un matériau à plus forte aimantation.

8.4 Elaboration technologique

L'élaboration technologique des micro/nano-pinces magnétiques a représenté la majeure partie du travail de thèse. Le procédé de fabrication a entièrement été développé à la PTA suivant les objectifs définis dans le chapitre **2**, c'est-à-dire de produire des pinces composées de deux couches métalliques déposées par évaporation électronique (les mâchoires) reliées par une charnière en or d'épaisseur nanométrique, évaporée sous incidence oblique sur l'un des flancs des pinces (**4.1**). La séparation entre les mâchoires est assurée par le dépôt d'une couche sacrificielle en aluminium qui est éliminée chimiquement à la fin du procédé de fabrication. Bien que cet objectif dépasse le cadre de cette thèse, la perspective de libérer les pinces en solution comme des colloïdes a toujours orienté le développement du procédé de fabrication.

Les techniques et moyens employés dans ce procédé de fabrication sont issus de la microélectronique, domaine d'expertise de Spintec qui fait partie des leaders dans la conception de mémoires magnétiques. Les besoins originaux de ce projet innovant ont cependant conduit au « détournement » de certaines de ces techniques, rendant ce travail aussi complexe que passionnant.

Ce procédé, élaboré à l'échelle du wafer, permet de produire assez rapidement et de manière reproductible une large collection de pinces facilement caractérisables lorsqu'elles sont maintenues attachées au wafer. Il se décline en 4 principales étapes :

- **Micro-structuration de la surface** du wafer en silicium par lithographie optique et gravure ionique de piliers dans le silicium. Cette méthode pourra être remplacée par une seule étape de lithographie optique une fois le reste du procédé validé.
- **Evaporation des couches métalliques qui constituent les pinces** : mâchoire inférieure (composition variable), couche sacrificielle en aluminium et mâchoire supérieure en NiFe. La couche d'aluminium est entourée de deux fines couches d'or qui permettront la fonctionnalisation chimique de l'intérieur des mâchoires une fois la couche sacrificielle retirée.
- **Evaporation de la nano-charnière en or sous incidence oblique** sur un seul flanc des pinces, les autres flancs étant ensuite débarrassés des redépôts d'or par gravure ionique. L'élaboration de la charnière est une étape délicate puisque l'alignement de l'échantillon dans le bâti d'évaporation et de gravure se fait à la main. De plus, chaque type et dimension de pince ayant ses spécificités, il est nécessaire d'adapter systématiquement

l'angle de dépôt et l'épaisseur de la charnière pour qu'elle se lie correctement aux deux mâchoires.

- **Libération des mâchoires par gravure chimique de la couche sacrificielle** d'aluminium (immersion dans une solution acide spécifique) et séchage. Une fois la mâchoire supérieure libre de mouvement, les pinces deviennent fragiles et le séchage peut les endommager s'il n'est pas effectué avec précaution. Le retrait du fluide contenu à l'intérieur des mâchoires conduit parfois à la fermeture des mâchoires qui se trouvent alors soudées entre elles par les forces de van der Waals et l'effet Casimir. Une gravure ionique supplémentaire est alors nécessaire.

Avec ce procédé, on produit typiquement des pinces de 2 µm de côté dont les mâchoires font 200 nm d'épaisseur (150 nm seulement pour les mâchoires en chrome) et qui sont reliées par une charnière en or de 350 nm de haut et 20 nm de large. Des pinces allant d'environ 500 nm à 10 µm de large ont aussi été fabriquées.

Deux types de pinces ont été produits, l'un fait de deux mâchoires en Permalloy (doux/doux) et l'autre composé d'une mâchoire supérieure en Permalloy associée à une mâchoire inférieure en chrome (doux/non-magnétique). Pour les pinces doux/dur, différents matériaux durs ont été testés mais de nombreux problèmes d'adhésion ont été rencontrés ; problèmes dont la résolution a été abandonnée dans le cadre de la thèse. La caractérisation expérimentale de ces deux types de pinces et l'analyse quantitative de leur comportement sont présentées dans le chapitre suivant (**5**).

8.5 Actionnement des pinces: caractérisation expérimentale et modélisation

Le but principal de la thèse était d'établir une preuve de la validité du concept en démontrant l'actionnement de micro/nano-pinces magnétiques par l'application d'un champ magnétique externe. Dans ce but, une expérience originale a été mise en place dans un microscope électronique à balayage (MEB) pour mettre en évidence l'ouverture des pinces (**5.1**), ces dernières étant trop petites pour permettre une observation quantitative de leur mouvement par microscopie optique.

Cependant, la présence de champs magnétiques à l'intérieur d'un MEB dévie les électrons collectés pour construire l'image, ce qui la dégrade fortement. Pour limiter cet effet, un champ magnétique très local a été généré à proximité immédiate des pinces. Pour ce faire, une microsphère magnétique de néodyme-fer-bore (NdFeB) d'environ 10 µm de diamètre a été soudée au bout d'une pointe AFM, elle-même fixée sur un bras micro-manipulé dont le mouvement à 3 degrés de liberté est contrôlé par des moteurs piézo-électriques. Le champ magnétique que la microsphère génère est si local qu'il ne permet d'intervenir que sur une pince à la fois, d'à peine quelques microns de distance.

Ce montage expérimental a permis l'observation directe de la première actuation magnétique de deux types de pince : doux/doux et doux/non-magnétique. En particulier, les comportements de deux pinces ont été enregistrés et analysés, l'une composée de deux mâchoires en NiFe de 2 µm de côté et 250 nm d'épaisseur (doux/doux) et l'autre composée d'une mâchoire de 250 nm de NiFe et une mâchoire de 150 nm de chrome mesurant aussi 2 µm de côté (doux/non-magnétique). Les deux pinces comportaient une charnière en or de 20 nm d'épaisseur nominale et 350 nm de haut.

L'analyse de ces images visait à déterminer la constante de raideur de la charnière en or. En effet, cette constante est le coefficient de proportionnalité entre le couple élastique et l'angle d'ouverture de la pince (chapitres **2** et **3**). Cette relation peut être déterminée dans le cadre de ces expériences en associant l'angle d'ouverture observé au couple magnétique exercé par le champ émis par la microsphère sur la mâchoire mobile, celui-ci étant égal au couple élastique (puisque les deux s'équilibrent).

Dans ce but, la position de la sphère par rapport à celle de la pince a été extraite sur une succession d'images et intégrée au modèle présenté précédemment (chapitre **2**). Le calcul a dû être modifié par rapport au cas théorique car le champ magnétique externe n'est plus uniforme mais dipolaire. Le couple magnétique ainsi calculé a enfin été associé à l'angle

d'ouverture observé sur la même succession d'images pour déterminer la rigidité de la charnière.

Suivant cette approche, la rigidité de la charnière de la pince doux/non-magnétique est estimée à $K_{doux/NM} = 3.02 \pm 0.4 \times 10^{-13}$ N.m, correspondant à une épaisseur effective de 22 ± 1 nm (dont la constante de raideur K dépend au cube, voir section 3.1, équation 17). Ce résultat, très proche de l'épaisseur nominale d'or déposée pour constituer la charnière, est en excellent accord avec nos prédictions.

Concernant la pince doux/doux, la rigidité de la charnière vaut $K_{doux/doux} = 1.95 \pm 0.8 \times 10^{-12}$ N.m, ce qui correspond à une épaisseur effective de 41 ± 5 nm. Cette charnière apparaît donc plus rigide qu'escompté bien qu'elle ait été fabriquée sous les mêmes conditions et au même moment que la précédente.

L'écart entre ces deux résultats peut être expliqué par le caractère aléatoire de l'épaisseur de la couche d'or en raison de ses conditions de dépôt particulières. En effet, celle-ci est évaporée sur le flanc de la couche sacrificielle en aluminium qui est particulièrement rugueuse. De plus, l'incidence oblique du dépôt induit un phénomène d'ombrage dû à la croissance en îlots caractéristique de l'or, ce qui génère une porosité à l'échelle nanométrique dans le film d'or.

L'augmentation de la rigidité effective de la charnière due à une distribution aléatoire de son épaisseur a été confirmée par les prédictions d'un modèle statistique simple, décrivant la distribution d'épaisseur selon une loi gaussienne. Néanmoins, plus d'expériences seraient nécessaires pour confirmer ce modèle et en affiner les paramètres statistiques.

Finalement, ce travail expérimental a rempli l'objectif principal de la thèse qui consistait à établir la preuve de concept de l'actionnement magnétique de micro/nano-pinces magnétiques. Cette étude a notamment validé la solidité et la flexibilité de la charnière en or qui permettent l'ouverture répétée d'une pince sans se briser. Le bon accord entre les résultats expérimentaux et nos prédictions théoriques corrobore les hypothèses employées dans le modèle analytique élaboré précédemment.

8.6 Conclusion générale et perspectives

8.6.1 Conclusion générale

Cette thèse proposait de réaliser des micro/nano-pinces magnétiques articulées dont l'actionnement est obtenu à distance par l'application d'un champ magnétique. La finalité de ces pinces est de saisir et exercer des forces sur des objets biologiques dans le cadre d'applications biotechnologiques et médicales. Ce projet novateur, qui a été initié par cette thèse, a nécessité un travail exploratoire important et très en amont d'éventuelles applications.

Les objectifs principaux de la thèse étaient de:

- modéliser le comportement magnéto-mécanique des micro/nano-pinces magnétiques pour prédire leur réaction à l'application d'un champ magnétique uniforme en fonction de divers paramètres physiques (composition et dimensions des mâchoires, dimensions de la charnière, orientation et intensité du champ externe),
- développer un procédé de fabrication inspiré des techniques de la microélectronique pour aboutir à la réalisation d'un prototype de pince fonctionnel, composé de deux microparticules magnétiques reliées par l'un de leur côté par une charnière en or flexible,
- démontrer l'actionnement à distance de ce prototype par l'application d'un champ magnétique.

Dans un premier temps, une analyse globale du système magnéto-mécanique que constituent les pinces a été effectuée (chapitre **2**). La description du comportement micromagnétique des mâchoires ferromagnétiques douces, ainsi que l'évaluation des couples magnétiques et élastiques impliqués dans l'ouverture d'une pince, ont orienté le choix des matériaux et déterminé les dimensions des pinces.

Dans un second temps, le modèle analytique visant à prédire plus précisément le comportement des pinces a été élaboré (**3.1.1**). Il permet de calculer la position de la mâchoire mobile pour laquelle les couples magnéto-mécaniques qui s'exercent sur elle s'équilibrent.

Trois types de pinces avec une mâchoire supérieure mobile dotées des propriétés magnétiques du Permalloy (ferromagnétique douce), et une mâchoire inférieure fixe dont les propriétés magnétiques sont modifiées d'un cas à l'autre (ferromagnétique douce, aimant permanent, non-magnétique) ont été étudiés. Les hypothèses ont été faites que le

matériau doux a une réponse linéaire au champ appliqué jusqu'à saturation (0.1 T) et que l'aimantation des mâchoires magnétiques (douces et dures) est confinée dans le plan.

La comparaison des résultats obtenus pour les trois types de pinces (**3.1.2**), soumises à un champ magnétique (de 0 à 0.2 T) appliqué sous différentes orientations, révèle la spécificité de chaque type de pince et indique notamment que l'interaction magnétostatique est faible par rapport à l'effet du champ externe. Commander l'ouverture d'une pince libérée en solution par l'application d'un champ magnétique nécessitera donc quelques ajustements. De manière générale, l'application d'un champ uniforme d'au moins 0.085 T à 45° par rapport au plan des pinces donne des ouvertures d'environ 30°, ce qui constitue un résultat tout à fait encourageant.

L'idée originale de ces pinces a ensuite pu être concrétisée par l'élaboration d'un procédé de fabrication, inspiré des techniques de la microélectronique et mis en œuvre dans la salle blanche de la Plateforme Technologique Amont (PTA) (**4.1**). Ce procédé permet de fabriquer des réseaux de pinces fonctionnelles de manière reproductible. Il peut être résumé en 4 étapes : i) micro-structuration de la surface en silicium par lithographie optique et gravure ionique réactive ; ii) dépôt par évaporation électronique des couches métalliques qui constituent les pinces (mâchoires séparées d'une couche sacrificielle en aluminium) ; iii) évaporation sous incidence oblique de la charnière en or sur un des flancs des pinces et gravure ionique des autres flancs ; iv) élimination de la couche sacrificielle par gravure chimique et séchage.

Des pinces de composition variées ont ainsi été produites, notamment des pinces faites de deux mâchoires magnétiques douces (Permalloy) et des pinces composées d'une seule mâchoire douce, l'autre étant non-magnétique (chrome). Les dimensions typiques pour les mâchoires sont de 2 µm de côté et 200 nm d'épaisseur et la charnière mesure 350 nm de haut et de 20 nm d'épaisseur.

Finalement, l'actuation magnétique de ces pinces a été démontrée avec succès à l'aide d'une expérience originale et développée spécialement dans ce but. Cette dernière a été installée dans un microscope électronique à balayage (MEB) pour permettre l'observation directe des pinces dont les dimensions ne permettent pas une observation quantitative par imagerie optique. Le montage expérimental consistait à générer un champ magnétique très localisé à l'aide d'une microsphère magnétique à proximité d'une pince, pour limiter la perturbation de l'image électronique.

Le comportement des pinces à l'approche de la microsphère magnétique a été analysé grâce aux images acquises lors des expériences (**5.3**). L'interprétation de ces résultats, effectuée à l'aide du modèle analytique élaboré précédemment et adapté pour correspondre à ces cas expérimentaux, a permis de quantifier les propriétés mécaniques de nano-charnières en or de 20 nm d'épaisseur.

Pour conclure, à travers ce travail de thèse, nous sommes parvenus à valider le concept initial des micro/nano-pinces magnétiques en démontrant leur actuation à distance par l'action d'un champ magnétique, ainsi que la flexibilité et robustesse de la nano-charnière en or. Le bon accord entre ces résultats expérimentaux et nos prédictions théoriques confirme les hypothèses sur les propriétés physiques des pinces utilisées dans le modèle analytique (micromagnétisme des mâchoires douces adoptant une configuration magnétique vortex, flexibilité du film d'or). Par ailleurs, ces prédictions théoriques sont elles-mêmes en très bon accord avec des calculs numériques par éléments finis réalisés avec Flux3D et COMSOL Multiphysics.

8.6.2 Perspectives et applications

Dans le cadre du projet « Nanoshark » soutenu par l'Agence Nationale de la Recherche (référence : ANR-11-NANO-001), cette étude a été poursuivie une année supplémentaire. Faisant suite à la présente thèse, cette étude vise à optimiser les pinces, le procédé de fabrication en particulier, sur la base de l'expérience acquise durant la thèse. Ces travaux ont été menés par Guillermo Tulio Ortiz, post-doctorant à Spintec.

Les paramètres techniques nécessaires à l'obtention de pinces fonctionnelles étant mieux connus à l'issue de ce travail de thèse, la technique de formation de micro-piliers dans le substrat en silicium qui permettait de varier aisément la taille des pinces (**4.1.2**) a pu être abandonnée au profit d'une technique plus simple. L'étape de micro-structuration du substrat peut donc être réalisée par une simple lithographie optique en vue de déposer les pinces au fond de trous de résine plutôt qu'au somment de piliers en silicium. La réalisation d'un masque dur de lithographie optique a été guidée par les résultats des premières expériences de caractérisation effectuées pendant la thèse.

En permettant la fabrication de pinces de différentes formes (carrée, rectangulaire plus ou moins allongée ou trapézoïdale) et tailles sur le même wafer, ce changement dans le procédé de fabrication va faciliter l'évaluation de l'impact de ces paramètres sur le comportement des pinces. Cette étude sera d'autant plus facilitée par la mise en place d'un

nouvel outil permettant l'actionnement simultané d'une collection de pinces à l'intérieur d'un MEB. Ce montage est conçu pour générer un champ macroscopique sans trop altérer la trajectoire des électrons (**6.2.1**).

Des simulations micromagnétiques ont notamment montré que la configuration magnétique en vortex n'était plus présente dans les mâchoires en NiFe dont la longueur fait trois fois la largeur, donnant lieu à une aimantation planaire dans les mâchoires, qui peuvent alors adopter une configuration antiparallèle en champ nul et parallèle sous l'application d'un champ magnétique. Il serait particulièrement intéressant valider cet effet expérimentalement. Dans la perspective de libérer les pinces en solution, l'intensité de l'interaction magnétostatique pourra aussi être augmentée, en modifiant le rapport de forme et en augmentant le volume des mâchoires.

La structure de charnière en or pourra être rendue plus homogène et reproductible en gravant les flancs des pinces préalablement au dépôt de l'or. Ceci devrait permettre de réaliser des charnières plus fines, jusqu'à 5 nm. Les résultats déjà obtenus dans ce sens par G. T. Ortiz sont très encourageants.

Les propriétés mécaniques de la charnière telles que sa raideur et sa durée de vie (en nombre de cycles d'ouverture et fermeture) pourront être caractérisées par microscopie à force atomique (AFM).

Il est par ailleurs envisageable de remplacer l'or par un polymère pour composer la charnière. La plupart des polymères possèdent une élasticité très supérieure à celle des métaux déposés par évaporation et permettraient donc un plus grand nombre de cycles et de plus amples ouvertures. Des idées de pinces dotées d'une charnière polymérique sont présentées dans la section **6.2.2**.

Dans la perspective de les intégrer dans des canaux microfluidiques ou de les relâcher en solution, les micro/nano-pinces magnétiques pourront voir leurs surfaces fonctionnalisées chimiquement pour interagir spécifiquement avec les objets biologiques ciblés. La stratégie envisagée consiste à passiver l'extérieur des pinces pour éviter les interactions non-spécifiques avec l'environnement, puis, après élimination de la couche sacrificielle, à activer chimiquement l'intérieur des mâchoires pour leur permettre de reconnaître et de se lier spécifiquement aux objets biologiques ciblés.

Ces travaux ont été démarrés au cours de la thèse et poursuivis par Nora Reinhardt, post-doctorante au SPrAM. Ainsi, le bon état des couches d'or à l'intérieur des mâchoires

suite à l'élimination chimique de la couche sacrificielle a été confirmé. Ensuite, la réalisation de particules Janus dont les deux surfaces d'or sont fonctionnalisées différemment a été démontrée par un test de fluorescence. Enfin, la résistance à l'attaque chimique de la couche sacrificielle du polyéthylène glycol (PEG) utilisé comme couche inerte sur les surfaces externes des pinces a été testée et validée. La capture de nanoparticules d'or de 40 et 80 nm de diamètre par les pinces est également à l'étude.

La fonctionnalisation de l'intérieur des mâchoires permet d'établir des liens chimiques avec les objets ciblés. Ainsi, la capture d'une cible peut maintenir une pince fermée (ou ouverte en fonction de la taille de l'objet) malgré l'application d'un champ magnétique. Ceci induit une différence de réflectivité entre les pinces vides et les pinces « chargées », détectable optiquement. Ainsi, un réseau de pinces fixées au fond de canaux microfluidiques pourra constituer une bio-puce à détection optique. On peut même imaginer conduire des expériences de mécano-transduction en masse, en appliquant un champ alternatif basse fréquence sur un réseau de pinces ayant capturé des cellules.

En augmentant le champ magnétique appliqué jusqu'à la rupture des liens chimiques avec ou au sein même de la cible (dans le cas d'assemblages biomoléculaires), et connaissant la valeur du couple magnétique ainsi appliqué, il sera possible d'effectuer des mesures des forces assurant ces liens.

Libérées en solution, les pinces pourront trouver des applications originales en interagissant avec des cellules. Par exemple, elles pourraient être employées à des fins de destruction cellulaire ciblée, soit par hyperthermie extrêmement localisée (sous l'application de champs magnétiques haute fréquence), soit par induction d'apoptose par stimuli mécaniques (sous l'application de champs basse fréquence). Les pinces pourront aussi servir pour pratiquer des nano-biopsies non invasives.

Par ailleurs, les micro/nano-pinces magnétiques présentent des propriétés magnéto-optiques qui pourront aussi trouver des applications en physique. En effet, elles constituent un réseau de micro-surfaces réfléchissantes dont la réflectivité varie en fonction du champ appliqué, ce qui peut permettre de détecter la présence de champs magnétiques et de les cartographier avec une grande résolution (qui correspond à l'espacement entre les pinces dans le réseau). Ce concept est déjà à l'étude à Spintec avec des micro-poutres flexibles dont le changement de réflectivité à l'approche d'un aimant macroscopique est visible à l'œil nu.

Les propriétés mécaniques des pinces peuvent aussi être exploitées en tant que micro-résonateurs, la mâchoire supérieure jouant le rôle d'un cantilever, dont la fréquence propre est estimée à l'ordre du MHz pour une charnière en or de 20 nm d'épaisseur. Le couplage avec un laser pourrait permettre une mesure très précise de la force exercée sur la mâchoire supérieure, l'adsorption d'une cible biologique par exemple.